

**Development of immuno-affinity mass spectrometry assays
for the detection and quantification of viral antigens and antibodies**

by

Delaram Dara

A thesis submitted in partial fulfillment of the requirements for the degree of

Master of Science

Department of Laboratory Medicine and Pathology

University of Alberta

© Delaram Dara, 2022

Abstract

Currently, immunoassays are the gold standard tools for the detection and measurement of proteins in biological samples. These methods have a high level of sensitivity but are prone to limitations, such as non-specific binding and limited specificity due to cross-reactivity. This research aimed at addressing these limitations. Multiplexing sensitive and highly specific immunoaffinity-mass spectrometry (IA-MS) assays were developed for the detection and quantification of immunoglobulins (Igs) generated against severe acute respiratory syndrome coronavirus (SARS-CoV-2), and the human endogenous retrovirus-K (HERV-K) envelope proteins.

For the first project, the developed IA-MS assays were applied for the multiplexing detection and quantification of antibody subclasses and isotypes (IgG1, IgG2, IgG3, IgG4, IgA1, IgA2, IgM, IgD, and IgE). Proteotypic peptides unique to the constant regions of various antibody subclasses and isotypes were selected, and stable-isotope labeled peptide internal standards were designed and optimized, enabling the differential quantification of human Igs. For immunoprecipitation (IP), the recombinant receptor binding domain (RBD) of the spike glycoprotein was used as a bait to capture human antibodies specifically targeting the RBD domain. Following IP, ultra performance liquid chromatography was used for the separation of peptides followed by selected reaction monitoring (SRM) assay for the detection and quantification of antibody subclasses and isotypes. Initially, 29 confirmed positive plasma samples and 12 pre-pandemic and confirmed negative serological samples were used to examine the sensitivity and specificity of the developed assay. There was a statistically significant increase in median concentrations of the anti-RBD IgG1, IgG3, total IgG, IgA1, total IgA and IgM in COVID-19 positive versus COVID-19 negative

samples. Additionally, there was 100% diagnostic specificity at 100% sensitivity when measuring anti-RBD IgG1 median concentrations to detect COVID-19 positive patients from negative patients. Subsequently, a larger sample size was used to evaluate the developed IA-SRM assay (82 positive plasma, and 142 pre-pandemic serum and plasma). The IgG1 cut-off for diagnosing SARS-CoV-2 positive versus negative patients was validated to be 407 ng/mL. IgG1 was found to be the most representative antibody in serological samples for distinguishing positive from negative patients. Additionally, with the multiplexing capacity of SRM assays and the assessment of both IgG1 and IgM antibodies, the sensitivity of the developed assay increased from 89.1% to 97.62%.

An IA-SRM assay was developed for the differential quantification of HERV-K *env* (envelope) proteins in MCF-7, MDA-MB-231 and LNCaP cancer cell lines as well as human placenta tissues. Two commercial antibodies (HERM 1811-5 and ERVK-7) targeting highly conserved protein sequences were used to capture HERV-K *env* proteins. HERV-K *env* proteins, however, were not detected in these cell lines nor the placenta tissues. Synthetic peptides containing the epitope region of these two antibodies were used to assess antibody affinity and revealed that the HERM 1811-5 and ERVK-7 antibodies potentially did not bind to the corresponding epitope peptides.

Overall, the developed IA-SRM assays showcase the potential to facilitate diagnosis of infectious diseases. In such cases, specific peptides or antibodies can be used for the capturing and enrichment of target proteins to then be detected with a high level of sensitivity and specificity using liquid chromatography coupled to mass spectrometry.

Preface

Some of the research conducted for this thesis forms part of a collaboration within the laboratory of my supervisor, Dr. Andrei P. Drabovich. The literature review, conduct of experiments and data analysis are my original work except for the proteotypic peptide selections (Table 2.2) and the statistical analysis/figure generation for Table 2.7 and Figure 2.6, which were performed by Dr. Drabovich using the data generated from my experiments. Both Table 2.7 and Figure 2.6 were included in a manuscript titled “Rational Design and Development of SARS-CoV-2 Serological Diagnostics by Immunoprecipitation-Targeted Proteomics” by Zhiqiang Fu (postdoctoral fellow), Yasmine Rais (doctoral student), Delaram Dara and Andrei P. Drabovich.

The research project, of which this thesis is a part, received the following research ethics approvals from the University of Alberta Research Ethics Board: (i) “RATIONAL DESIGN AND STANDARDIZATION OF COVID-19 SEROLOGY DIAGNOSTICS”, Pro00104098_REN1, 2021-2023 and (ii) COVID-19 SURVEILLANCE COLLABORATION, CoCollab; Pro00100207_REN1, July 6, 2020

Acknowledgments

I would like to express my utmost gratitude to my two supervisors, Dr. Andrei Drabovich and Dr. X. Chris Le for their guidance through the program. I have learned a lot about the field of proteomics. I would like to also thank my lab members, Yasmine Rais, Zhiqiang Fu, and fellow members within the Division of Analytical and Environmental Toxicology. Additionally, I would like to thank Dr. Monika Keelan and Dr. Jelena Holovati immensely for their guidance through the steps to complete the program. Lastly, I would like to thank my supervisory committee member Dr. Olivier Julien and Dr. Richard Fahlman for serving as arm's length examiner at my final examination.

Table of Contents

1	The use of Immunoaffinity Mass Spectrometry for the Detection of Proteins.....	1
1.1	Introduction to Proteomics	1
1.2	Immunoassays and their Limitations.....	3
1.3	Introduction to Mass Spectrometry	5
1.4	Mass Spectrometry Coupled to Liquid Chromatography	8
1.5	Bottom-up Proteomics.....	9
1.6	Targeted Mass Spectrometry.....	10
1.7	Method Development using Targeted Mass Spectrometry	10
1.8	Immunoaffinity Mass Spectrometry.....	14
1.9	Clinical Diagnosis of SARS-CoV-2.....	15
1.10	Human Endogenous Retroviruses	17
1.11	Research Rationale	18
1.12	References	19
2	Development of Immuno-Affinity Mass Spectrometry Assay for the Serological Testing of Immunity against SARS-CoV-2	22
2.1	COVID-19 Pandemic	22
2.2	Immune Response Following SARS-CoV-2 Infection	24
2.3	B-cell Activation and Antibody Production.....	24
2.4	Antibody Class Switching.....	25
2.5	The use of immuno-affinity mass spectrometry assays for detection and quantification of immunity against SARS-CoV-2	27
2.6	Materials and Methods	29
2.7	High Performance Liquid Chromatography Gradient Optimization.....	39

2.8	Optimization of Immunoassay’s Blocking Buffer	43
2.9	Optimization of Immunoassay’s Washing Buffer.....	45
2.10	Results	46
2.10.1	Quantification of anti-SARS-CoV-2 antibodies	46
2.10.2	Assessment of the Developed Immuno-affinity Mass Spectrometry Assay in Larger Cohort	49
2.10.3	Comparison of Plasma and Saliva Immunoglobulin Levels.....	51
2.10.4	Clinical Outcome Assessment	54
2.10.5	Benefits of the Multiplexing Potential of Immuno-affinity Mass Spectrometry Assay	56
2.10.6	Assessment of SARS-CoV-2 Mutants and Common Cold Coronaviruses	57
2.11	Discussion	63
2.12	References	68
3	The use of immuno-affinity mass spectrometry for the detection and quantification of the Human Endogenous Retrovirus proteins	71
3.1	Materials and Methods.....	73
3.2	Results	82
3.2.1	Assessment of the HERV-K <i>env</i> Protein Expression in MCF-7, MDA-MB-231, and LNCaP Cell Lines	82
3.2.2	HERV-K Envelope Protein Expression in Placental Tissue.....	87
3.2.3	Assessment of Binding of HERV-K <i>env</i> Antibodies to their Specific Epitope.....	88
3.3	Discussion	91
3.4	References	92
4	Conclusions.....	93
4.1	References	96

List of Tables

Table	Page
Table 1.1 The neXtprot human proteome statistics (v2.43.2), including the unique human proteins, splicing isoforms, single amino acid variants, and post translational modifications	1
Table 2.1. Structure and function of subclasses and isotypes of the human immunoglobulins	27
Table 2.2. Selected proteotypic tryptic peptides	33
Table 2.3. Proteotypic tryptic peptides, unique for each antibody isotypes and subclasses with their optimized parameters	35-38
Table 2.4. Optimization of HPLC gradients by altering percentage of Buffer B	40
Table 2.5. Assessment of various blocking reagents of sample preparation for immunoprecipitation	44
Table 2.6. Assessment of various washing buffers of sample preparation for immunoprecipitation	45
Table 2.7. Concentrations of the various subclasses and isotypes of anti-SARS-CoV-2 antibodies.	47
Table 2.8. Median concentration of antibody subclasses and isotypes amongst RT-PCR confirmed SARS-CoV-2 positive patients categorized based on clinical endpoints	55
Table 2.9. Multiplexing potential of IgG1 with other antibody isotypes and subclasses for the diagnosis of SARS-CoV-2 positive patients	57
Table 3.1. Proteotypic tryptic peptides of HERV-K <i>env</i> proteins	76-80
Table 3.2. ELISA detection of HERV-K <i>env</i> proteins in human placenta tissue and MCF-7 cell line	88

List of Figures

Figure	Page
Figure 1.1. The twenty different amino acids that make up all proteins.	2
Figure 1.2. The three most common ELISA assay types used to detect proteins.	4
Figure 1.3. Setup of the triple quadrupole mass analyzer	7
Figure 1.4. Exemplary optimization of SRM assay using internal standard tryptic peptides.	13
Figure 2.1. SARS-CoV-2 structural proteins	23
Figure 2.2. Design of IA-MS assay for the serological testing of immune response against SARS-CoV-2.	28
Figure 2.3. The detection of top product ion transitions for the identification of tryptic peptides with high level of sensitivity.	34
Figure 2.4. Mass spectra of three UPLC-SRM gradients composed of all proteotypic tryptic peptides.	42
Figure 2.5. HPLC gradient composition.	43
Figure 2.6. Quantification of RBD-specific antibody isotypes and subclasses in smaller sample size using the IA-HPLC-SRM assay.	49
Figure 2.7. Quantification of RBD-specific antibody isotypes and subclasses in a larger sample size using the IA-HPLC-SRM assay.	51
Figure 2.8A. Comparison of anti-RBD IgG levels in plasma versus saliva samples (n=26) of the same patient, collected on the same day	53
Figure 2.8B. Comparison of anti-RBD IgA and IgM levels in plasma versus saliva samples (n=26) of the same patient, collected on the same day	54
Figure 2.9. Comparison of anti-RBD IgG1 antibody levels amongst hospitalized, ICU taken, non-hospitalized, and patients who passed away.	55

Figure 2.10. Benefits of the multiplexing capacity of IA-HPLC-SRM assay for enabling multiple anti-RBD antibodies to be detected simultaneously.	56
Figure 2.11. IgG1 immunoglobulin levels against three SARS-CoV-2 antigens belonging to the RBD, the B.1.1, and B.1.351 variants alongside four common cold coronavirus antigens (HKU1, OC43, 229E, and NL63).	59
Figure 2.12. IgM immunoglobulin levels against three SARS-CoV-2 antigens belonging to the RBD, the B.1.1, and B.1.351 variants alongside four common cold coronavirus antigens (HKU1, OC43, 229E, and NL63)	60
Figure 2.13. Antibody subclasses and isotype levels against the RBD, the B.1.1, and B.1.351 variants alongside four common cold coronavirus antigens (HKU1, OC43, 229E, and NL63)	62
Figure 3.1. Depiction of the high level of homology through the alignment of HERV-K <i>env</i> sequences.	72
Figure 3.2 Optimized HERV-K <i>env</i> proteotypic tryptic peptides shared amongst various HERV-K genes	81
Figure 3.3. SRM results from two representative tryptic peptides (IVSPVSGPEHPELWR, LWNSQSSIDQK) shared by HERV-K <i>env</i> proteins tested in MCF-7 cell line lysates	83
Figure 3.4. SRM results from two representative tryptic peptides (IVSPVSGPEHPELWR, LWNSQSSIDQK) shared by HERV-K <i>env</i> proteins tested in LNCaP cell line lysates	84
Figure 3.5. SRM results of a representative tryptic peptide (QTVIWMGDR) shared by HERV-K <i>env</i> proteins tested in MCF-7 cell line lysates cultured and passaged in trypsin exposed vs. no-enzyme exposed cells	86
Figure 3.6. Assessment of binding of HERV-K <i>env</i> antibodies to their specific epitope	90

Symbols and Abbreviations

IA-MS	Immunoaffinity-mass spectrometry
Igs	Immunoglobulins
IP	Immunoprecipitation
RBD	Receptor binding domain
SRM	Selected reaction monitoring
UPLC	Ultra performance liquid chromatography
HPLC	High performance liquid chromatography
MRM	Multiple reaction monitoring
ELISA	Enzyme-linked immunosorbent assay
COVID-19	Coronavirus Disease 19
Nano-LC	Nano-liquid chromatography
RIA	Radioimmunoassay
m/z	Mass-to-charge
ESI	Electrospray ionization
TOF	Time-of-flight
LC	Liquid chromatography
CE	Collision energies
Env	Envelope
SARS-CoV-2	Severe acute respiratory syndrome coronavirus 2

1 The use of Immunoaffinity Mass Spectrometry for the Detection of Proteins

1.1 Introduction to Proteomics

Although DNA is the basis for building the genetic code, the dynamics of biological systems and the majority of biological functions are determined at the protein level (1). Proteins impact all components of life, such as immunity, metabolism, DNA replication to translation, and cell-cell communications (1). With the extensive variability in protein variants (**Table 1**), there remains many proteins whose function(s) have not been identified. Proteins are composed of combinations of individual amino acids which are linked together via peptide bonds (1). There are twenty different amino acids (**Figure 1.1**) each sharing an alpha carbon atom that is bonded to a carboxyl group, amino group, a hydrogen atom, and a variable side chain (1). The chemical and physical properties of these amino acids are determined by these variable side chains (1). These side chains can be polar and non-polar, resulting in different levels of hydrophobicity and hydrophilicity (1). As a whole, the field of proteomics refers to the combination of the terms "proteins" and "genomics" and entails the discovery, quantification, and determination of the functionality and dynamics of the proteome (2).

Table 1.1. The neXtprot human proteome statistics (v2.43.2), including the unique human proteins, splicing isoforms, single amino acid variants, and post translational modifications (3).

Unique protein entries	Splicing isoforms	Single amino acid variants	Post translational modifications
20,359	42,329	9,719,593	192,917

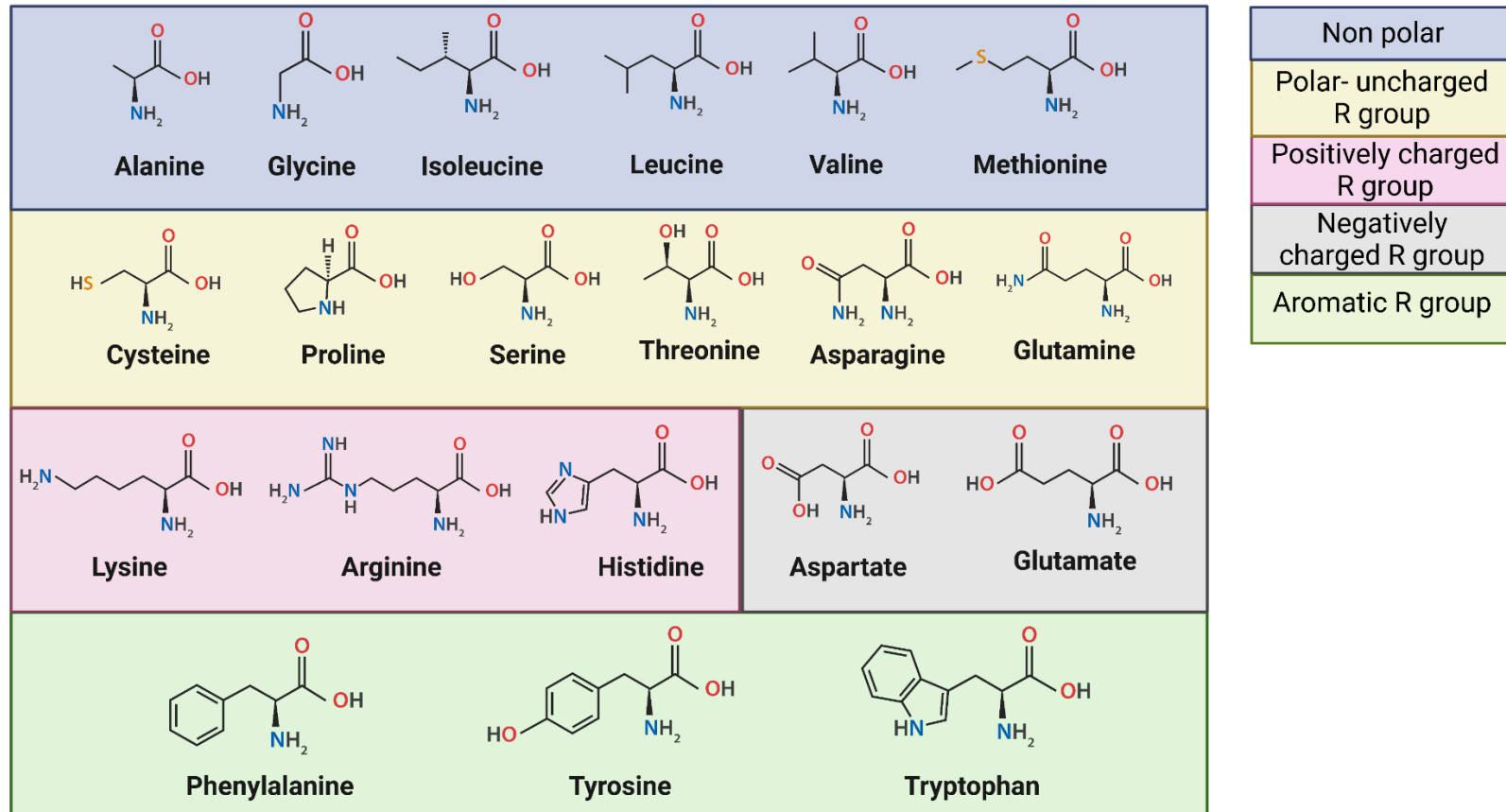


Figure 1.1. The twenty different amino acids that make up all proteins. Created with [BioRender.com](https://www.biorender.com)

1.2 Immunoassays and their Limitations

When it comes to studying proteins in biological samples, there are two main methods used: immunoassays and mass spectrometry. Immunoassays have been used since 1959, when Berson and Yalow developed the first radioimmunoassay (RIA) for insulin (4). Ever since then, there have been many evolving immunoassay techniques developed and thousands of proteins studied. As a whole, immunoassays encompass an umbrella of analytical methods used for the detection and quantification of proteins in biological samples which share the fundamental commonality of using the affinity of antibodies to their respective antigens (5). Enzyme-linked immunosorbent assay (ELISA) is one of the well-known immunoassays and is composed of 3 major types (**Figure 1.2**): direct, indirect, and sandwich ELISA (5). In ELISA, the antigen is detected directly or indirectly, using a labeled primary antibody or a labeled secondary antibody, respectively (5). As the name suggests, the direct ELISA involves a primary antibody directly interacting with the antigen (5). In this case this antibody is labeled with a fluorescent tag or reporter enzyme (5). Indirect ELISA involves a primary antibody that interacts with the target antigen (5). Following this, a labeled secondary antibody then binds to this primary antibody and facilitates detection (5). In sandwich ELISA, the plate is coated with a capture antibody that is specific for the target antigen (5, 6, 38). Following antigen capture, the labeled secondary antibody that has specificity for a different epitope region is utilized for the antigen detection (5, 6, 38). Additionally, sandwich ELISA can be of two forms, direct or indirect (38). In direct form, the detection antibody is enzyme conjugated. However, in the indirect form, a secondary enzyme-conjugated antibody is needed (5, 6, 38).

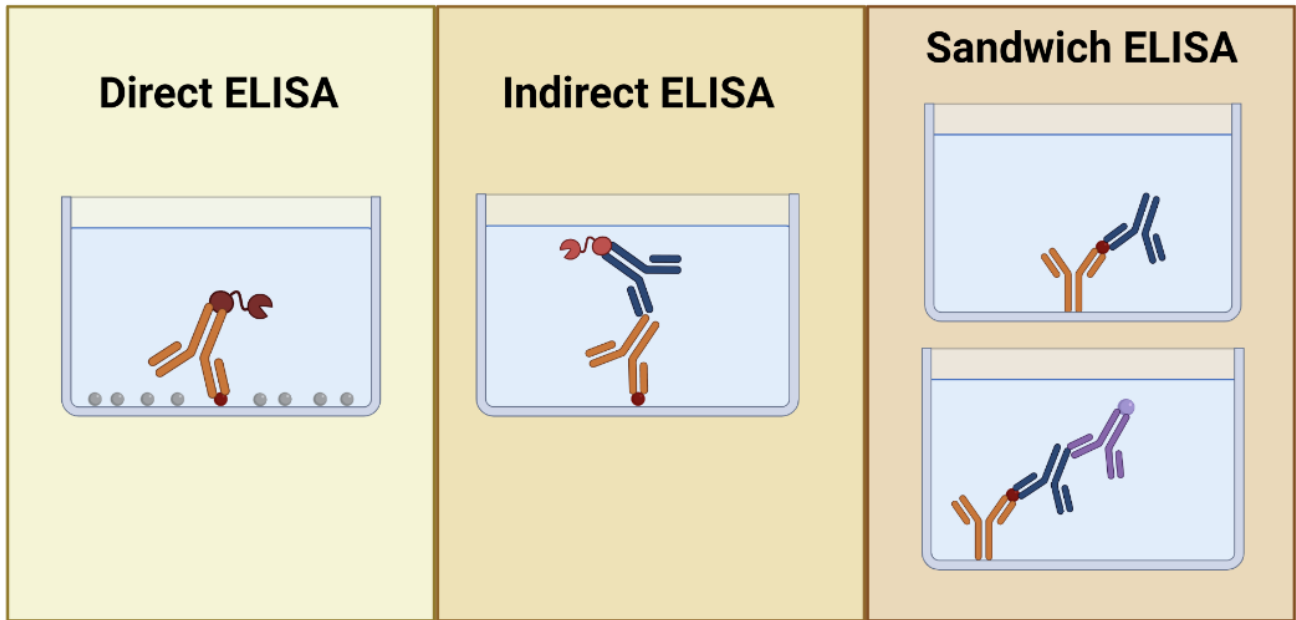


Figure 1.2. The three most common ELISA assay types used to detect proteins (5, 6, 38). (Left) Direct ELISA. (Centre) Indirect ELISA. (Right) Sandwich ELISA. Created with [BioRender.com](https://www.biorender.com)

Although immunoassays are very sensitive, their specificity could be compromised due to poor differential quantification of proteoforms and protein variants. Such limitations in specificity arise from cross reactivity where antibodies bind to similarly structured and result in false positive signal (7). Additionally, autoantibodies produced endogenously may inhibit the binding of capture antibodies to their target antigens and lead to falsely low immunoassay results (7). Another limiting factor is the lack of standardization of immunoassays, where the ELISA calibrators vary from lab-to-lab (7). As such the same assay must be used continuously in research laboratories and clinical diagnostics (7). A striking example would be an assay for the CA 19-9 (Carbohydrate Antigen 19-9) 19-9, a biomarker for pancreatic cancer (8). CA 19-9 immunoassay results in one hospital may suggest cancer recurrence, but another hospital would be suggesting cancer remission (7, 8). Subsequently, it is time consuming to immunize animals with a target protein antigen and produce and purify antibodies to be used in immunoassays (42).

1.3 Introduction to Mass Spectrometry

Mass spectrometry (MS) is another tool for detecting and quantifying proteins, but in this case, such information is acquired via the analysis of mass-to-charge (m/z) values of peptide ions corresponding to the proteins present in biological samples. There are three main components to a typical mass spectrometer: (i) the ionization source (ii) the mass analyzer and (iii) the ion detector (9).

The first step mass spectrometry analysis encompasses the molecules within a particular sample to be ionized where they are transformed into gaseous ions (9). An example and commonly used ionization technique is electrospray ionization (ESI) (9). As the name suggests, ESI involves the

formation of ionized gaseous particles to then be subjected to the mass analyzer (10). The first step involves the formation and ejection of charged droplets via the electric field created by the high potential difference between the capillary tube carrying the sample and the surrounding atmospheric pressure of the chamber (9, 10). Following this, these charged droplets are vaporized via a heated gas (air or nitrogen) and further broken down to smaller droplets and the individual ions. These charged ions then enter the mass analyzer (9, 10). The second step involves the use of the mass analyzer in which the m/z ratios of the gas-phase ions as well as their corresponding intensities are measured (ion trap or Orbitrap mass analyzers) or filtered (quadrupole analyzers) (9-11). An example of a hybrid mass spectrometer with multiple analyzers is a triple quadrupole mass spectrometer (**Figure 1.3**) (9, 10). In the first quadrupole (Q1), a predetermined precursor ion is selected and filtered amongst all other ions ejected into the mass analyzer (10). Subsequently, in the second quadrupole (Q2) collision-induced dissociation occurs where specific collision gas (nitrogen or argon) breaks down this precursor ion into fragments (10). Lastly, in the third quadrupole (Q3), the fragmented ions are filtered again, and the intensities of selected fragments are measured using the electron multiplying detectors (10). This results in the production of mass spectrums which are plots showcasing the various retention times of different product ions (m/z ratios) represented by the various peaks/curves and their corresponding intensities/abundances (**Figure 1.3**). Another well known mass analyzer is called the time-of-flight (TOF). Using the TOF, ions gain the same kinetic energy and are accelerated via an electric field towards the detector (37). While traveling towards the detector, the ions with the smaller m/z ratio will travel quicker than those with heavier m/z ratios (37). This enables ion separation based on the time it takes for them to reach the detector (37).

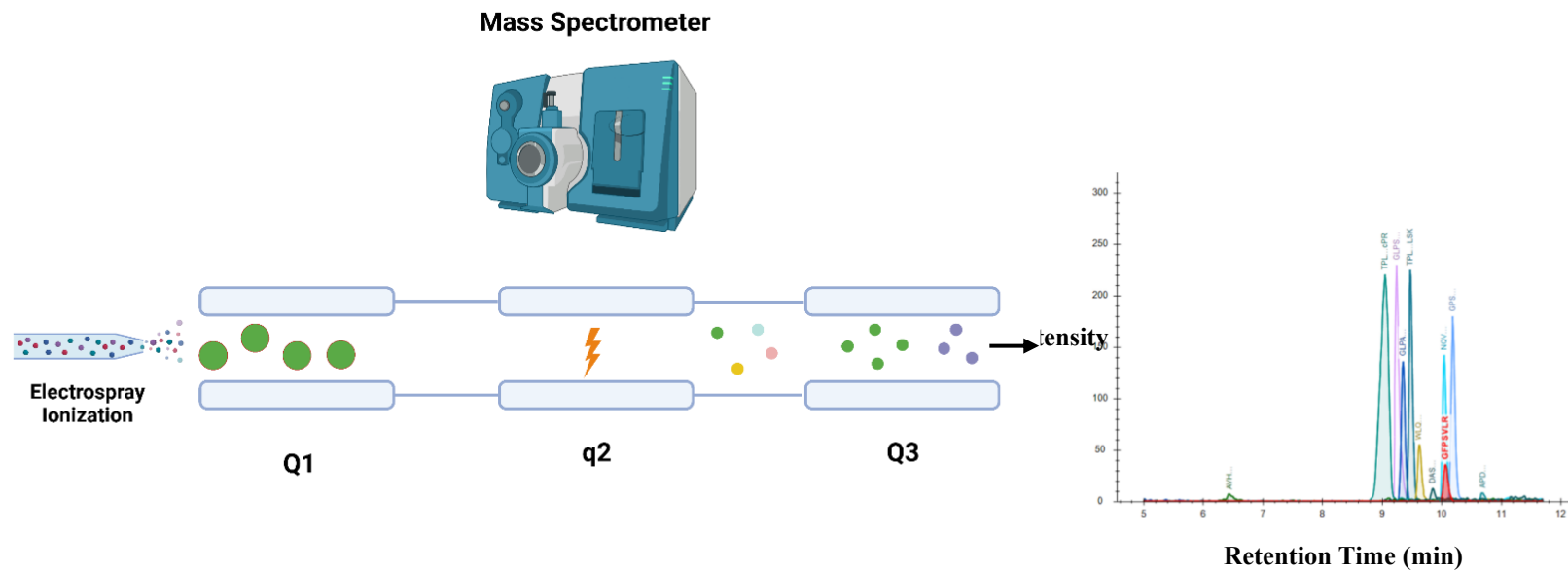


Figure 1.3. Setup of the triple quadrupole mass analyzer. The predetermined ions are selected in the Q1 and fragmented into product ions in Q2. These fragmented product ions are selected and filtered in the Q3 and detected with the ion detector to produce mass spectra. Created with [BioRender.com](https://www.biorender.com)

1.4 Mass Spectrometry Coupled to Liquid Chromatography

To enhance the detection of various compounds using MS, MS is commonly coupled to chromatography. One of such chromatography instruments is liquid chromatography. Liquid chromatography (LC) is an analytical tool that enables the separation of analytes (e.g., peptides) to be analyzed using the mass spectrometer (12). This coupled technique is known as LC-MS. There are 2 main components to LC which includes the mobile phase and the stationary phase (12, 13). Initially, the sample is picked up and injected into the sample loop and then introduced into the flowing mobile solvent (12, 13). As the mobile solvent is continuously flowing throughout the columns of the LC and carrying the sample (e.g., peptides), the sample then encounters the stationary phase such as C18 particles (typically, silica particles covalently linked to the long alkyl chains) (12-14). C18 as the name suggests is composed of 18 carbons bound to silica (12-14). These 18 carbons increase the surface area in which the mobile phase carrying our analyte can interact with to enable the separation of various components of the analyte (e.g., peptides) based on their hydrophobicity (12-14). The C18 in the column creates a hydrophobic environment in which nonpolar analytes in our sample interact stronger and are retained longer, while more polar compounds are eluted earlier and reach the ionization source faster (e.g., ESI) (12-14).

The mobile phase can be optimized by changing the gradient flow composition over the time frame of each run. For example, the gradient eluting solution usually starts with a higher concentration of water. Gradually there is then a decrease in water concentration while concurrently an increase in acetonitrile concentration. This incremental gradient change enables both hydrophobic and hydrophilic peptides to be eluted. For instance, in our project such pre-made buffers included buffer A containing 95% water, 0.1% formic acid, and 5% dimethyl sulfoxide (DMSO) while

buffer B containing 95% acetonitrile, 0.1% formic acid, and 5% DMSO. Notably it is important to optimize LC gradients to find the best configuration that enables all analytes to be eluted within the stationary phase of the column in the span of the run and to simultaneously get the most optimal separation of analytes in the sample. The optimization of LC gradients is key for detecting analytes with high level of analytical selectivity.

There are numerous types of liquid chromatography. Two of such include high performance liquid chromatography (HPLC) and nano-liquid chromatography (nano-LC). HPLC is a kind of column chromatography designed to use high pressure to move the sample and the mobile phase buffer through the stationary phase (12-13). Another type of LC is the nanoscale liquid chromatography. Nano-LC are useful in particular when low abundant analytes (e.g., peptides) want to be detected as this type of chromatography increases the sensitivity (15). This is done by the reduction in the inner diameter (less than 100 μm) of the columns used in the nano-LC which concentrates the analytes being measured (15).

1.5 Bottom-up Proteomics

One approach of studying proteins includes bottom-up proteomics. The fundamental component of this approach entails the proteolysis of the protein matrix and the subsequent protein analysis using mass spectrometry (2, 16). Shot-gun proteomics is a sub-field of bottom-up proteomics in which a mixture of proteins is broken down into smaller peptides and then analyzed using LC-MS/MS (liquid chromatography and tandem mass spectrometry) (2, 16). The shot-gun approach enables the identification and quantification of proteins on a global scale (2, 16, 17). It does this indirectly meaning using the fragmented peptides that are matched to proteomic databases in order

to detect and measure proteins (2, 16, 17). This works by comparing the MS/MS mass spectra identified in the sample to reference proteome databases (2, 16). Some uses of shot-gun proteomics have been in assessing protein-protein interactions, profiling of the proteome, protein quantification, and biomarker discovery (2, 18). Because of the database dependence of shot-gun mass spectrometry, a challenge that arises includes identification of the mismatches of non-unique digested peptides (2). While the shot-gun mass spectrometry analysis is designed to allow for detection of lower abundance peptide ions, the higher abundance peptides and proteins are identified more frequently and thus more accurately (17).

1.6 Targeted Mass Spectrometry

Another sub-field of bottom-up proteomics includes targeted mass spectrometry. As opposed to the global profiling of proteins in samples using shot-gun mass spectrometry, targeted methods enable the identification and quantification of pre-determined peptide of interest. In addition, stable isotope-labeled internal standards could be used for the accurate relative or “absolute” quantification (17). Markedly, this approach enables the detection of peptides with a high level of analytical selectivity and sensitivity (17).

1.7 Method Development using Targeted Mass Spectrometry

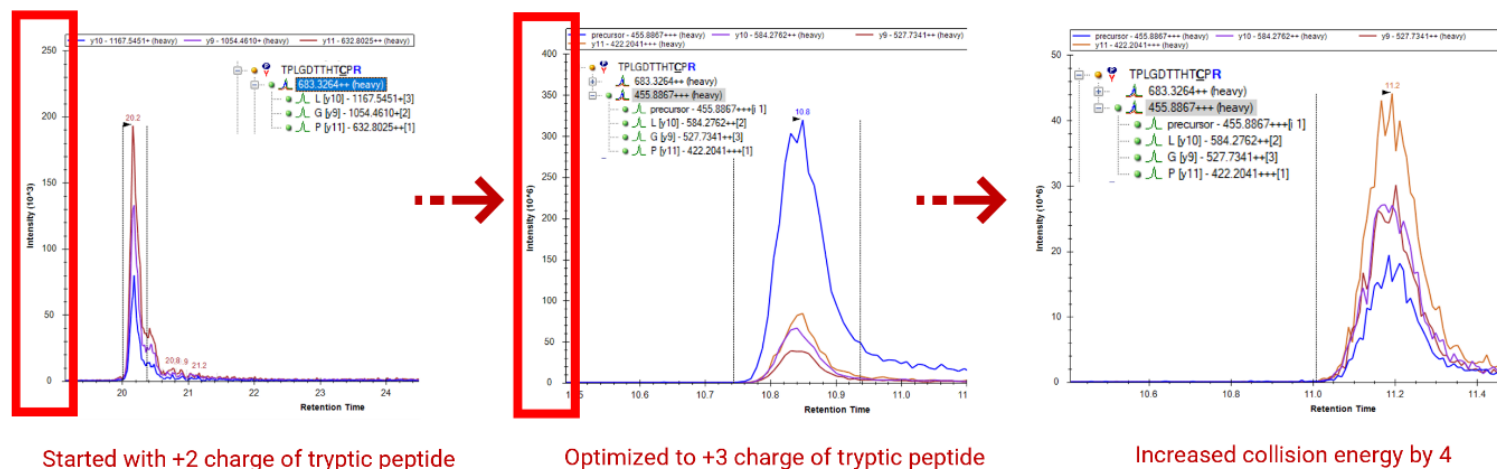
In order to develop selective reaction monitoring/multiple reaction monitoring SRM/MRM methods, various online databases such as Peptide Atlas, and neXtProt were utilized in order to select specific enzymatically (trypsin) digestible peptides that are unique to our proteins of interest, enabling the differential identification and quantification of such proteins in the samples (3, 39).

Such tryptic peptides are then synthesized, purified, and provided with known concentrations (such as SpikeTides_L peptides). These tryptic SpikeTides_L peptides are designed in such a way that they are stable-isotope labelled internal standards where “heavy” (^{13}C and ^{15}N) labeled lysine or arginine amino acids are incorporated (19). The “heavy” internal standard peptides have the same chromatographic properties as the endogenous unlabeled “light” peptides in biological samples (19). Additionally, the heavier mass of these isotopes creates a m/z difference that can be used for the identification and quantification of endogenous peptides by comparing their abundance to that of the known amounts of internal standards (19).

Following this, these internal standards are subjected to tandem mass spectrometry (MS/MS) mode where precursor ions with specific mass-to-charge (m/z) ratios are selected in the first quadrupole and then fragmented into product ions that are detected. Using the MS/MS modality of the mass spectrometer we can determine the best product ions also known as transitions which show the highest abundance and intensity. These fragmented product ions are denoted as 'b' or 'y' ions depending on whether the original precursor ion was fragmented from the N- or C- terminal of the peptide, respectively (17). These transitions in return enable us to detect our tryptic peptides of interest with a high degree of accuracy and specificity.

Another parameter that can be adjusted to enhance the detection of target analytes includes the optimization of collision energies (CE). As explained previously (**Figure 1.4**) in the second quadrupole of a triple quadrupole mass spectrometer, specific CEs facilitate extensive fragmentation of the analyte. These CEs can be optimized to create the highest abundance of particular product ions that are selected in the third quadrupole of the mass spectrometer.

Additionally, these methods can be further optimized selecting the charged state of the specific tryptic peptides of interest. For example, tryptic peptides of interest could be present as +2 or +3 forms with varying intensities. Notably, it is important to assess which charged state is present with a higher abundance used for quantification. By doing so, the developed assay has higher sensitivity in detecting lower abundant tryptic peptides.



Sources of optimization include adjusting:

- ✓ Gradient
- ✓ Charge
- ✓ Detecting Top Transitions
- ✓ Collision Energy

Figure 1.4. Exemplary optimization of SRM assay using internal standard tryptic peptides. The most abundant charge, collision energy, and transitions for a tryptic peptide needs to be examined and chosen.

After optimizing the various parameters as explained above, specific product ion transitions are chosen to indirectly detect and measure the selected precursor ion(s). These transitions are then inputted into the MRM/SRM methods of the mass spectrometer.

An advantage of using MS is its high level of analytical selectivity in which we can distinguish between even single amino acid variances between different peptides and proteins. This feature becomes particularly useful when we need to differentiate between highly homologous proteins. Additionally, as mentioned previously with MS we can develop multiplexing assays where hundreds of proteins can be measured simultaneously in one run. On the other hand, a limitation of MS lies in its sensitivity in which many low abundant proteins can not be detected using this technology. To address this issue, a more recently developed approach known as immunoaffinity-mass spectrometry (IA-MS) has been explored.

1.8 Immunoaffinity Mass Spectrometry

As the name suggest, IA-MS is a hybrid technique in which there is a combination of use of immunoassays alongside mass spectrometry (21). This approach is particularly powerful to analyze low abundance proteins (21, 40). To delineate, the first step of this hybrid approach involves the use of antibodies or antigens coated onto wells to capture specific proteins of interest (21, 40). IA step provides concentration or enrichment of the specific proteins of interest by antibodies while eliminating non-specific and highly abundant proteins in our sample (21, 40). Notably, using antibodies/antigens to capture certain proteins has shown to enrich samples by 1000-fold, enabling the study of many low abundant proteins that could not be assessed before (40).

In this thesis paper, I will be presenting results from the IA-MS assay development projects for the detection, identification, and quantification of 1) antibodies against SARS-CoV-2 and 2) human endogenous retrovirus proteins (HERVs).

1.9 Clinical Diagnosis of SARS-CoV-2

The current gold standard method for the clinical diagnosis of SARS-CoV-2 has been nucleic acid testing (NAT) (22, 23). Other developed and used methods include immunoassays for viral antigen detection, and immunoassays for the detection of immune response against SARS-CoV-2 (23). Some common NATs include reverse transcriptase polymerase chain reaction (RT-PCR), droplet digital PCR (ddPCR), reverse transcription loop-mediated isothermal amplification (RT-LAMP), next generation sequencing, and clustered regularly interspaced short palindromic repeats (CRISPR)-based detection (23). Focusing on the most commonly used NAT, RT-PCR, there are certain limitations that must be considered. Some limitations include relatively high false-negative rates which can result from improper sample collection and handling (e.g., inappropriate sample type, storage, transportation), narrow detection window (e.g., testing too early post infection), viral mutations, and low viral load (23, 24). Additionally, there is a need for skilled personnel for sample collection and the use of biosafety level (BSL)-2 labs (23). Alternatively, immunoassays can be used as direct antigen tests for detecting SARS-CoV-2 with the benefits of enabling a quick diagnosis, low purchasing cost, no need for trained personnel, and overall convenience of at home testing kits (23). Limitations of these tests include improper sample collection/handling, narrow detection windows, and potential cross-reactivity (23).

Another avenue for assessing COVID-19 prevalence is examining the anti-viral antibodies (23). Measuring antibody levels in blood can act as a surveillance tool for detecting past COVID-19 infections, many of which were asymptomatic, assessing efficacy of vaccines, and the development of therapeutic antibodies (23). When compared to nucleic acid-based testing, some of the useful benefits of assessing antibody levels include greater stability of antibodies relative to nucleic acids and a longer detection window (23). Some of the most widely used method for detecting and quantifying anti-viral antibodies against SARS-CoV-2 is the use of enzyme linked immunosorbent assay (ELISA) and lateral flow immunoassay (LFA) (25, 26). These methods portray a high level of sensitivity but are prone to limitations (23, 25, 26). Such limitations include non-specific binding and limited specificity due to cross-reactivity (23, 41). Additionally, these assays cannot be multiplexed meaning not all antibody classes and their isotypes (IgG1, IgG2, IgG3, IgG4, IgA1, IgA2, IgM, IgD, and IgE) can be measured all at once. As such when considering throughput and turnaround time, only a limited number of subclasses are routinely measured in indirect ELISAs which misses other potential diagnostic and prognostic information that other antibody isotypes would deliver.

Alternatively, MS is another analytical method that can be utilized for the detection of viral protein antigens, as well as antibodies, for those infected naturally or vaccinated patients. The benefits of using mass spectrometry include its high level of selectivity, capacity to differentiate between distinct proteins, and multiplexing potential. Notably, the use of MS has been applied during the 2019 pandemic for the detection and quantification of SARS-CoV-2 proteins in various clinical samples (27-29). The issue remaining is the limited analytical and diagnostic sensitivity when MS is used without thorough fractionation. To address this limitation, IA-MS can be utilized which

combines the best of both worlds, enabling a highly sensitive and selective approach in detecting proteins of interest.

1.10 Human Endogenous Retroviruses

HERVs make up approximately 8% of the human genome (30, 31). They were originally exogenous retroviruses that infected our ancestors' germline cells millions of years ago (30, 31). These retroviruses were double-stranded positive sense RNA viruses that integrated into the human genome (30). HERV are composed of 3 classes: class I to class III (30, 31). The most recently integrated HERV group into our genome is HERV-K group belonging to class II (30, 31). There are 11 subclasses in this subgroup denoted as HML (human mouse mammary tumour virus like)-1 to HML-11 (30). HERVs are composed of 4 main open reading frames which include *gag* (group-specific antigen), *pol* (polymerase), *pro* and *env* (envelope) genes that are flanked by long terminal repeats (LTRs) (30, 31). The *gag* gene encodes for the matrix, capsid, and nucleocapsid proteins (32). The *pol* gene encodes for the reverse transcriptase, integrase, and ribonuclease (32). The *pro* gene encodes for a nucleotidohydrolase and protease (32). Lastly the *env* gene encodes for an envelope surface glycoprotein (32). The HERV-K *env* transcript expression has been associated with some cancers including breast cancer, prostate cancer, lung cancer, melanomas, hepatocellular carcinoma etc. (33-35). The exact molecular mechanism for cancer development and HERV-K *env* gene has not been discovered. One hypothesis is that HERV can result in insertional mutagenesis, resulting in the activation of certain oncogenes and inhibition of tumor suppressor genes (31, 33-35). Currently, immunoassays are the gold standard analytical tool for the quantification of proteins (43). However, due to the high homology and potential cross-reactivity, the differential quantification of HERV-K *env* proteins and their evaluation as cancer

biomarkers can hardly be achieved by immunoassays. The development of methodologies that are highly sensitive and selective, such as by using IA-MS is important as having such assays that can differentially detect and quantify these proteins can enable future studies to evaluate the role of each individual HERV-K *env* protein in different cancers.

1.11 Research Rationale

The development of MS has revolutionized the field of proteomics by enabling proteins to be detected with a high level of selectivity, in which each amino acid of a protein sequence can be identified (40). The limitation of using MS solely for the detection and identification of proteins lies in its limited sensitivity (40). This limitation can be addressed by combining the technique of immunoassays with MS, a more novel tool known as IA-MS. The applicability of this novel tool can be beneficial in the detection and quantification antibodies produced against SARS-CoV-2. Another application of this tool is in the detection of potentially low-abundant and highly homologous HERV-K *env* proteins. To date, there has been assessment of the expression of these HERV-K *env* genes at the transcript level, and protein expression using indirect ELISA, immunohistochemistry and shot-gun proteomics (31, 34-36). However, there hasn't been studies that use IA-MS and more precisely targeted mass spectrometry approaches to detect these HERV-K *env* proteins. In this thesis, it is hypothesized that IA-MS facilitates the highly sensitive and specific detection of 1. SARS-CoV-2 antibodies in serological samples and 2. The highly homologous HERV-K *env* proteins.

1.12 References

1. Breda A VN, Norberto de Souza O, Garratt RC. *Bioinformatics in Tropical Disease Research: A Practical and Case-Study Approach*. 2006.
2. Zhang Y, Fonslow BR, Shan B, Baek MC, Yates JR, 3rd. Protein analysis by shotgun/bottom-up proteomics. *Chem Rev*. 2013;113(4):2343-94.
3. Zahn-Zabal M, Michel PA, Gateau A, Nikitin F, Schaeffer M, Audot E, et al. The neXtProt knowledgebase in 2020: data, tools and usability improvements. *Nucleic Acids Res*. 2020;48(D1):D328-D34.
4. Wu AH. A selected history and future of immunoassay development and applications in clinical chemistry. *Clin Chim Acta*. 2006;369(2):119-24.
5. Alhadj M FA. *Enzyme Linked Immunosorbent Assay*. StatPearls Publishing 2022.
6. Sakamoto S, Putalun W, Vimolmangkang S, Phoolcharoen W, Shoyama Y, Tanaka H, et al. Enzyme-linked immunosorbent assay for the quantitative/qualitative analysis of plant secondary metabolites. *J Nat Med*. 2018;72(1):32-42.
7. Hoofnagle AN, Wener MH. The fundamental flaws of immunoassays and potential solutions using tandem mass spectrometry. *J Immunol Methods*. 2009;347(1-2):3-11.
8. La'ulu SL, Roberts WL. Performance characteristics of five automated CA 19-9 assays. *Am J Clin Pathol*. 2007;127(3):436-40.
9. Glish GL, Vachet RW. The basics of mass spectrometry in the twenty-first century. *Nat Rev Drug Discov*. 2003;2(2):140-50.
10. Ho CS, Lam CW, Chan MH, Cheung RC, Law LK, Lit LC, et al. Electrospray ionisation mass spectrometry: principles and clinical applications. *Clin Biochem Rev*. 2003;24(1):3-12.
11. Dass C. *Fundamentals of Contemporary Mass Spectrometry 2007*. Wiley-Blackwell, Chichester, England
12. Pitt JJ. Principles and applications of liquid chromatography-mass spectrometry in clinical biochemistry. *Clin Biochem Rev*. 2009;30(1):19-34.
13. Petrova OE, Sauer K. High-Performance Liquid Chromatography (HPLC)-Based Detection and Quantitation of Cellular c-di-GMP. *Methods Mol Biol*. 2017;1657:33-43.
14. Shabir GA. Development and Validation of a Reversed-phase HPLC Method for the Determination of Hydroxybenzene in a Cream Formulation. *Indian J Pharm Sci*. 2010;72(3):307-11.
15. Wilson SR, Olsen C, Lundanes E. Nano liquid chromatography columns. *Analyst*. 2019;144(24):7090-104.
16. Fournier ML, Gilmore JM, Martin-Brown SA, Washburn MP. Multidimensional separations-based shotgun proteomics. *Chem Rev*. 2007;107(8):3654-86.
17. Liebler DC, Zimmerman LJ. Targeted quantitation of proteins by mass spectrometry. *Biochemistry*. 2013;52(22):3797-806.
18. Fredolini C, Pathak KV, Paris L, Chapple KM, Tsantilas KA, Rosenow M, et al. Shotgun proteomics coupled to nanoparticle-based biomarker enrichment reveals a novel panel of extracellular matrix proteins as candidate serum protein biomarkers for early-stage breast cancer detection. *Breast Cancer Res*. 2020;22(1):135.
19. Osinalde N, Aloria K, Omaetxebarria MJ, Kratchmarova I. Targeted mass spectrometry: An emerging powerful approach to unblock the bottleneck in phosphoproteomics. *J Chromatogr B Analyt Technol Biomed Life Sci*. 2017;1055-1056:29-38.

20. SCIEX™ A. Powerful Scan Modes of QTRAP® System Technology 2019 [Available from: <https://sciex.com/content/dam/SCIEX/pdf/tech-notes/all/QTRAP-Scan-Modes.pdf>].
21. Neubert H, Shuford CM, Olah TV, Garofolo F, Schultz GA, Jones BR, et al. Protein Biomarker Quantification by Immunoaffinity Liquid Chromatography-Tandem Mass Spectrometry: Current State and Future Vision. *Clin Chem.* 2020;66(2):282-301.
22. Coiras MT, Perez-Brena P, Garcia ML, Casas I. Simultaneous detection of influenza A, B, and C viruses, respiratory syncytial virus, and adenoviruses in clinical samples by multiplex reverse transcription nested-PCR assay. *J Med Virol.* 2003;69(1):132-44.
23. Liu G, Rusling JF. COVID-19 Antibody Tests and Their Limitations. *ACS Sens.* 2021;6(3):593-612.
24. Kanji JN, Zelyas N, MacDonald C, Pabbaraju K, Khan MN, Prasad A, et al. False negative rate of COVID-19 PCR testing: a discordant testing analysis. *Virol J.* 2021;18(1):13.
25. Chen Z, Zhang Z, Zhai X, Li Y, Lin L, Zhao H, et al. Rapid and Sensitive Detection of anti-SARS-CoV-2 IgG, Using Lanthanide-Doped Nanoparticles-Based Lateral Flow Immunoassay. *Anal Chem.* 2020;92(10):7226-31.
26. Faustini SE, Jossi SE, Perez-Toledo M, Shields AM, Allen JD, Watanabe Y, et al. Development of a high-sensitivity ELISA detecting IgG, IgA and IgM antibodies to the SARS-CoV-2 spike glycoprotein in serum and saliva. *Immunology.* 2021;164(1):135-47.
27. Cardozo KHM, Lebkuchen A, Okai GG, Schuch RA, Viana LG, Olive AN, et al. Establishing a mass spectrometry-based system for rapid detection of SARS-CoV-2 in large clinical sample cohorts. *Nat Commun.* 2020;11(1):6201.
28. Cazares LH, Chaerkady R, Samuel Weng SH, Boo CC, Cimbri R, Hsu HE, et al. Development of a Parallel Reaction Monitoring Mass Spectrometry Assay for the Detection of SARS-CoV-2 Spike Glycoprotein and Nucleoprotein. *Anal Chem.* 2020;92(20):13813-21.
29. Ihling C, Tanzler D, Hagemann S, Kehlen A, Huttelmaier S, Arlt C, et al. Mass Spectrometric Identification of SARS-CoV-2 Proteins from Gargle Solution Samples of COVID-19 Patients. *J Proteome Res.* 2020;19(11):4389-92.
30. Gonzalez-Cao M, Iduma P, Karachaliou N, Santarpia M, Blanco J, Rosell R. Human endogenous retroviruses and cancer. *Cancer Biol Med.* 2016;13(4):483-8.
31. Salavatiha Z, Soleimani-Jelodar R, Jalilvand S. The role of endogenous retroviruses-K in human cancer. *Rev Med Virol.* 2020;30(6):1-13.
32. Xue B, Sechi LA, Kelvin DJ. Human Endogenous Retrovirus K (HML-2) in Health and Disease. *Front Microbiol.* 2020;11:1690.
33. Chen J, Foroozesh M, Qin Z. Transactivation of human endogenous retroviruses by tumor viruses and their functions in virus-associated malignancies. *Oncogenesis.* 2019;8(1):6.
34. Dervan E, Bhattacharyya DD, McAuliffe JD, Khan FH, Glynn SA. Ancient Adversary - HERV-K (HML-2) in Cancer. *Front Oncol.* 2021;11:658489.
35. Wang-Johanning F, Frost AR, Johanning GL, Khazaeli MB, LoBuglio AF, Shaw DR, et al. Expression of human endogenous retrovirus k envelope transcripts in human breast cancer. *Clin Cancer Res.* 2001;7(6):1553-60.
36. Weldemariam MM, Han CL, Shekari F, Kitata RB, Chuang CY, Hsu WT, et al. Subcellular Proteome Landscape of Human Embryonic Stem Cells Revealed Missing Membrane Proteins. *J Proteome Res.* 2018;17(12):4138-51.
37. Haag AM. *Modern Proteomics – Sample Preparation, Analysis and Practical Applications; Mass Analyzers and Mass Spectrometers*: Springer, Cham; 2016.
38. Crowther JR. *Systems in ELISA. The Elisa Guidebook*: Humana Press; 2001.

39. Desiere F, Deutsch EW, King NL, Nesvizhskii AI, Mallick P, Eng J, et al. The PeptideAtlas project. *Nucleic Acids Res.* 2006;34(Database issue):D655-8.
40. Ackermann BL. Understanding the role of immunoaffinity-based mass spectrometry methods for clinical applications. *Clin Chem.* 2012;58(12):1620-2
41. Guven E, Duus K, Lydolph MC, Jorgensen CS, Laursen I, Houen G. Non-specific binding in solid phase immunoassays for autoantibodies correlates with inflammation markers. *J Immunol Methods.* 2014;403(1-2):26-36.
42. Leenaars M, Hendriksen CF. Critical steps in the production of polyclonal and monoclonal antibodies: evaluation and recommendations. *ILAR J.* 2005;46(3):269-79.
43. Thiha A, Ibrahim F. A Colorimetric Enzyme-Linked Immunosorbent Assay (ELISA) Detection Platform for a Point-of-Care Dengue Detection System on a Lab-on-Compact-Disc. *Sensors (Basel).* 2015;15(5):11431-41

2 Development of Immuno-Affinity Mass Spectrometry Assay for the Serological Testing of Immunity against SARS-CoV-2*

2.1 COVID-19 Pandemic

On March 11, 2020, the World Health Organization (WHO) declared the COVID-19 pandemic caused by the severe acute respiratory syndrome coronavirus 2 (SARS-CoV-2) (2, 3). SARS-CoV, Middle East respiratory syndrome coronavirus (MERS-CoV), and SARS-CoV-2 have emerged as the three coronaviruses in the 21st century that have spread inter-species, now affecting humans (2). MERS-CoV appeared in the Arabian Peninsula in 2012 and resulted in 2494 infections, of which 858 resulted in deaths, with a fatality rate of 34% (2, 3). In 2002, SARS-CoV appeared in Guangdong, China, infecting 8098, of which 774 individuals died, resulting in a fatality rate of 9.7% (2, 3). SARS-CoV-2 was first detected in Hubei, China, in December 2019 (2, 3). As of Jan 17, 2022 there has been over 300 million cases of infections, of whom approximately 5 million have resulted in mortality (4). If nothing else, the 2019 pandemic should be a reminder that future endemics, epidemics, and pandemics are not intangible, emphasizing the need for the development of timely and robust methods for the detection and further investigation of the emerging infectious diseases.

SARS-CoV-2 is categorized under the Betacoronavirus genus's Coronaviridae family (5). Similar to other corona-like viruses, the SARS-CoV-2 virus can result in acute respiratory distress syndrome (ARDS) which is typically characterized by hypoxaemia and pulmonary oedema (6). SARS-CoV-2 is an enveloped positive sense single-stranded RNA virus composed of four main

* Table 2.7 and Figure 2.6 are included in a manuscript titled “Rational Design and Development of SARS-CoV-2 Serological Diagnostics by Immunoprecipitation-Targeted Proteomics” by Zhiqiang Fu, Yasmine Rais, Delaram Dara and Andrei P. Drabovich.

structural proteins: envelope (E), spike (S), membrane (M), and nucleocapsid (N) (**Figure 2.1**) (5). Following entrance into the body via respiratory droplets, the virus's spike glycoprotein binding to angiotensin-converting enzyme 2 (ACE2) receptors enables viral entry into host cell by membrane fusion and endocytosis (2, 5, 7). The spike protein is a homotrimer containing S1 and S2 subunit in each monomer (2, 7). One key structure enabling this viral-host membrane fusion is the receptor binding domain (RBD) located in the S1 subunit (2, 7). The RBD is composed of a receptor binding motif (RBM) that contains the residues needed for SARS-CoV-2 interaction with ACE-2 receptor (8).

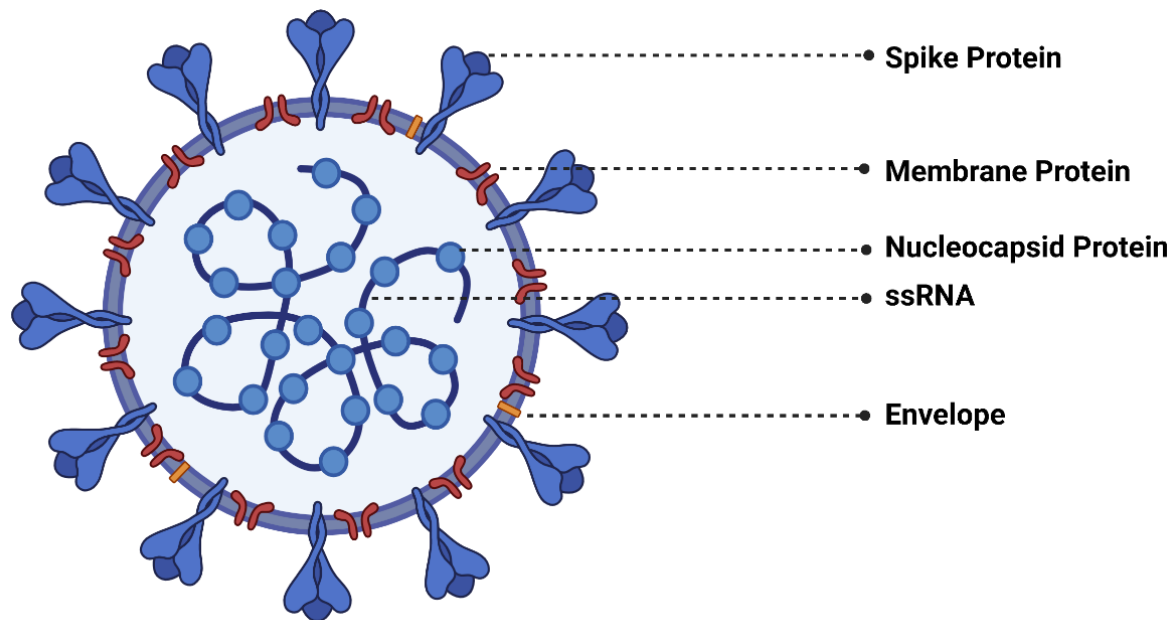


Figure 2.1. SARS-CoV-2 structural proteins. Four structural proteins include: spike glycoprotein (SPIKE_SARS2), nucleoprotein (NCAP_SARS2), membrane protein (VME1_SARS2), and envelope small membrane protein (VEMP_SARS2). Host cell entry is initiated by the binding of the receptor binding domain of the spike glycoprotein of SARS-CoV-2 to the angiotensin-converting enzyme 2 (ACE2) receptor located on the surface of human cells. ssRNA denotes the genetic makeup of SARS-CoV-2 which is composed of a positive-stranded RNA (2, 5, 7). Created with [BioRender.com](https://www.biorender.com)

2.2 Immune Response Following SARS-CoV-2 Infection

Following a viral infection, the innate and adaptive immune systems play a role in clearing out the pathogen and defending the body (9, 11). The innate immune system is known as the "general" response which is composed of the skin barrier, mucosal surfaces, and proteins (e.g., enzymes) that hinder the ability of foreign pathogen from infiltrating the body (9, 11). Phagocytes are one type of white blood cells (WBC) that surround and digest the foreign pathogen (9, 11). Phagocytes also expose certain components of the digested pathogen on their surface to signal the adaptive immune system (9, 11). If the innate immune system is not able to fully clear out the pathogen, the adaptive or "specialized" immune system is called into action (9). The two main players of the adaptive system include T and B lymphocytes (9, 11). T-lymphocytes also known as T-cells are originally made in the bone marrow and they mature in the thymus (10). T-helper cells are a type of T-cells that notify and activate other WBCs to fight off the pathogen (9, 11). Cytotoxic T-cells are another group which directly detects and destroys virally infected and tumour cells (9, 11). B-lymphocytes also known as B-cells are made and mature in the bone marrow (9, 11). T-helper cells play the key role in activating B-cells. Activated B-cells replicate and mature into plasma cells which are antibody producing cells (9, 11).

2.3 B-cell Activation and Antibody Production

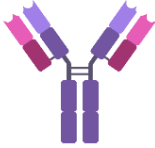
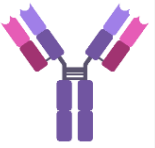
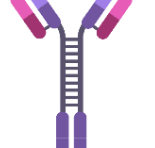
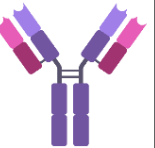
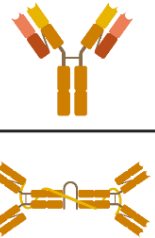
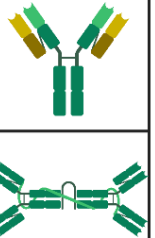
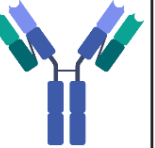
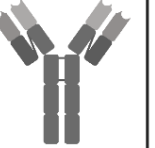
On the surface of B-cells, there are antigen receptors that bind to antigens of pathogens (11). Following this they degrade and present pieces of this antigen on their surface on what are called major histocompatibility complex (MHC) class II (11). The MHC class II presenting this antigen is then detected by helper T-cells (11). The interaction between the helper T-cell and the

corresponding B-cell is mediated through the binding of CD40 ligand (on T-helper cell) and the CD40 (on B-cell) and is known as linked recognition (11). This in turn stimulates the helper T-cell to produce proteins and cytokines such as interleukin-4 (IL-4) that activate the B-cell to multiply and mature into plasma cells (antibody producing cells) (11).

2.4 Antibody Class Switching

Antibodies are composed of 5 classes: IgM, IgG, IgA, IgD, and IgE (11). These classes are further divided into subclasses which include IgG1, IgG2, IgG3, IgG4, IgA1, and IgA2 (11). These antibody classes and subclasses have various functionalities to fight against foreign bodies (**Table 2.1**). The process by which B-cells differentiate into the different classes and subclasses of antibodies is known as isotype switching (11). Isotype switching occurs via recombination events on the DNA that are induced by different cytokines (11). These naïve B-cells are transported from the bone marrow throughout the blood to the lymph node and encounter pathogens and activated T-helper cells (11). Based on the specific cytokines exposed to the B-cell, the heavy chain of the constant C gene region undergoes unique recombination events, giving rise to different antibody classes and subclasses (11).

Table 2.1. Structure and function of subclasses and isotypes of the human immunoglobulins (11).

	IgG1	IgG2	IgG3	IgG4	IgA1	IgA2	IgD	IgE	IgM
Structure									
Function	<ul style="list-style-type: none"> - produced in response to proteins - fights against viral pathogens - relative abundance: 60% of all IgGs 	<ul style="list-style-type: none"> - produced in response to bacterial capsular polysaccharides - fights against encapsulated pathogens - relative abundance: 32% of all IgGs 	<ul style="list-style-type: none"> - produced in response to proteins - activates complement system, phagocytosis, and antibody mediated cellular cytotoxicity - relative abundance: 4% of all IgGs 	<ul style="list-style-type: none"> - produced in response to proteins and allergens - anti-inflammatory functionality - relative abundance: 4% of all IgGs 	<ul style="list-style-type: none"> - produced in response to proteins - maintaining homeostatis of the immune system - relative abundance: 85% of all IgAs 	<ul style="list-style-type: none"> - produced in response to polysaccharides - activates inflammatory response - relative abundance: 15% of all IgAs 	<ul style="list-style-type: none"> - exact function is unknown - may play a role in activating B cells 	<ul style="list-style-type: none"> - produced in response to parasites and allergens 	<ul style="list-style-type: none"> - plays a role in immune regulation - activation of complement and agglutination - relative abundance: 10% of all serum Ig antibodies
Cytokine Class Switching	<ul style="list-style-type: none"> Activation of: IFN-γ, IL-10 Inhibition of: IL-4 	<ul style="list-style-type: none"> Activation of: IFN-γ, IL-4 Inhibition of: TGF-β 	<ul style="list-style-type: none"> Activation of: IFN-γ, IL-10 Inhibition of: TGF-β, IL-4 	<ul style="list-style-type: none"> Activation of: IL-4 	<ul style="list-style-type: none"> Activation of: IL-5, TGF-β 	<ul style="list-style-type: none"> Activation of: IL-5, TGF-β 	N/A	<ul style="list-style-type: none"> Activation of: IL-4 Inhibition of: IFN-γ 	<ul style="list-style-type: none"> Inhibition of: IL-4, IFN-γ, TGF-β

IgA antibodies are present in monomer form mainly in serological samples, while they form dimers in secretory saliva samples (12).
 Created with [BioRender.com](https://www.biorender.com)

2.5 The use of immuno-affinity mass spectrometry assays for detection and quantification of immunity against SARS-CoV-2

As mentioned previously, immuno-affinity mass spectrometry assays can be applied for the identification and quantification of antibodies generated against SARS-CoV-2. The capture and enrichment of endogenous antibodies in various samples (e.g., serum, plasma, saliva) via specific SARS-CoV-2 antigens followed by the highly specific detection of these antibodies using mass spectrometry and the multiplexing capacity of such assays to detect various antibody isotypes and subclasses are major benefits of applying IA-MS for the diagnosis of current and past SARS-CoV-2 infections.

The setup of IA-MS assay is shown in **Figure 2.2**. High-binding 96-well microplates are coated with the recombinant SARS-CoV-2 receptor binding domain antigen. Following overnight incubation, these plates are washed with designated wash buffer and blocked with the blocking buffer. Subsequently, patient samples (serum, plasma, saliva) are added to these wells and if patients have developed antibodies against SARS-CoV-2, these antibodies are captured and immunoprecipitated. Following this, potentially captured immunoglobulins are then digested using the enzyme trypsin and undergo separation and detection using targeted mass spectrometry.

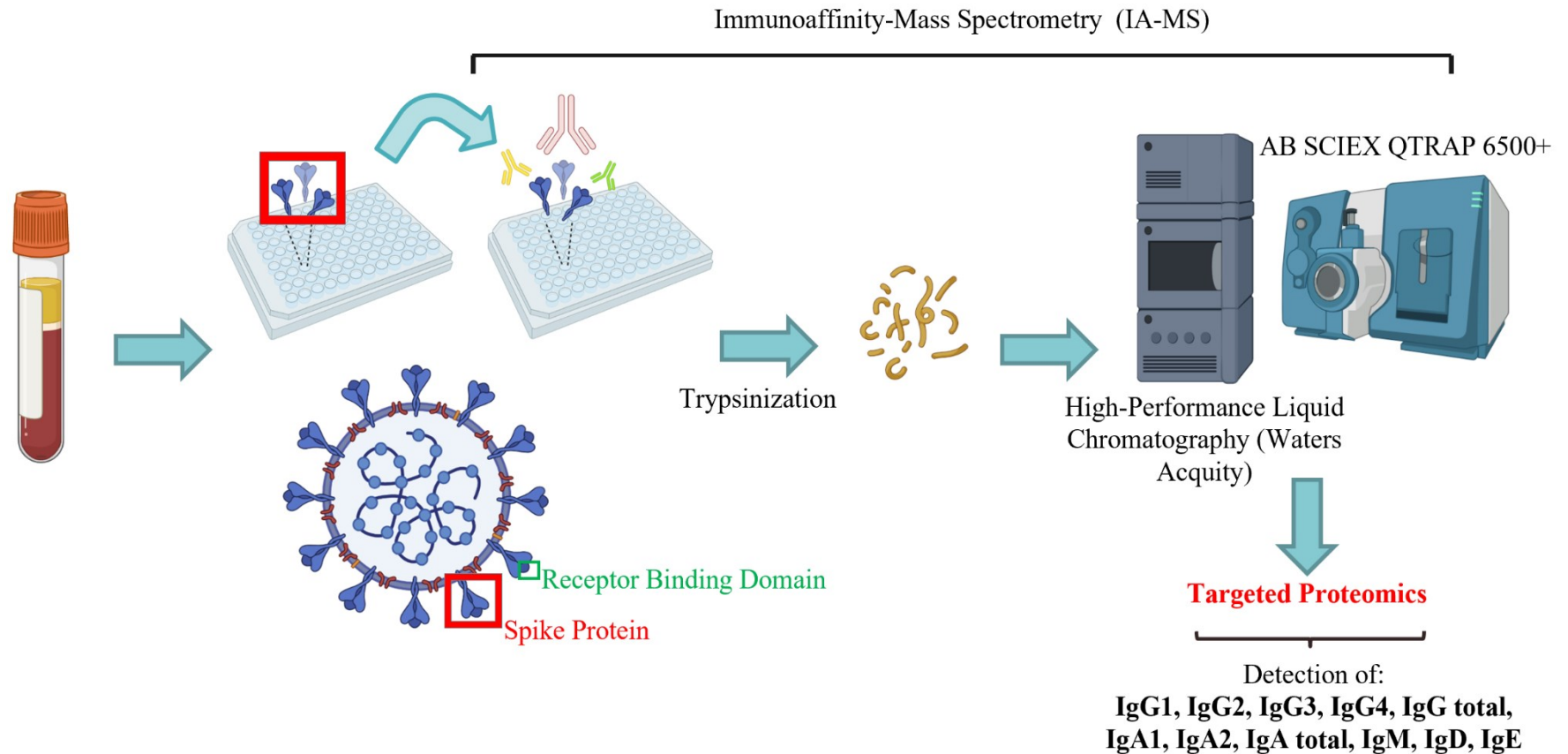


Figure 2.2. Design of IA-MS assay for the serological testing of immune response against SARS-CoV-2. Patient serological samples exposed to immunoaffinity setup: coating with recombinant SPIKE_SARS2 receptor binding domain (RBD) antigen to capture specific antibodies formed against SARS-CoV-2. Captured antibodies are digested using trypsin. Tryptic peptides are separated using Ultra Performance Liquid Chromatography (UPLC) and detected using shotgun mass spectrometry (MS/MS). Tryptic proteotypic peptides are selected and synthesized as stable heavy isotope-labeled internal standards. Top SRM transitions for each tryptic peptide are identified showing the highest signal-to-noise ratios, enabling the detection and quantification of anti-SARS-CoV-2 immunoglobulin IgG, IgM, IgA, IgD, IgE subclasses and IgG1, IgG2, IgG3, IgG4, IgA1, IgA2 isotypes. Created with [BioRender.com](https://www.biorender.com)

2.6 Materials and Methods

Study Population

Two set of experiments were performed. In the initial experiment, a smaller sample size was assessed. SARS-CoV-2 positive EDTA plasma (n=29, collected 14 days to 3 months post RT-PCR confirmed positivity) and SARS-CoV-2 negative plasma samples (n=5, RT-PCR confirmed negative), and negative serum samples (n=7, pre-pandemic). For the larger experiment, SARS-CoV-2 negative EDTA plasma samples (n=87, pre-pandemic, collected 2-3 weeks post RT-PCR confirmed positivity) and negative serum samples (n=56, collected pre-pandemic) alongside positive EDTA plasma samples (n=82, all collected 20-35 days post RT-PCR confirmed positivity) were obtained. All samples were from the Canadian Biosample Repository and the Alberta COVID-19 Bio-repository. The study was approved by the University of Alberta (ethics approvals # Pro00104098_REN1, Pro00100207_REN1).

Chemicals and reagents

Dithiothreitol, iodoacetamide, and trifluoroacetic acid (TFA) were purchased from Thermo Fisher Scientific (Burlington, ON, Canada). Mass spectrometry-grade acetonitrile (ACN) and water were obtained from Fisher Scientific (Fair Lawn, NJ). Formic acid (FA), Dimethyl sulfoxide (DMSO), and dimethylated SOLu-trypsin were obtained from Sigma-Aldrich (Oakville, ON). Synthetic stable isotope-labeled peptides (SpikeTide_TQL) were provided by JPT Peptide Technologies GmbH (Germany). Recombinant SARS-CoV-2 antigens were obtained from Sino Biological (Beijing, China).

Immunoprecipitation Protocol

High-binding 96-well microplates (Greiner Bio-One) were coated with 500 ng/well of recombinant SARS-CoV-2 antigens diluted in phosphate-buffered saline (PBS, pH 7.4) to make a final volume

of 100 μ l/well and kept overnight at room temperature. Following this, wells were washed 3 times with 300 μ l/well of wash buffer (0.05% Tween20 in PBS) using an automated microplate washer. For the larger experiment, the wells were then blocked for 1 hour with green buffer 2 (50mM Tris-HCl, pH 7.6), 6% BSA, 0.01% goat γ -globulin, 0.1% bovine IgG γ -globulin, 0.15% mouse IgG, 0.05% Tween20, and 500mM potassium chloride (KCl). For the smaller experiment, solely 6% BSA was utilized as the blocking reagent. The 3 times washing step was repeated. Subsequently, 22 μ l of human serological samples were diluted in 78 μ l of dilution buffer (green buffer 2 for large experiment and 6% BSA for small experiment), creating a total volume of 100 μ l to be added to each well. Additionally, 33 μ l of human saliva samples were diluted in 67 μ l of dilution buffer, where an overall total of 100 μ l of diluted samples were added to each well. The samples were incubated for 2 hours on a plate shaker at room temperature. Following this, the 3 times washing step was repeated.

Proteomic Sample Preparation

100 fmol of heavy isotope-labeled SpikeTide_TQL were added to each well for the quantification of immunoglobulins. The immunoprecipitated wells were reduced using 10 mM of dithiothreitol at 70°C for 15 min. Following this, 20 mM of iodoacetamide was added for 1 hour at room temperature and kept in the dark. Samples were then digested using 0.25 μ g of SOLu-trypsin (Sigma-Aldrich) per well and incubated at 37°C overnight. The next day, the digestion was stopped using 1% v/v trifluoroacetic acid (TFA).

High Performance Liquid Chromatography and Shotgun Mass Spectrometry Performance and Analysis

A 12-minute gradient was developed on the Waters Acquity ultra-performance liquid chromatography to enable the fast separation of peptides. The gradient started with 95% buffer A

(95% MS gradient water, 0.1% FA, 5% DMSO) and 5% of buffer B (95% ACN, 0.1%FA, 5% DMSO) for 1.4 minutes, to 25% of buffer B and 75% of buffer A for 0.7 minutes, to 37% of buffer B and 63% buffer A for 4.1 minutes, to 44% of buffer B and 56% of buffer A for 0.6 minutes, to 95% of buffer B and 5% of buffer A for 0.5 minutes, and to a final concentration of 95% buffer A and 5% buffer B for 1.4 minutes. For the smaller sized experiment, for sample loading (injection volume: 17 μ l at 300 μ l/min), a Luna C18 (2 \times 30 mm, 3 μ m, 100 Å; #00A-4114-B0; Phenomenex, Torrance, CA) was used as a trap column. Additionally, for peptide separation, a Luna C18(2) column (2 \times 100 mm, 3 μ m, 100 Å, 25°C; #00D-4251-B0; Phenomenex, Torrance, CA). For the larger sized experiment, for sample loading (injection volume: 40 μ l at 50 μ l/min), a Kinetex C18 (30 \times 2.1 mm, 2.6 μ m, 100 Å; #00A-4462-AN; Phenomenex, Torrance, CA) was used as a trap column. Furthermore, a Kinetex C18 column (50 \times 2.1 mm, 1.3 μ m, 100 Å; #00B-4515-AN; Phenomenex, Torrance, CA) was used for peptide separations. Waters Acquity ultra-performance liquid chromatography coupled to a quadrupole ion-trap mass spectrometer (AB SCIEX QTRAP 6500+) was used for running optimized SRM assays. The specifications of the SRM assay include: 500°C source temperature, +4700V electrospray ionization voltage; 25 psi air curtain gas, 15 psi for atomizing gas Gas 1 and auxiliary Gas 2, 80V declustering potential, 10V entrance potential, 11V collision cell exit potential, and collision gas “Medium”. Skyline Targeted Proteomics Environment v20.1.0.76 (MacCoss Lab) software was used for the analysis of SRM experiments. The peak window were adjusted manually to determine the light-to-heavy ratios for the quantification of endogenous peptides.

Immunoglobulin Measurements and Quantification

Endogenous levels of Igs were measured by adding known amounts of the isotope-labeled internal standards. By doing so, the light-to-heavy (L/H) ratios which showcase the area under the peak of

endogenous peptides in relation to the area under the peak of internal standards were used. Additionally, the molar mass of each antibody isotype and subclass (IgG total: 150000 g/mol, IgG1, IgG2, IgG4: 146000 g/mol, IgG3: 170000 g/mol, IgA total, IgA2, IgA2: 162000 g/mol, IgM: 950000) was used for calculating the endogenous concentrations in the clinical samples. IgGs were counted as being monomers in both plasma and saliva samples. IgAs were counted as being monomers in plasma samples while dimers in saliva samples. IgMs were counted as being pentamers in both plasma and saliva samples. GraphPad Prism 9 software was used for the performing statistical tests and generating figures for the larger cohort size experiment. A one-tail Mann-Whitney test was used as it was predicted that following SARS-CoV-2 infection, there would be antibody production and an increase in antibody levels against this virus in those infected.

Selection of Proteotypic Tryptic Peptides and their Optimization for Detection using SRM Assay

The use of IA-MS assays was applied for the detection of all human Ig classes and subclasses (IgG1, IgG2, IgG3, IgG4, IgG total, IgA1, IgA2, IgA total, IgM, IgD, and IgE). In order to develop these assays, specific tryptic peptides shown in **Table 2.2** were found via online proteomics database searches. Peptide Atlas, GnomAB database v2.1.1, and previous literature were used to find proteotypic peptides that exist in the constant region of human immunoglobulins and show low frequency of polymorphic missense variants (1, 35, 36). Additionally, absence of glycosylation sites and post-translational modifications was ruled out using the NextProt database (37).

Table 2.2. Selected proteotypic peptides[†].

Immunoglobulin	Anti-SARS-CoV-2 Tryptic Peptides
GPSVFPLAPSSK	IGHG1
GLPAPIEK	IGHG2
EEQFNSTFR	IGHG2
TPLGDTHTCPR	IGHG3
GLPSSIEK	IGHG4
NQVSLTCLVK	IGHG 1-4 (total)
DASGVTFTWTPSSGK	IGHA1
TPLTATLSK	IGHA1
TFTCTAAYPESK	IGHA1
DASGATFTWTPSSGK	IGHA2
TPLTANITK	IGHA2
WLQGSQELPR	IGHA 1-2 (total)
DGFFGNPR	IGHM
GFPSVLR	IGHM
FTCTVTHDLPSPLK	IGHM
APDVFPIISGCR	IGHD
AVHEAASPSQTVQR	IGHE

The peptides belonging to the constant heavy chain of human immunoglobulins and unique for each antibody class and subclass (IgG1, IgG2, IgG3, IgG4, IgG total, IgA1, IgA2, IgA total, IgM, IgD, and IgE). Selected peptides show low frequency polymorphic missense variance alongside absence of glycosylation and post-translational modifications. For IgGs, there are 2 copies of each proteotypic peptide per one antibody molecule. For IgAs, there are 2 copies of each proteotypic peptide per one antibody molecule. For IgMs, there are 10 copies of each proteotypic peptide per one antibody molecule

These proteotypic internal standard peptides were optimized by initially running them on the tandem (MS/MS) modality of the mass spectrometer followed by then creating MRM methodologies containing the top selected product ion transitions (**Figure 2.3**). As previously explained, by using the MS/MS modality, our precursor ion is broken down into all its product ions. Following this, the top product ion transitions which have the highest abundance are chosen in order for the SRM assay to detect the specific peptides with the most optimal level of sensitivity.

[†] Specific tryptic peptides were selected by Dr Andrei Drabovich.

The overall summary for the optimization of various parameters including precursor charges, top transitions, collision energies, and retention times is shown on **Table 2.3**.

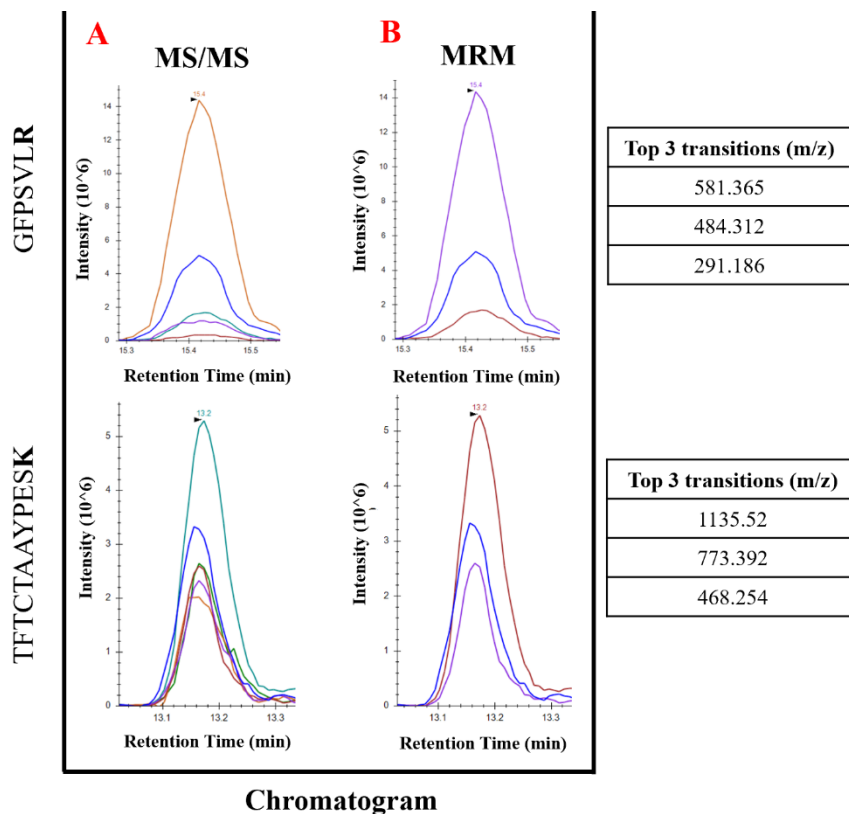


Figure 2.3. The detection of top product ion transitions for the identification of tryptic peptides with high level of sensitivity. (A) The depiction of MS/MS spectra containing top 6 product ion transitions for two proteotypic tryptic peptides (GFPSVLR, TFTCTAAYPESK) used in SRM assay. **(B)** The depiction of MRM spectra containing the finalized top 3 product ion transitions for two proteotypic tryptic peptides (GFPSVLR, TFTCTAAYPESK) used in SRM assay.

Table 2.3. Proteotypic tryptic peptides, unique for each antibody isotypes and subclasses with their optimized parameters.
Optimized parameters enable accurate detection of peptides using SRM assays.

Anti-SARS-CoV-2 tryptic peptides	Precursor Q1 (m/z)	Precursor Charge	Product Q3 (m/z)	Fragment Charge	Fragment Ion type	Collision Energy (V)	Declustering Potential (V)	Retention Time (min)
GPSVFPLAPSSK	593.827	++	846.472	+	y8	28.1	80	9.0
GPSVFPLAPSSK			699.404	+	y7	28.1	80	9.0
GPSVFPLAPSSK			418.23	+	y4	28.1	80	9.0
GPSVFPLAPSSK (Heavy)	597.834	++	854.486	+	y8	28.1	80	9.0
GPSVFPLAPSSK (Heavy)			707.418	+	y7	28.1	80	9.0
GPSVFPLAPSSK (Heavy)			426.244	+	y4	28.1	80	9.0
GLPAPIEK	412.748	++	486.292	+	y4	19.2	80	8.6
GLPAPIEK			654.382	+	y6	19.2	80	8.6
GLPAPIEK			327.695	++	y6	19.2	80	8.6
GLPAPIEK (Heavy)	416.755	++	494.306	+	y4	19.2	80	8.6
GLPAPIEK (Heavy)			662.396	+	y6	19.2	80	8.6
GLPAPIEK (Heavy)			331.702	++	y6	19.2	80	8.6
WYVDGVEVHNAK	472.902	+++	615.809	++	y11	22.7	80	8.6
WYVDGVEVHNAK			534.278	++	y10	22.7	80	8.6
WYVDGVEVHNAK			484.743	++	y9	22.7	80	8.6
WYVDGVEVHNAK (Heavy)	475.573	+++	619.816	++	y11	22.7	80	8.6
WYVDGVEVHNAK (Heavy)			538.285	++	y10	22.7	80	8.6
WYVDGVEVHNAK (Heavy)			488.751	++	y9	22.7	80	8.6

Anti-SARS-CoV-2 tryptic peptides	Precursor Q1 (m/z)	Precursor Charge	Product Q3 (m/z)	Fragment Charge	Fragment Ion type	Collision Energy (V)	Declustering Potential (V)	Retention Time (min)
TPLGDTTHTCPR	452.551	+++	579.272	++	y10	23.7	80	8.4
TPLGDTTHTCPR			522.73	++	y9	23.7	80	8.4
TPLGDTTHTCPR			418.868	+++	y11	23.7	80	8.4
TPLGDTTHTCPR (Heavy)	455.887	+++	584.276	++	y10	23.7	80	8.4
TPLGDTTHTCPR (Heavy)			527.734	++	y9	23.7	80	8.4
TPLGDTTHTCPR (Heavy)			422.204	+++	y11	23.7	80	8.4
GLPSSIEK	415.735	++	660.356	+	y6	19.4	80	8.6
GLPSSIEK			563.304	+	y5	19.4	80	8.6
GLPSSIEK			330.682	++	y6	19.4	80	8.6
GLPSSIEK (Heavy)	419.742	++	668.371	+	y6	19.4	80	8.6
GLPSSIEK (Heavy)			571.318	+	y5	19.4	80	8.6
GLPSSIEK (Heavy)			334.689	++	y6	19.4	80	8.6
NQVSLTCLVK	581.318	++	243.109	+	b2	27.5	80	8.9
NQVSLTCLVK			820.46	+	y7	27.5	80	8.9
NQVSLTCLVK			919.528	+	y8	27.5	80	8.9
NQVSLTCLVK (Heavy)	585.326	++	243.109	+	b2	27.5	80	8.9
NQVSLTCLVK (Heavy)			828.474	+	y7	27.5	80	8.9
NQVSLTCLVK (Heavy)			927.542	+	y8	27.5	80	8.9
TPLTATLSK	466.277	++	733.445	+	y7	21.8	80	8.6
TPLTATLSK			620.361	+	y6	21.8	80	8.6
TPLTATLSK			415.753	++	y8	21.8	80	8.6
TPLTATLSK (Heavy)	470.284	++	741.46	+	y7	21.8	80	8.6
TPLTATLSK (Heavy)			628.376	+	y6	21.8	80	8.6
TPLTATLSK (Heavy)			419.76	++	y8	21.8	80	8.6

Anti-SARS-CoV-2 tryptic peptides	Precursor Q1 (m/z)	Precursor Charge	Product Q3 (m/z)	Fragment Charge	Fragment Ion type	Collision Energy (V)	Declustering Potential (V)	Retention Time (min)
TFTCTAAYPESK	688.314	++	1127.5	+	y10	33.7	80	8.5
TFTCTAAYPESK			765.378	+	y7	33.7	80	8.5
TFTCTAAYPESK			460.24	+	y4	33.7	80	8.5
TFTCTAAYPESK (Heavy)	692.321	++	1135.52	+	y10	33.7	80	8.5
TFTCTAAYPESK (Heavy)			773.392	+	y7	33.7	80	8.5
TFTCTAAYPESK (Heavy)			468.254	+	y4	33.7	80	8.5
DASGATFTWTPSSGK	756.852	++	863.426	+	y8	36.1	80	8.8
DASGATFTWTPSSGK			762.378	+	y7	36.1	80	8.8
DASGATFTWTPSSGK			475.251	+	y5	36.1	80	8.8
DASGATFTWTPSSGK (Heavy)	760.859	++	871.44	+	y8	36.1	80	8.8
DASGATFTWTPSSGK (Heavy)			770.392	+	y7	36.1	80	8.8
DASGATFTWTPSSGK (Heavy)			483.265	+	y5	36.1	80	8.8
WLQGSQELPR	607.320	++	786.41	+	y7	28.8	80	8.6
WLQGSQELPR			914.469	+	y8	28.8	80	8.6
WLQGSQELPR			385.256	+	y3	28.8	80	8.6
WLQGSQELPR (Heavy)	612.324	++	796.419	+	y7	28.8	80	8.6
WLQGSQELPR (Heavy)			924.477	+	y8	28.8	80	8.6
WLQGSQELPR (Heavy)			395.264	+	y3	28.8	80	8.6
DGFFGNPR	455.214	++	443.236	+	y4	21.3	80	8.9

Anti-SARS-CoV-2 tryptic peptides	Precursor Q1 (m/z)	Precursor Charge	Product Q3 (m/z)	Fragment Charge	Fragment Ion type	Collision Energy (V)	Declustering Potential (V)	Retention Time (min)
DGFFGNPR			590.305	+	y5	21.3	80	8.9
DGFFGNPR			320.124	+	b3	21.3	80	8.9
DGFFGNPR (Heavy)	460.218	++	453.244	+	y4	21.3	80	8.9
DGFFGNPR (Heavy)			600.313	+	y5	21.3	80	8.9
DGFFGNPR (Heavy)			320.124	+	b3	21.3	80	8.9
GFPSVLR	388.227	++	571.356	+	y5	18	80	8.9
GFPSVLR			474.304	+	y4	18	80	8.9
GFPSVLR			286.182	++	y5	18	80	8.9
GFPSVLR (Heavy)	393.231	++	581.365	+	y5	18	80	8.9
GFPSVLR (Heavy)			484.312	+	y4	18	80	8.9
GFPSVLR (Heavy)			291.186	++	y5	18	80	8.9
APDVFPIISGCR	666.343	++	802.424	+	y7	31.7	80	9.6
APDVFPIISGCR (Heavy)	671.347	++	812.432	+	y7	31.7	80	9.6
AVHEAASPSQTVQR	494.255	+++	487.257	++	y9	21.7	80	8.9
AVHEAASPSQTVQR (Heavy)	497.591	+++	492.261	++	y9	21.7	80	8.9

2.7 High Performance Liquid Chromatography Gradient Optimization

Another parameter in the IA-MS assay that was optimized was the HPLC gradient (**Table 2.4, Figure 2.4**). The goal of this optimization is to find the shortest (timewise) gradient that enables the differentiation and detection of tryptic peptides including hydrophobic and hydrophilic, with a high-level sensitivity. The most optimal gradient was found to start with 95% buffer A (95% MS gradient water, 0.1% FA, 5% DMSO) and 5% of buffer B (95% ACN, 0.1%FA, 5% DMSO) for 1.4 minutes, to 25% of buffer B and 75% of buffer A for 0.7 minutes, to 37% of buffer B and 63% buffer A for 4.1 minutes, to 44% of buffer B and 56% of buffer A for 0.6 minutes, to 95% of buffer B and 5% of buffer A for 0.5 minutes, and to a final concentration of 95% buffer A and 5% buffer B for 1.4 minutes, for a total of a 12-minute gradient as shown in **Figure 2.5**.

Table 2.4. Optimization of HPLC gradients by altering percentage of Buffer B.

Buffer B (%)	Area Under Curve/Peak										
	IgG1	IgG2	IgG3	IgG4	Total IgG	IgA1	IgA2	Total IgA	IgD	IgE	IgM
7-20-40	1.0E+06	6.7E+05	2.4E+06	1.2E+06	7.1E+05	1.1E+06	5.7E+03	2.1E+05	4.6E+04	3.4E+04	6.4E+05
7-20-43	9.7E+05	5.9E+05	2.2E+06	1.1E+06	6.1E+05	1.0E+06	3.9E+04	2.6E+05	4.6E+04	3.3E+04	4.6E+05
7-20-37	1.1E+06	7.0E+05	2.1E+06	1.1E+06	6.8E+05	1.1E+06	4.8E+04	2.1E+05	4.7E+04	N/A	5.8E+05
7-20-38	1.2E+06	7.2E+05	2.3E+06	1.0E+06	7.7E+05	1.2E+06	5.8E+04	1.9E+05	4.6E+04	2.8E+04	6.0E+05
7-20-39	1.2E+06	7.1E+05	2.3E+06	1.2E+06	7.6E+05	1.2E+06	5.1E+04	2.1E+05	3.1E+04	2.0E+04	6.9E+05
7-20-40	2.9E+06	7.8E+05	3.3E+06	1.2E+06	1.8E+06	1.3E+06	1.0E+05	3.8E+05	2.2E+04	3.0E+04	1.2E+06
5-25-37-44	9.0E+06	8.5E+05	3.9E+06	1.2E+06	5.4E+06	2.2E+06	5.4E+05	1.2E+06	2.1E+05	1.6E+05	2.2E+06

N/A (not applicable) denotes the absence of peaks and thus no numerical quantification of areas for corresponding antibodies.

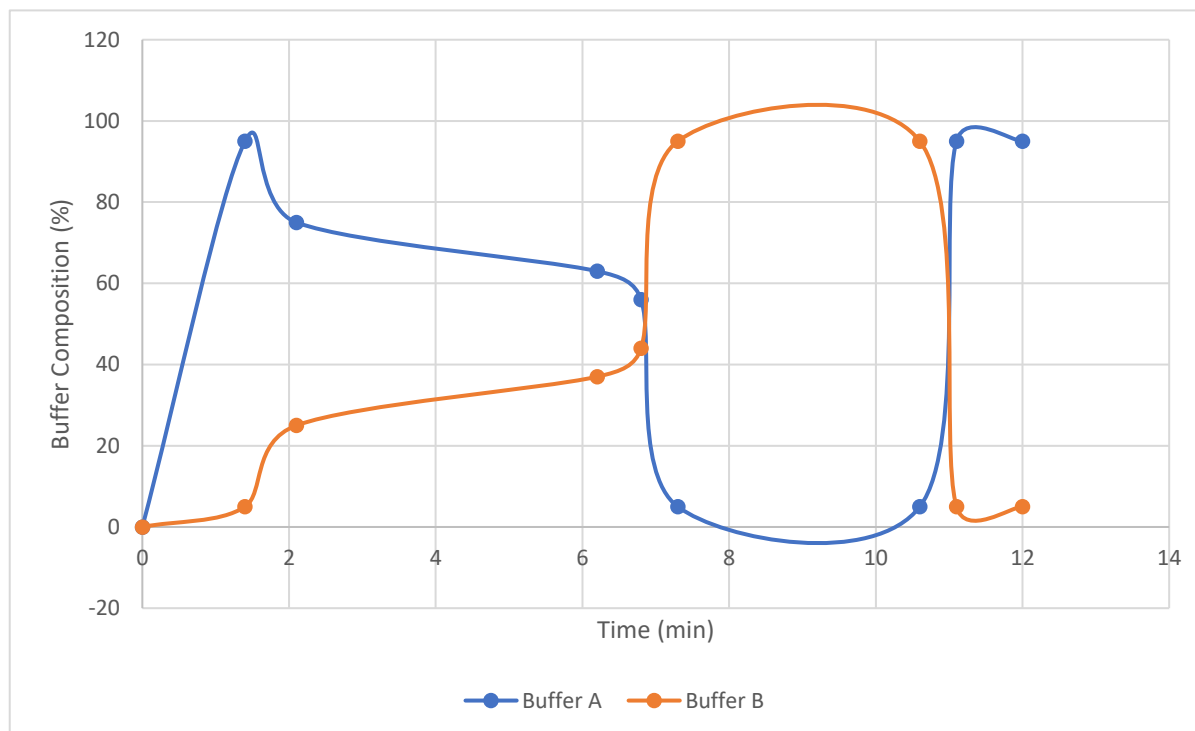


Figure 2.5. HPLC gradient composition. 12-minute gradient run composed of varying percentages of buffer A (95% MS gradient water, 0.1% FA, 5% DMSO) and buffer B (95% ACN, 0.1%FA, 5% DMSO) for optimal detection of peptides.

2.8 Optimization of Immunoassay's Blocking Buffer

Another parameter in the immunoassay that was optimized included the blocking buffer. A wide array of blocking buffers were utilized which included 3% bovine serum albumin (BSA), 3% dried milk (DM), 3% DM combined with 3% BSA, Thermo Scientific SuperBlock T20, 3% fish gelatin, 3% fish gelatin combined with 3% DM and 3% BSA, yellow buffer (50mM Tris-HCl: pH 7.6, 6% BSA, 0.01% goat γ -globulin, 0.1% bovine IgG γ -globulin, 0.15% mouse IgG, and 0.05% Tween20), green buffer 1 (50mM Tris-HCl: pH 7.6, 6% BSA, 0.01% goat γ -globulin, 0.1% bovine IgG γ -globulin, 0.15% mouse IgG, 0.05% Tween20, and 100mM potassium chloride (KCl)), and green buffer 2 (50mM Tris-HCl: pH 7.6, 6% BSA, 0.01% goat γ -globulin, 0.1% bovine IgG γ -globulin, 0.15% mouse IgG, Tween20, and 500mM potassium chloride (KCl)). It was found that there was a high level of non-specific binding when 3%BSA, 3% DM, 3% BSA combined with 3% DM, SuperBlock T20, 3% fish gelatin, and 3% fish gelatin combined with 3% DM and 3% BSA was used. This is evident as the difference between RBD coated wells in comparison to the PBS coated wells when it came to the IgA antibody classes showed minimal variation, signifying the occurrence of non-specific binding (**Table 2.5**). Notably, the green buffer 2 which is composed of cocktail of various compounds showed to have the highest amount of variation between RBD coated wells versus PBS coated wells, signifying the highest level of blocking using this buffer as opposed to the other blocking buffers.

Table 2.5. Assessment of various blocking reagents of sample preparation for immunoprecipitation.

	3% BSA	3% BSA and 3% DM	SuperBlock T20	3% Fish Gelatin	3% Fish Gelatin, 3% DM, 3% BSA
IgG1	5.59	5.04	3.52	5.27	4.25
IgG Total	15.44	28	3.5	14.36	4.07
IgA1	2.65	0.84	0.76	1.55	1.51
IgA Total	2.23	1.07	0.59	0.72	0.73

	3% DM	Yellow Buffer	Green Buffer 1	Green Buffer 2
IgG1	20.92	15.63	19.43	20.92
IgG Total	7.38	6.71	9.25	11.1
IgA1	0.48	1.56	2.24	3.28
IgA Total	0.81	3.41	3.79	5.72

Numbers showcase the fold difference in L/H ratios of four antibodies (IgG1, IgG total, IgA1, IgA total) immunoprecipitated in wells coated with the RBD antigen versus PBS (no antigen) controls.

2.9 Optimization of Immunoassay's Washing Buffer

The last parameter that was optimized included the washing buffer. Various washing buffer solutions were assessed, and these included 0.1% Tween 20 combined with 0.1% Triton, 0.5% Tween 20, and 0.05% Tween 20. As shown in **Table 2.6.**, when harsher washing buffers (0.1% Tween 20 combined with 0.1% Triton, 0.5% Tween 20) were used, there was a loss of specific binding. Ultimately, the most optimal washing buffer was determined to be 0.05% Tween 20 which showed to not result in high degree of loss of the specific binding of antibodies.

Table 2.6. Assessment of various washing buffers of sample preparation for immunoprecipitation.

	0.05% Tween 20	0.1% Tween20 + 0.1% Triton	0.5% Tween20
IgG1	20.92	28.67	18.88
IgG Total	7.375	8.13	5.17
IgA1	0.48	0.56	0.73
IgA Total	0.81	1.12	1.11

Numbers showcase the fold difference in L/H ratios of four antibodies (IgG1, IgG total, IgA1, IgA total) immunoprecipitated in wells coated with the RBD antigen versus PBS (no antigen) controls.

2.10 Results

2.10.1 Quantification of anti-SARS-CoV-2 antibodies

Using the developed assays, IgG1, IgG2, IgG3, IgG4, IgG total, IgA1, IgA2, IgA total were detected in patient serological samples (n=29 RT-PCR positive plasma, n=12 RT-PCR negative plasma and pre-pandemic serum). The data were analyzed using Skyline software. The IA-HPLC-SRM assay was developed using injection of digested samples onto a trap column at a flow rate of 300 $\mu\text{l}/\text{min}$. Following this, an analytical column was used for peptide separation at a flow rate of 100 $\mu\text{l}/\text{min}$. A QTRAP 6500+ was used for peptide detection. The median concentrations of the various antibody classes and subclasses in positive plasma and negative serological samples are shown in **Table 2.7**. Notably, IgG1 median values showed a 22 times difference between positive versus negative samples. Additionally, there was a statistically significant difference between positive and negative COVID-19 samples in IgG1 ($P=3.3\times 10^{-7}$), IgG3 ($P=3.9\times 10^{-7}$), total IgG ($P=5.2\times 10^{-7}$), IgM ($P=1.4\times 10^{-6}$), IgA1 ($P=2.0\times 10^{-3}$), and total IgA ($P=1.8\times 10^{-3}$) (**Figure 2.5**). Markedly, the IgG1 subclass was found to be the most representative antibody group in patient serological samples in which median concentration levels in positive patients was 2,138 ng/mL versus negative patients (95 ng/mL). Additionally, the cut-off concentration of 385 ng/mL in IgG1 resulted in 100% sensitivity at 100% specificity in distinguishing positive versus negative COVID-19 serological samples. Notably, endogenous IgE and IgD were not detected using our developed assay.

Table 2.7. Concentrations of the various isotypes and subclasses of anti-SARS-CoV-2 antibodies.§

Antibody Subclass	Median Serological Antibody Concentration		Mann–Whitney U test*		Diagnostic Cut-off (ng/mL)	Diagnostic Specificity at 100% Sensitivity, % [95%CI]
	Positive (ng/mL)	Negative (ng/mL)	<i>P</i> -value	AUC [95% CI] *		
IgG1	2,138	95	3.3×10^{-7}	1.00 [1.00-1.00]	385	100 [74-100]
IgG3	92	13	3.9×10^{-7}	0.997[0.99-1.00]	25	92 [62-100]
IgG	2,017	218	5.2×10^{-7}	0.99 [0.97-1.01]	457	92 [62-100]
IgM	1,100	156	1.4×10^{-6}	0.97 [0.93-1.01]	166	58 [28-85]
IgA1	269	76	2.0×10^{-3}	0.79 [0.64-0.94]	44	42 [15-72]
IgA	293	90	1.8×10^{-3}	0.79 [0.65-0.94]	50	33 [10-65]
IgA2	26	22	0.24	0.57 [0.38-0.76]	-	-
IgG2	46	52	0.51	0.50 [0.30-0.70]	-	-
IgG4	4.9	6.3	0.87	0.60 [0.41-0.79]	-	-

Positive samples were RT-PCR confirmed EDTA plasma (n=29).

Negative samples were RT-PCR confirmed EDTA plasma (n=5), and pre-pandemic serum (n=7).

*Nonparametric Mann–Whitney U test, AUC (area under the curve), CI (confidence interval).

§ Statistical analysis of the data generated for Table 2.7 was performed by Dr Andrei Drabovich.

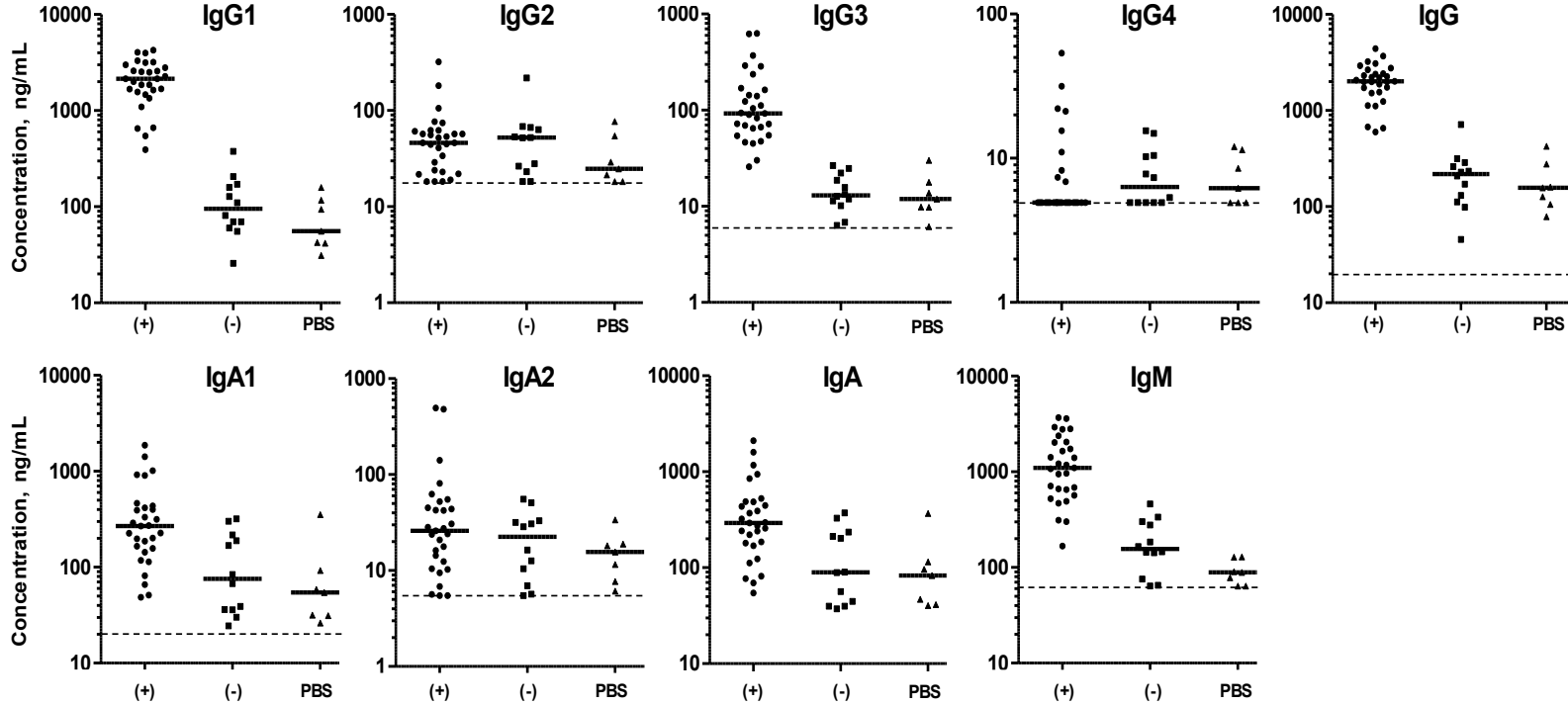


Figure 2.6. Quantification of RBD-specific antibody isotypes and subclasses using IA-HPLC-SRM assay in smaller sample size study.^{††}

PBS (phosphate buffered saline) coated wells represent the negative control to assess the level of non-specific binding in the assay.

(+) denotes n=29 RT-PCR COVID-19 positive EDTA plasma.

(-) denotes n=5 RT-PCR COVID-19 negative EDTA plasma and n=7 pre-pandemic serum.

Statistical significance ($P < 0.05$) using nonparametric Mann–Whitney U test. IgG1 ($P = 3.3 \times 10^{-7}$), IgG3 ($P = 3.9 \times 10^{-7}$), IgG total ($P = 5.2 \times 10^{-7}$), IgM ($P = 1.4 \times 10^{-6}$), IgA1 ($P = 2.0 \times 10^{-3}$), and IgA total ($P = 1.8 \times 10^{-3}$).

Dash (---) lines represent limits of detection (LOD) in which values below the limit were counted to be the LOD.

RBD-specific IgE and IgD immunoglobulins were not detected using this assay.

^{††} Statistical analysis and figure generated for Figure 2.6 was performed by Dr Andrei Drabovich.

2.10.2 Assessment of the Developed Immuno-affinity Mass Spectrometry Assay in Larger Cohort

To validate the IA-SRM assay developed and to incorporate the optimized blocking buffer, an independent larger sample size was tested (n=82 RT-PCR positive plasma, n=143 pre-pandemic plasma and serum). Notably, all these serological samples were collected 21 to 32 days post RT-PCR positivity testing. Using this larger cohort, the cut-off for the previously found most representative antibody subclass, IgG1 in differentiating positive versus negative serological samples was validated to be 407 ng/ml. There was a statistically significant difference in IgG1, IgG3, IgG4, IgG total, IgA1, IgA total, and IgM between COVID-19 positive and negative serological samples (**Figure 2.6**). Notably, there was incomplete digestion for the IgG total and IgG4 internal standards in this validation experiment which rendered the concentration of this antibody class to be different from the initial developing assay experiment.

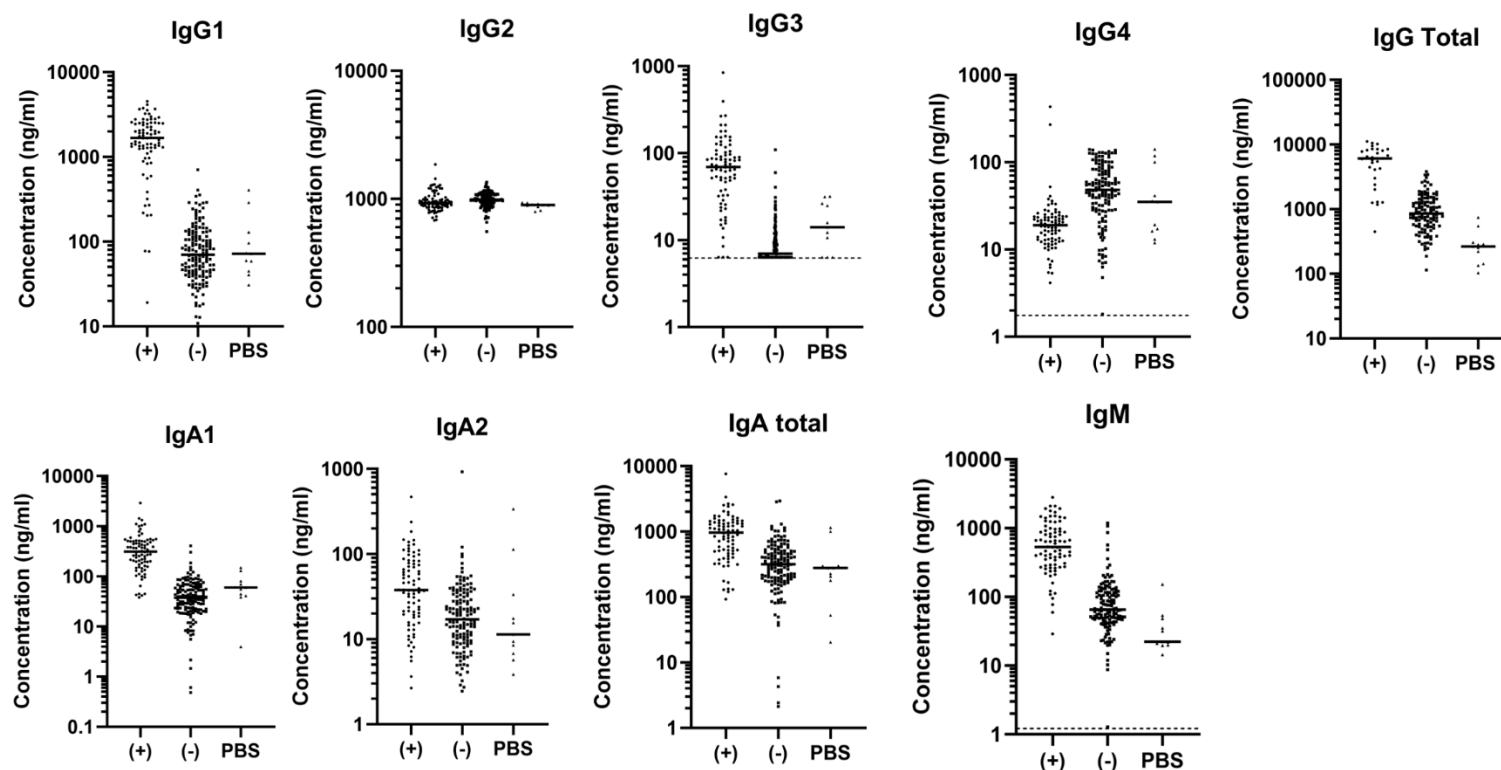


Figure 2.7. Quantification of RBD-specific antibody isotypes and subclasses using the IA-HPLC-SRM assay in larger sample size study.

PBS (phosphate buffered saline) coated wells represent the negative control to assess the level of non-specific binding in our assay. (+) denotes n=82 RT-PCR COVID-19 positive EDTA plasma.

(-) denotes n=87 and n=56 pre-pandemic serum.

Statistical significance ($P < 0.05$) using nonparametric Mann–Whitney U test. IgG1, IgG3, IgG4, IgG total, IgM, IgA1, IgA2 and IgA total ($P < 0.0001$).

Dash (---) lines represent limits of detection (LOD) in which values below the limit were counted to be the LOD.

RBD-specific IgE and IgD immunoglobulins were not detected using this assay.

2.10.3 Comparison of Plasma and Saliva Immunoglobulin Levels

The saliva and plasma Igs of the same patient collected (RT-PCR confirmed positive) on the same day (day 21-32 post positivity) was examined. Three patient saliva samples were excluded due to high sample viscosity. The results showed that the developed IA-SRM assay can be applied to detecting Igs in saliva samples (**Figure 2.7**). Future studies are needed in order to assess whether saliva samples can be used as an alternative sample type for the diagnosis of past SARS-CoV-2 infections using this developed assay.

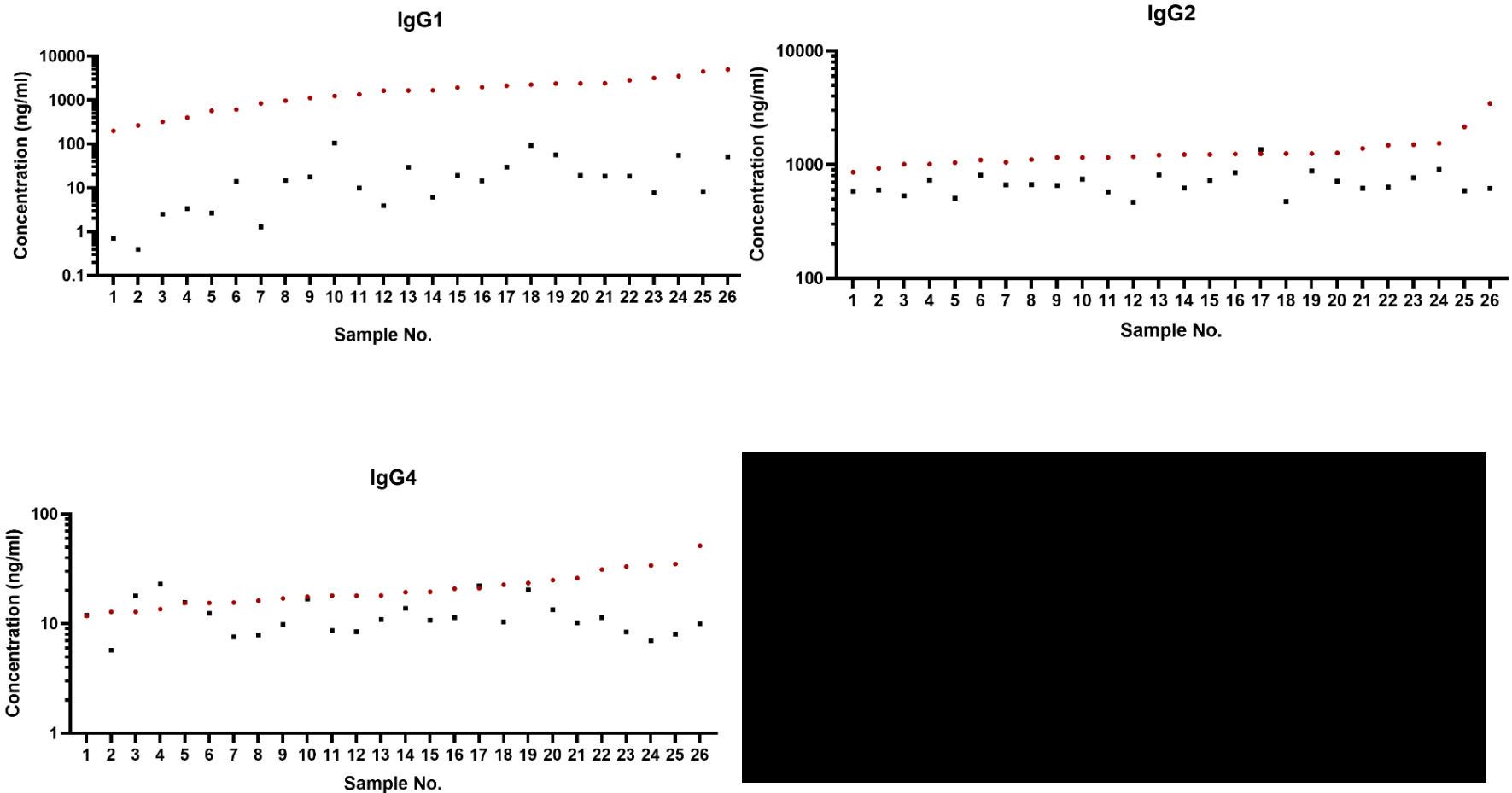


Figure 2.8A. Comparison of anti-RBD IgG levels in plasma versus saliva samples (n=26) of the same patient, collected on the same day. Anti-RBD IgG3 were not detected in saliva samples. Red data points (●) represent plasma Ig concentrations. Black data points (●) represent saliva Ig concentrations.

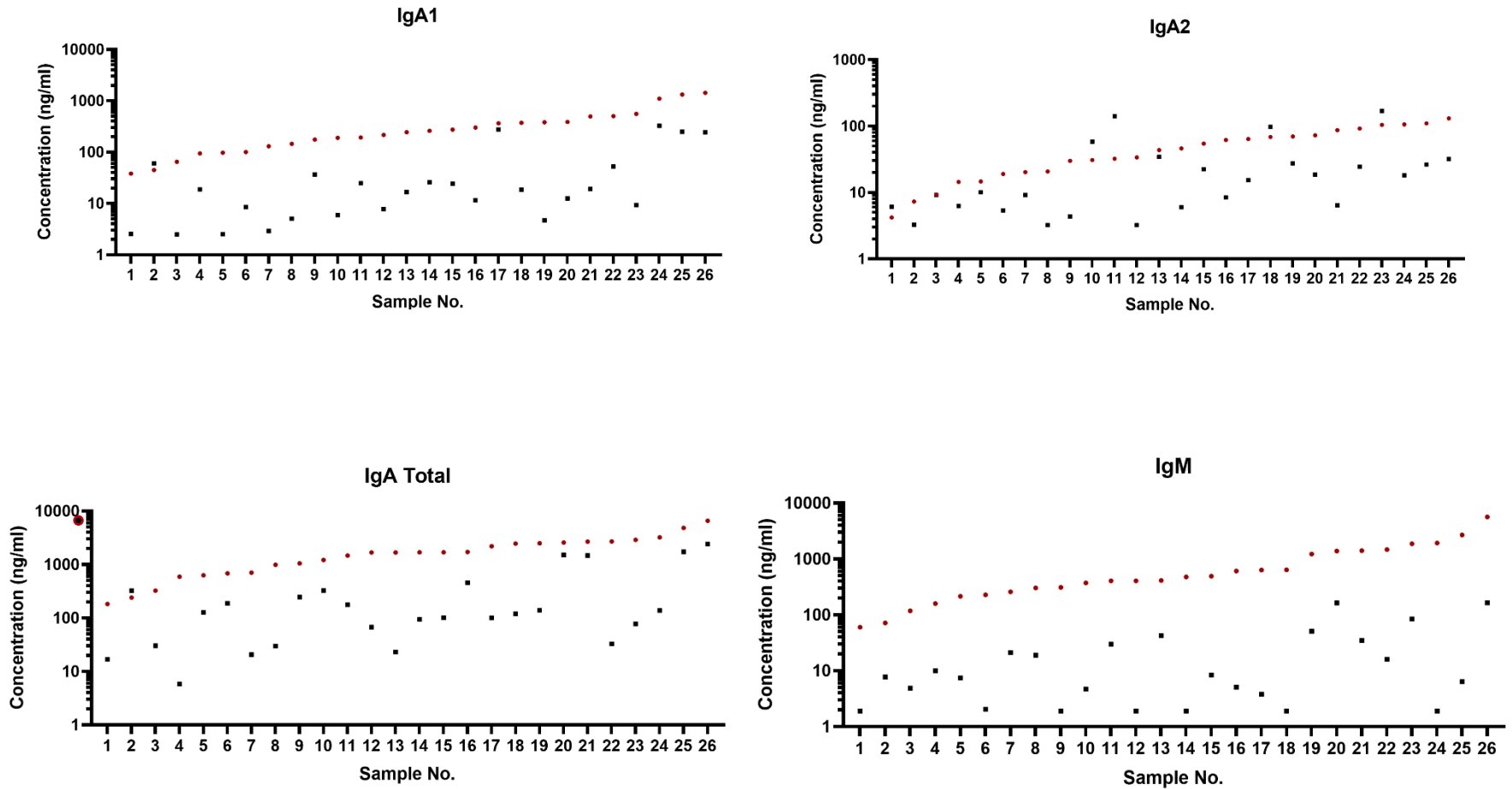


Figure 2.8B. Comparison of anti-RBD IgA and IgM levels in plasma versus saliva samples (n=26) of the same patient, collected on the same day. Anti-RBD IgG3 were not detected in saliva samples. Red data points (●) represent plasma Ig concentrations. Black data (●) points represent saliva Ig concentrations.

2.10.4 Clinical Outcome Assessment

In order to know whether specific antibody subclasses can have prognostic value, antibody levels were grouped based on patient clinical endpoints. There were four different clinical endpoints which included hospitalized, ICU, death, and non-hospitalized. The majority of the samples were from patients who were either hospitalized or taken to the ICU. There was a statistically significant higher level of IgG1 than other Igs in patients who were taken to the ICU in comparison to those who were hospitalized ($P=0.0087$) (Figure 2.8, Table 2.8). Conclusions regarding clinical endpoints for patients that were non-hospitalized or died cannot be made due to the small sample sizes. As such, further studies with larger sample sizes need to be examined in order to discover and validate potential prognostic Igs.

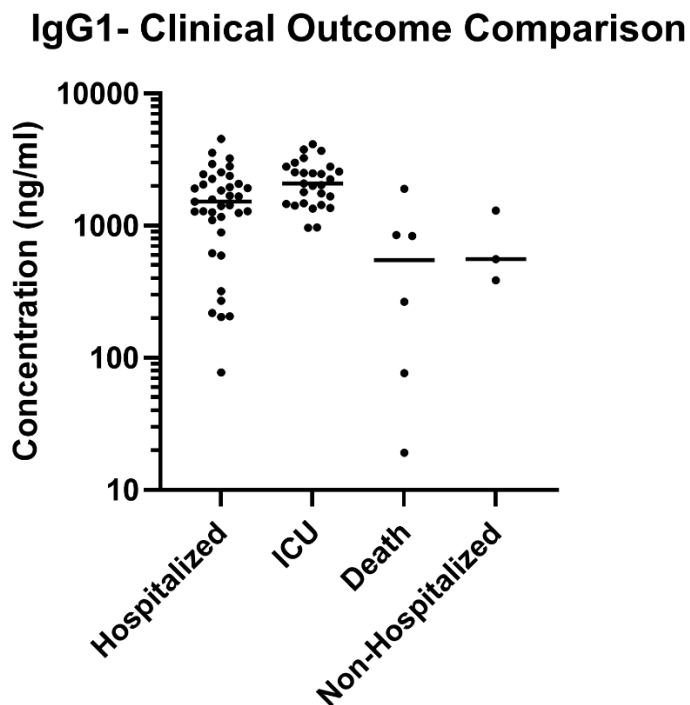


Figure 2.9. Comparison of anti-RBD IgG1 antibody levels amongst patients who were hospitalized, in ICU, died or were non-hospitalized. (n=37 hospitalized, n=27 ICU ward, n=6 passed away, n=3 non-hospitalized). Significantly higher IgG1 antibody levels in patients taken to the ICU versus those in hospital ($P=0.0087$), passed away ($P=0.0003$), and non-hospitalized ($P=0.0020$). Nonparametric Mann–Whitney U test was performed to assess statistical significance.

Antibody	Median Antibody Concentrations (ng/mL)			
	Hospitalized	ICU	Death	Non-hospitalized
IgG1	1513.6	2085.3	548.5	558.7
IgG2	1094.6	1048.5	1147.1	1122.6
IgG3	73.1	88.7	26.9	28.7
IgG4	18.3	19.5	12.5	23.8
IgA1	260.2	320.2	344.4	510.1
IgA2	36.9	38.0	55.8	62.6
IgA total	838.8	1031.5	1332.4	1318.4
IgM	467.0	522.5	658.2	349.7

Table 2.8. Median concentration of antibody subclasses and isotypes amongst RT-PCR confirmed SARS-CoV-2 positive patients categorized based on clinical endpoints. Hospitalized (n=37), ICU ward (n=27), death (n=6), non-hospitalized (n=3).

2.10.5 Benefits of the Multiplexing Potential of Immuno-affinity Mass Spectrometry Assay

SRM's multiplexing capacity allows multiple antibody subclasses and isotypes to be measured simultaneously. If IgG1 is used solely for the diagnosis of COVID-19 positive versus COVID-19 negative patients in the larger dataset, the specificity is 99.33% with a sensitivity of 89.1%. In this case, it was found that by combining IgG1 and IgM results, the specificity is maintained but the sensitivity increases to 97.62% (Figure 2.9, Table 2.7). In other words, when these two Igs are considered together, the patients with false negative results with IgG1 only, will now be correctly diagnosed as COVID-19 positive.

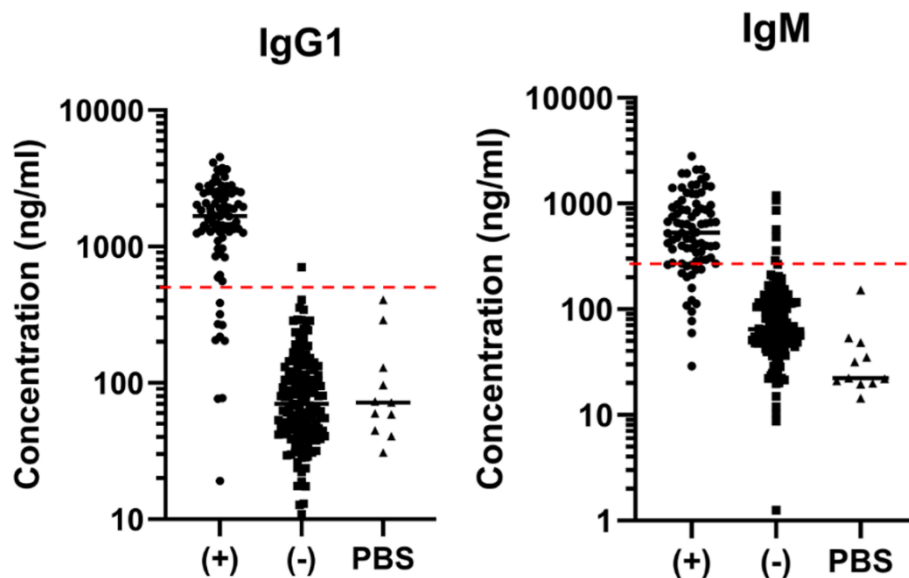


Figure 2.10. Benefits of the multiplexing capacity of IA-UPLC-SRM assay for simultaneous detection of multiple anti-RBD antibodies. IgG1 cut-off = 407 ng/ml (---), IgM cut-off = 267 ng/ml (---). RT-PCR COVID-19 confirmed (n=82) positive (+) EDTA plasma versus negative (-) EDTA plasma (n=87) and pre-pandemic serum (n=56).

Table 2.9. Multiplexing potential of IgG1 with other antibody isotypes and subclasses for the diagnosis of SARS-CoV-2 positive patients.

Combination of Antibodies	Specificity (%)	Sensitivity (%)
IgG1-IgM	99.3	97.6
IgG1-IgA1	99.3	95.3
IgG1-IgG3	99.3	91.1

Sensitivity and specificity measurements are based on n=10 COVID-19 positive patients who had below cut-off levels of IgG1 antibody (**Figure 2.9**) in which each of the IgM, IgA1, and IgG3 were individually examined in combination with IgG1.

2.10.6 Assessment of SARS-CoV-2 Mutants and Common Cold Coronaviruses

The antibody levels against the RBD, and two other SARS-CoV-2 variants which included the B.1.1 mutant and B.1.351 mutant alongside four other common cold coronaviruses (HKU1, OC43, 229E, and NL63) were examined in 10 RT-PCR confirmed positive patients. The results revealed that in most of these positive patients whose plasma was collected 21 to 35 days post RT-PCR positive testing, there was higher levels of IgG1 antibody against the SARS-CoV-2 RBD and two other mutants while lower levels against the common cold coronaviruses (**Figure 2.10**). While for the IgM antibody, there was a much more pronounced difference between antibody levels in the RBD and two other SARS-CoV-2 mutants in comparison to the four common cold coronaviruses (**Figure 2.11**). This can be explained by the biology behind the timing of antibody class switching. To delineate, IgM antibodies are the first line of defense when it comes to antibody production against a pathogen (11, 12). IgM antibodies then undergo class switching as explained previously

and transform into other immunoglobulin subclasses and isotypes, one being IgG1 (11, 12). Notably, IgM antibody levels drop as time passes post infection, while IgG1 antibodies are long lasting (13). As such, because these serological samples were collected in the early stages of SARS-CoV-2 infection, there are more pronounced differences between IgM antibodies against SARS-CoV-2 antigens versus previous infections from common cold coronaviruses.

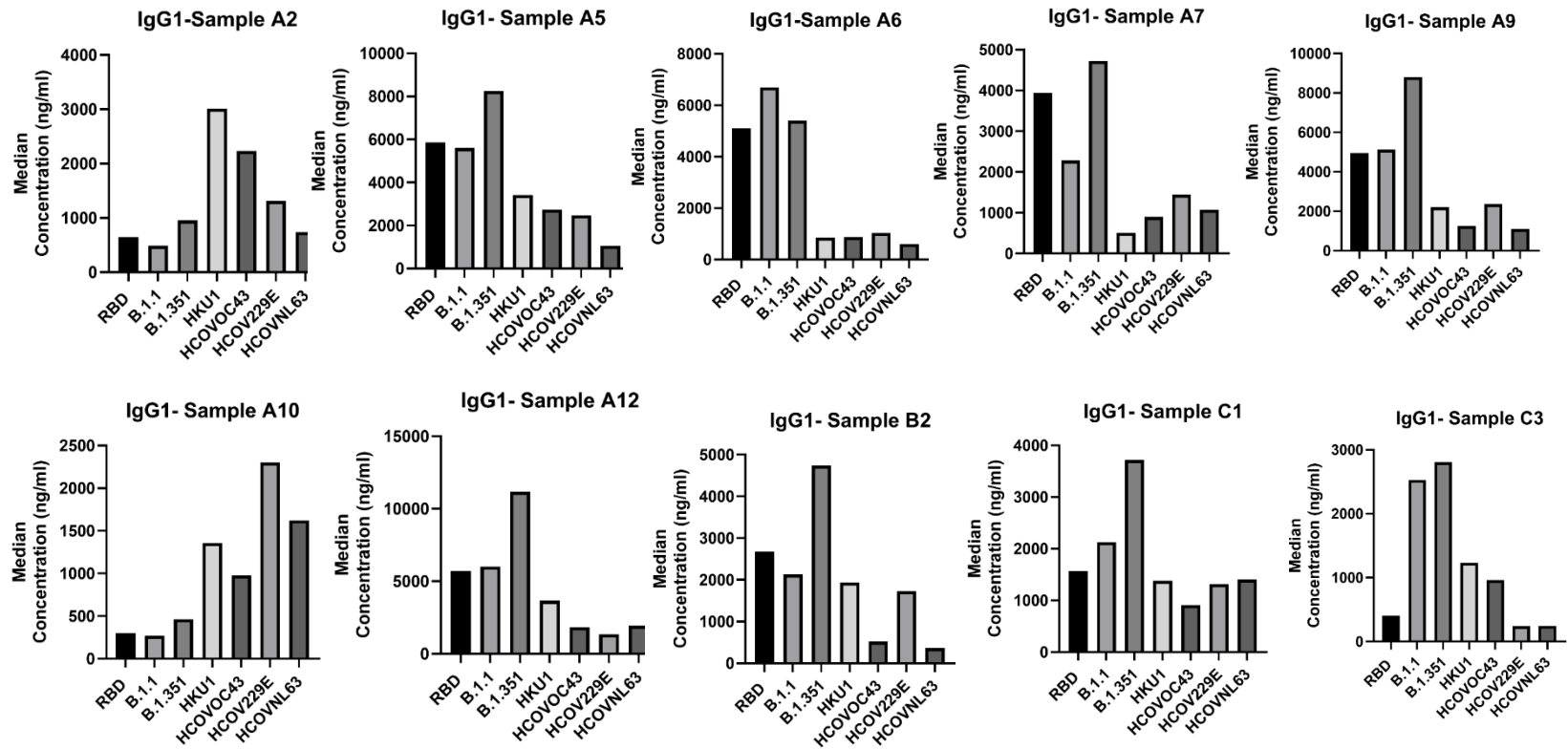


Figure 2.11. IgG1 levels against three SARS-CoV-2 antigens (RBD, the B.1.1, and B.1.351 variants) alongside four common cold coronavirus antigens (HKU1, OC43, 229E, and NL63). n=10 patients are COVID-19 positive, day 21-35 post RT-PCR positivity.

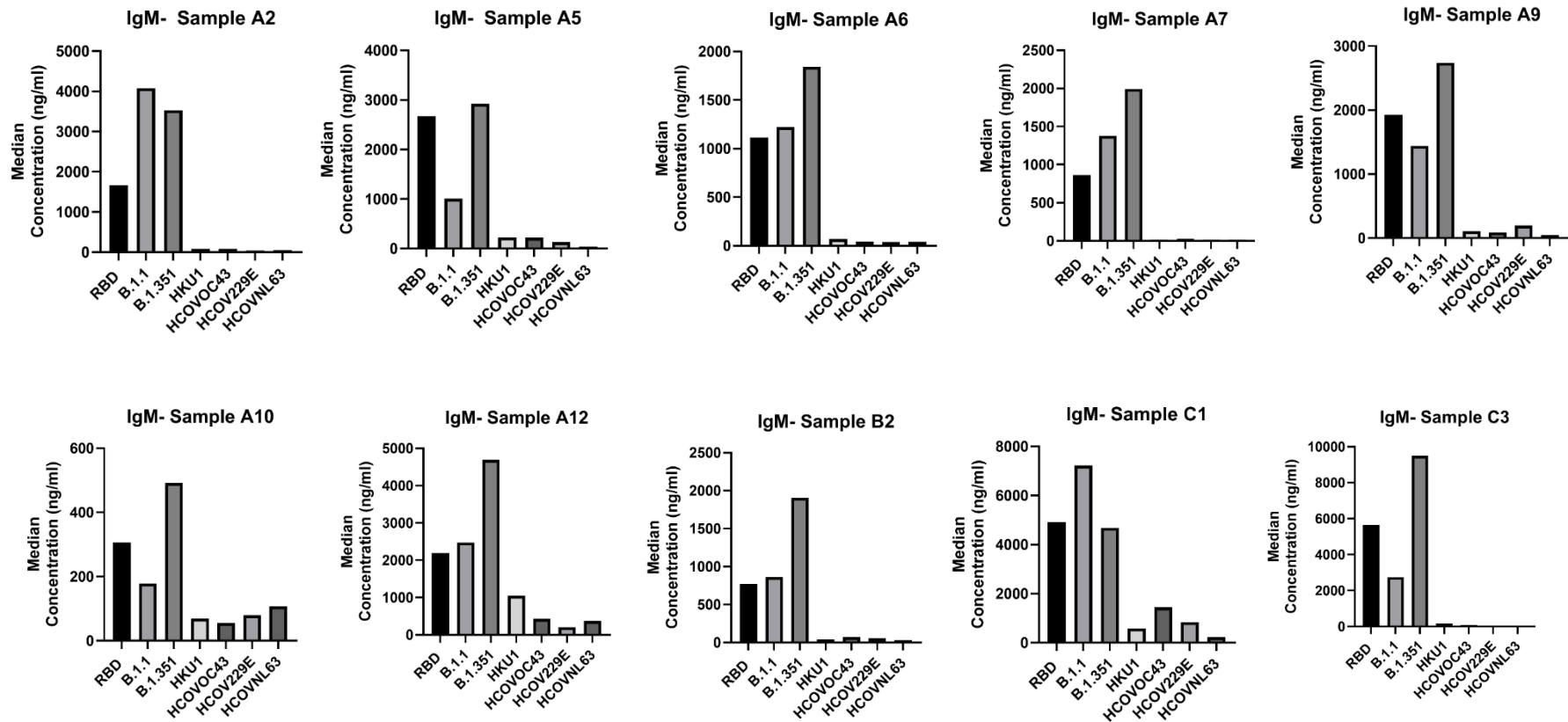


Figure 2.12. IgM levels against three SARS-CoV-2 antigens belonging to the RBD, the B.1.1, and B.1.351 variants alongside four common cold coronavirus antigens (HKU1, OC43, 229E, and NL63). All ten patients are COVID-19 positive, day 21-35 post RT-PCR positivity.

In another experiment SARS-CoV-2 positive plasma pool alongside 10 pre-pandemic plasma were compared to assess their levels of antibodies produced against the RBD, B.1.1 mutant, B.1.351 mutant, HKU1, OC43, 229E, and NL63 common cold coronaviruses. The results revealed that the positive plasma pool samples showed higher levels of antibodies against the RBD, B.1.1 mutant, and B.1.351 mutant in comparison to the pre-pandemic plasma samples. Additionally, it was found that similar levels of antibodies exist amongst all SARS-CoV-2 positive samples and pre-pandemic samples, signifying the existence of persisting antibodies/immunity against previous infections against the four common cold coronaviruses (HKU1, OC43, 229E, and NL63) (**Figure 2.12**).

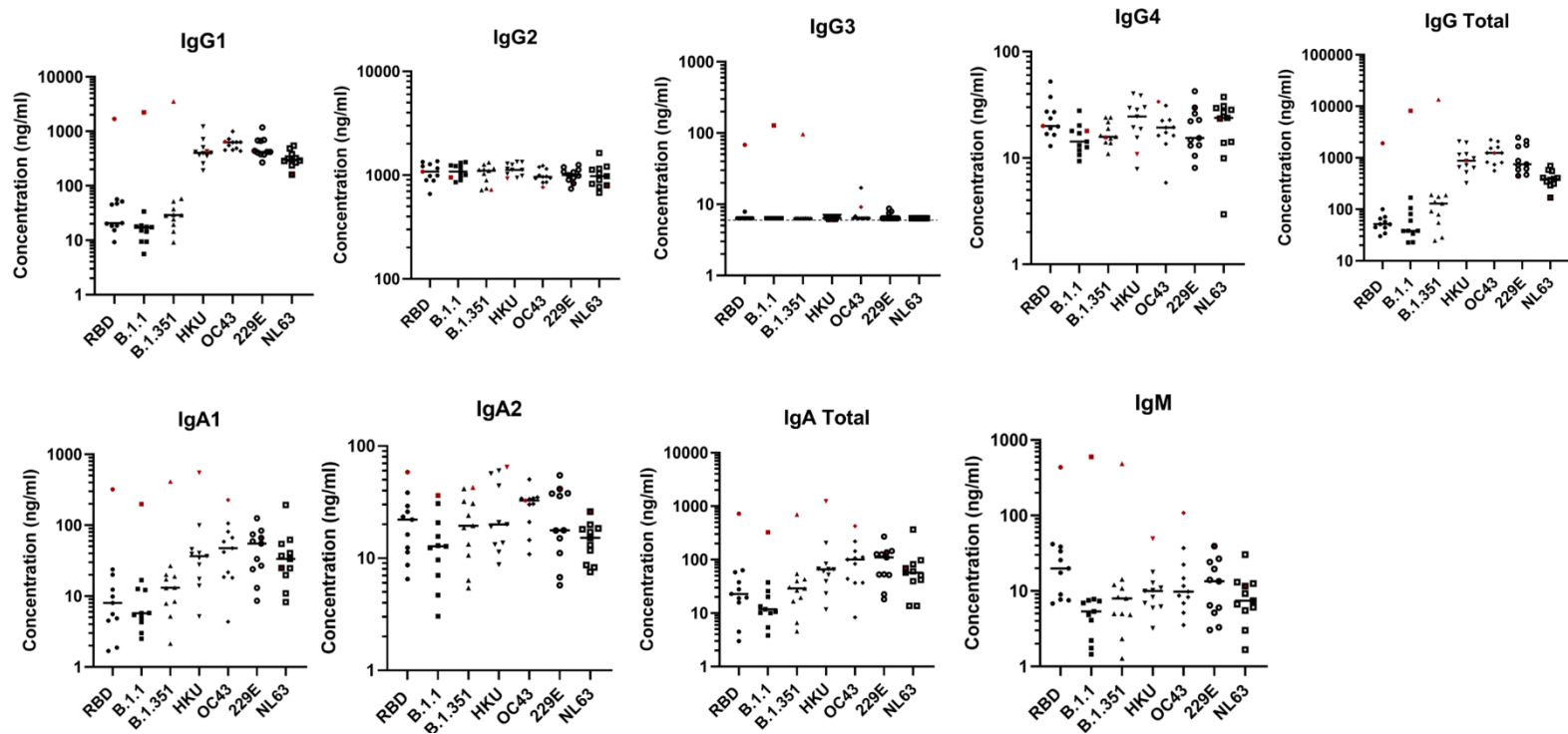


Figure 2.13. Antibody subclasses and isotype levels against the SARS-CoV-2 (RBD, the B.1.1, and B.1.351 variants) alongside four common cold coronavirus antigens (HKU1, OC43, 229E, and NL63). Samples include ten pre-pandemic patients alongside one human positive plasma pool. Points in red (●) signify the human EDTA plasma pool antibody levels. Points in black (●) signify negative EDTA plasma samples. Dash lines (---) represent limits of detection (LOD) shown in IgG3 panel in which values below the limit were counted to be the LOD.

2.11 Discussion

Having robust tools to identify and measure immunoglobins is important to determine whether convalescent and/or vaccinated individuals have developed immunity against infectious agents, to assess the seroprevalence of disease, and to select suitable convalescent plasma donors. Assessing the levels of different antibody subclasses and isotypes during different phases post infection, enables a better understanding of immunoglobulin dynamics and class switching. MS-based proteomic assays have the advantage of direct measurements (e.g., avoiding secondary antibodies) which decrease cross-reactivity and non-specific binding, and provide a wider dynamic range. When it comes to measuring immune response against pathogens, such as SARS-CoV-2, it is important to understand the biology of antibody production and the timing of it. In general, IgM antibodies are produced in the initial stage of infection and are then diminished and seroconverted into other antibody classes (13-15). Our hypothesis of the benefits of using IA-MS assays in detecting a wide array of antibody subclasses and isotypes in one run has shown to be beneficial. This is evident as SARS-CoV-2 infected patients can be diagnosed with a higher level of accuracy by examining multiple Ig subclasses and isotypes as opposed to relying on solely one antibody. This becomes even more important when we consider the previously explained seroconversion process in which different patients undergo various class switching of antibodies depending on the days post infection. As such, having assays that provide the levels of all antibody subclasses and isotypes will be beneficial to enhance diagnostic sensitivity.

In our experiments, we realized the necessity of blocking reagent to be optimized for specific assays depending on the matrix of the samples being utilized (saliva, plasma, etc.). As explained previously a limitation of immunoassays lies in their specificity which if not thoroughly assessed

can undermine the accuracy of results obtained. A root cause of limitations in specificity lies in non-specific binding, such as non-specific adsorption of proteins and antibodies on the surface of microplates, resulting in a high background signal (16). In terms of projects that rely on using immunoassays for COVID-19 diagnosis or assessment of immunity, such non-specific bindings will lead to false positive results and incorrect cut-off levels/concentrations for distinguishing positive from negative samples. Many studies assessing the immune response to SARS-CoV-2 in serological samples as well as saliva samples have utilized commonly used blocking buffers such as 3%-5% w/v dried milk (DM), 1%-5% bovine serum albumin (BSA) and not optimized these based on their sample type (17-22). Our findings reveal that a more stringent blocking buffer (green buffer 2) which is composed of BSA, Goat γ -globulin, Bovine IgG γ -globulin, mouse IgG, Tween20, and potassium chloride (KCl) is suitable for more effective blocking of plasma and saliva samples. Notably, the concentration of IgGs and total IgA in RBD coated wells was not affected by blocking with 3% DM versus green buffer 2. Significantly, this shows that by blocking with green buffer 2 we do not have a loss of specific binding. Going back to our issues with non-specific binding of IgAs, we can see that the concentration of IgA1 did decrease by blocking with green buffer 2 as opposed to 3% DM in PBS coated wells. This reveals that by using green buffer 2, we get a better blocking of surfaces. Overall, these results reveal that with more stringent blocking solutions such as green buffer 2, we can get much lower non-specific binding and background noise without compromising our true signal.

Although this chapter focuses on the development of an IA-SRM assay for measurement of the immune response against SARS-CoV-2 but the applicability of our assays can be for both detecting antigens and antibodies against this virus. Our lab has previously demonstrated a similar

methodology of IA coupled to SRM, yet different in terms of setup where plates were coated with anti-NCAP_SARS2 and anti- SPIKE_SARS2 antibodies. By using such a setup, we then captured and quantified endogenous NCAP_SARS2 and SPIKE_SARS2 proteins (antigens) found in patient serum samples for the serological diagnosis of SARS-CoV-2. Another avenue that can be studied using the IA-SRM assay discussed in this paper is to examine whether antibodies developed in individuals (naturally or vaccine induced) can neutralize other variants of SARS-CoV-2 (e.g., delta, omega, etc.). This can be done by simply coating plates with the mutated proteins (antigens) specific to different variants and assessing whether antibodies in patient samples can bind to these mutated peptide sequences. This is noteworthy as even when the COVID-19 pandemic diminishes, this virus may remain present with lower prevalence and thus with minor adjustments in the presented IP-SRM assay, we can have methods to diagnose and assess immunity against all emerging variants in a timely manner.

The applicability of our developed assay can be broadened to other diseases and/or conditions and not just restricted to diagnosing and measuring immune response against SARS-CoV-2. One example can be for the detection of Human Immunodeficiency Virus (HIV) by using the well studied and distinctive p24 viral antigen as well as antibodies specific to this virus (23-25). Immunoassays show limitations when detecting HIV due to their sensitivity (23), but they have been commonly used to detect both p24 and anti-HIV antibodies (24, 25). In such cases, IA-SRM assays can be used to address the limitations of sensitivity when using immunoassays. Such assays can be developed using a similar procedure of coating wells with either recombinant monoclonal antibodies against p24 or peptide sequences with specific epitopes against endogenously made antibodies in HIV infected individuals. Subsequently, SRM methods can be developed to detect

and quantify peptides of interest, enabling a highly sensitive and specific assay for the diagnosis of HIV. Overall, such IA-SRM assays can be used for other diseases that rely on detecting proteins (antibodies or antigens) including but not limited to hepatitis B virus, rubella, and influenza (26-28).

Another avenue for the use of IA-MS assays includes their application for therapeutic purposes. Therapeutic monoclonal antibodies have played a major role in treatments for various conditions ranging from cancer to autoimmune disorders (29). Some examples include trastuzumab for breast cancer, daclizumab for multiple sclerosis, and omalizumab for asthma (30). Particularly during the COVID-19 pandemic, bamlanivimab is a monoclonal antibody derived from a convalescent blood donor and now approved by various health agencies to be used for treating COVID-19 patients (31). One approach for finding novel therapeutic antibodies can be using IA-MS to capture and detect in particular low-abundance endogenous antibodies in patients battling certain diseases and to then use these developed antibodies to produce large scale therapeutic monoclonal antibodies to fight off diseases in other individuals.

Another approach in which MS-based proteomics can be an asset is in the sequencing of antibodies. The commonly used shot-gun proteomics approaches rely on matching sequenced peptides with readily available human proteome databases, enabling the identification of peptides in samples (32). But, when it comes to *de novo* sequencing of peptides, there are no reference databases for the variable regions of antibodies (32). These variable regions arise from recombination events, somatic hypermutations, and isotype switching (33). Currently, *de novo* sequencing of proteins and in this case for unknown antibodies using MS is still a challenge.

Overall, such approaches will enable more efficient development of therapeutic monoclonal antibodies alongside identification of epitopes and better understanding of antibody-antigen binding (34).

2.12 References

1. Weldemariam MM, Han CL, Shekari F, Kitata RB, Chuang CY, Hsu WT, et al. Subcellular Proteome Landscape of Human Embryonic Stem Cells Revealed Missing Membrane Proteins. *J Proteome Res.* 2018;17(12):4138-51.
2. Walls AC, Park YJ, Tortorici MA, Wall A, McGuire AT, Velesler D. Structure, Function, and Antigenicity of the SARS-CoV-2 Spike Glycoprotein. *Cell.* 2020;181(2):281-92 e6.
3. Petersen E, Koopmans M, Go U, Hamer DH, Petrosillo N, Castelli F, et al. Comparing SARS-CoV-2 with SARS-CoV and influenza pandemics. *Lancet Infect Dis.* 2020;20(9):e238-e44.
4. Organization WH. WHO Coronavirus (COVID-19) Dashboard 2022 [Available from: <https://covid19.who.int/>].
5. Feng W, Newbigging AM, Le C, Pang B, Peng H, Cao Y, et al. Molecular Diagnosis of COVID-19: Challenges and Research Needs. *Anal Chem.* 2020;92(15):10196-209.
6. Meyer NJ, Gattinoni L, Calfee CS. Acute respiratory distress syndrome. *Lancet.* 2021;398(10300):622-37.
7. Lan J, Ge J, Yu J, Shan S, Zhou H, Fan S, et al. Structure of the SARS-CoV-2 spike receptor-binding domain bound to the ACE2 receptor. *Nature.* 2020;581(7807):215-20.
8. Yi C, Sun X, Ye J, Ding L, Liu M, Yang Z, et al. Key residues of the receptor binding motif in the spike protein of SARS-CoV-2 that interact with ACE2 and neutralizing antibodies. *Cell Mol Immunol.* 2020;17(6):621-30.
9. Vivier E, Malissen B. Innate and adaptive immunity: specificities and signaling hierarchies revisited. *Nat Immunol.* 2005;6(1):17-21.
10. Yan F, Mo X, Liu J, Ye S, Zeng X, Chen D. Thymic function in the regulation of T cells, and molecular mechanisms underlying the modulation of cytokines and stress signaling (Review). *Mol Med Rep.* 2017;16(5):7175-84.
11. Janeway CA J, Travers P, Walport M, and Shlomchik MJ. *Immunobiology: The Immune System in Health and Disease.*: New York: Garland Science; 2001.
12. Steffen U, Koeleman CA, Sokolova MV, Bang H, Kleyer A, Rech J, et al. IgA subclasses have different effector functions associated with distinct glycosylation profiles. *Nat Commun.* 2020;11(1):120.
13. Arkhipova-Jenkins I, Helfand M, Armstrong C, Gean E, Anderson J, Paynter RA, et al. Antibody Response After SARS-CoV-2 Infection and Implications for Immunity : A Rapid Living Review. *Ann Intern Med.* 2021;174(6):811-21.
14. Galipeau Y, Greig M, Liu G, Driedger M, Langlois MA. Humoral Responses and Serological Assays in SARS-CoV-2 Infections. *Front Immunol.* 2020;11:610688.
15. Ghaffari A, Meurant R, Ardakani A. COVID-19 Serological Tests: How Well Do They Actually Perform? *Diagnostics (Basel).* 2020;10(7).
16. Waritani T, Chang J, McKinney B, Terato K. An ELISA protocol to improve the accuracy and reliability of serological antibody assays. *MethodsX.* 2017;4:153-65.
17. Isho B, Abe KT, Zuo M, Jamal AJ, Rathod B, Wang JH, et al. Persistence of serum and saliva antibody responses to SARS-CoV-2 spike antigens in COVID-19 patients. *Sci Immunol.* 2020;5(52).
18. MacMullan MA, Ibrayeva A, Trettner K, Deming L, Das S, Tran F, et al. ELISA detection of SARS-CoV-2 antibodies in saliva. *Sci Rep.* 2020;10(1):20818.

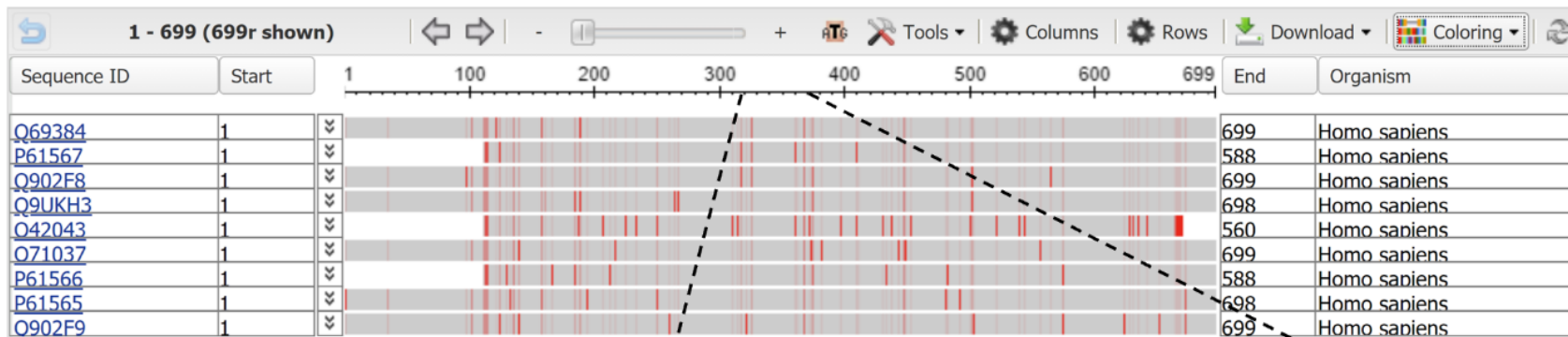
19. Melani RD, Soye BJD, Kafader JO, Forte E, Hollas M, Blagojevic V, et al. Next-generation Serology by Mass Spectrometry: Readout of the SARS-CoV-2 Antibody Repertoire. medRxiv. 2021.
20. Sweeney N, Merrick B, Pedro Galao R, Pickering S, Botgros A, Wilson HD, et al. Clinical utility of targeted SARS-CoV-2 serology testing to aid the diagnosis and management of suspected missed, late or post-COVID-19 infection syndromes: Results from a pilot service implemented during the first pandemic wave. PLoS One. 2021;16(4):e0249791.
21. Vernet R, Charrier E, Grogg J, Mach N. A Quantitative ELISA Protocol for Detection of Specific Human IgG against the SARS-CoV-2 Spike Protein. Vaccines (Basel). 2021;9(7).
22. Zhou C, Bu G, Sun Y, Ren C, Qu M, Gao Y, et al. Evaluation of serum IgM and IgG antibodies in COVID-19 patients by enzyme linked immunosorbent assay. J Med Virol. 2021;93(5):2857-66.
23. Passaes C, Delagreverie HM, Avettand-Fenoel V, David A, Monceaux V, Essat A, et al. Ultrasensitive Detection of p24 in Plasma Samples from People with Primary and Chronic HIV-1 Infection. J Virol. 2021;95(14):e0001621.
24. Gauthier DK, Turner JG. Anti-HIV antibody testing: procedures and precautions. Am J Infect Control. 1989;17(4):213-25.
25. Sutthent R, Gaudart N, Chokpaibulkit K, Tanliang N, Kanoksinsombath C, Chaisilwatana P. p24 Antigen detection assay modified with a booster step for diagnosis and monitoring of human immunodeficiency virus type 1 infection. J Clin Microbiol. 2003;41(3):1016-22.
26. Dimech W, Panagiotopoulos L, Marler J, Laven N, Leeson S, Dax EM. Evaluation of three immunoassays used for detection of anti-rubella virus immunoglobulin M antibodies. Clin Diagn Lab Immunol. 2005;12(9):1104-8.
27. Kimura T, Rokuhara A, Matsumoto A, Yagi S, Tanaka E, Kiyosawa K, et al. New enzyme immunoassay for detection of hepatitis B virus core antigen (HBcAg) and relation between levels of HBcAg and HBV DNA. J Clin Microbiol. 2003;41(5):1901-6.
28. Lu CY, Chang LY, Chen PJ, Xia NS, Shao PL, Huang LM. A highly specific ELISA for diagnosis of 2009 influenza A (H1N1) virus infections. J Formos Med Assoc. 2012;111(12):693-7.
29. Marshall MJE, Stopforth RJ, Cragg MS. Therapeutic Antibodies: What Have We Learnt from Targeting CD20 and Where Are We Going? Front Immunol. 2017;8:1245.
30. Lu RM, Hwang YC, Liu IJ, Lee CC, Tsai HZ, Li HJ, et al. Development of therapeutic antibodies for the treatment of diseases. J Biomed Sci. 2020;27(1):1.
31. Mahase E. Covid-19: FDA authorises neutralising antibody bamlanivimab for non-admitted patients. BMJ. 2020;371:m4362.
32. Cheng J, Wang L, Rive CM, Holt RA, Morin GB, Chen DDY. Complementary Methods for de Novo Monoclonal Antibody Sequencing to Achieve Complete Sequence Coverage. J Proteome Res. 2020;19(7):2700-7.
33. Sen KI, Tang WH, Nayak S, Kil YJ, Bern M, Ozoglu B, et al. Automated Antibody De Novo Sequencing and Its Utility in Biopharmaceutical Discovery. J Am Soc Mass Spectrom. 2017;28(5):803-10.
34. Peng W, Pronker MF, Snijder J. Mass Spectrometry-Based De Novo Sequencing of Monoclonal Antibodies Using Multiple Proteases and a Dual Fragmentation Scheme. J Proteome Res. 2021;20(7):3559-66.
35. Desiere F, Deutsch EW, King NL, Nesvizhskii AI, Mallick P, Eng J, et al. The PeptideAtlas project. Nucleic Acids Res. 2006;34(Database issue):D655-8.

36. Karczewski KJ, Francioli LC, Tiao G, Cummings BB, Alfoldi J, Wang Q, et al. The mutational constraint spectrum quantified from variation in 141,456 humans. *Nature*. 2020;581(7809):434-43.
37. Zahn-Zabal M, Michel PA, Gateau A, Nikitin F, Schaeffer M, Audot E, et al. The neXtProt knowledgebase in 2020: data, tools and usability improvements. *Nucleic Acids Res*. 2020;48(D1):D328-D34.

3 The use of immuno-affinity mass spectrometry for the detection and quantification of the Human Endogenous Retrovirus proteins

The human endogenous retrovirus group K's envelope proteins show a high level of homology in their peptide sequence (**Figure 3.1**). As explained previously, HERV-K *env* RNA transcript and protein overexpression has been associated with cancer development and autoimmune disorders (1, 2, 3-6). Due to the very high homology of HERV-K *env* sequences (few single amino acid differences), immunoassays are not capable of differentiating HERV-K *env* proteins (products of 14 distinct human genes, according to UniProt) (7, 8). Notably, this differentiation is needed in order to validate HERV-K *env* proteins as novel disease biomarkers. As such, we propose that IA-MS assays with the nearly absolute analytical selectivity and high sensitivity can be used for the unambiguous differentiation and quantification of the various HERV-K *env* proteins.

Figure 3.1. The high level of homology of HERV-K env protein sequences. Grey regions depict amino acid sequences that are the same and red regions depict amino acids that are variable between various proteins (8).



endogenous retrovirus group K member 6 Env polyprotein
 endogenous retrovirus group K member 7 Env polyprotein
 endogenous retrovirus group K member 8 Env polyprotein
 endogenous retrovirus group K member 9 Env polyprotein
 endogenous retrovirus group K member 18 Env polyprotein
 endogenous retrovirus group K member 21 Env polyprotein
 endogenous retrovirus group K member 24 Env polyprotein
 endogenous retrovirus group K member 113 Env polyprotein

```

PKI V SPVSGPEHPELWRLTVASHHIRIWSGNQTLETRDRKPFYTIDLNSS
PKI V SPVSGPEHPELWRLTVASHHIRIWSGNQTLETRD KPFYTIDLNSS
PKI V SPVSGPEHPELWRLTVASHHIRIWSGNQTLETRDRKPFYTVDLNSS
PKI I SPVSGPEHPELWRLTVASHHIRIWSGNQTLETR V RKPFFYTVDLNSS
PKI I SPVSGPEHPELWRLTVASHHIRIWSGNQTLETRDRKPFYTVDLNSS
PKI I SPVSGPEHPELWRLTVASHHIRIWSGNQTLETRDRKPFYTVDLNSS
PKI I SPVSGPEHPELWRLTVASHHIRIWSGNQTLETRDRKPFYTVDLNSS
PKI I SPVSGPEHPELWRLTVASHHIRIWSGNQTLETRDRKPFYTVDLNSS
    
```

Depiction of
 Frequency-Based
 Differences
 feature

3.1 Materials and Methods

Chemicals and Reagents

Dithiothreitol, iodoacetamide, and trifluoroacetic acid (TFA) were purchased from Thermo Fisher Scientific (Burlington, ON, Canada). Mass spectrometry-grade acetonitrile (ACN) and water were obtained from Fisher Scientific (Fair Lawn, NJ). Formic acid (FA), Dimethyl sulfoxide (DMSO), and dimethylated SOLu-trypsin were obtained from Sigma-Aldrich (Oakville, ON). SpikeTides_TQL peptides were ordered from JPT (innovative peptide solutions-Germany) as stable isotope-labeled peptides.

Cell Lysis

Cell pellets were exposed to 20 μ l of EDTA-free protease inhibitor cocktail (Roche) to prevent protein degradation. Following this, cells were lysed using 50 μ l of 0.1% RapiGest SF (Waters), vortexed and probe sonicated at 20 kHz for 1 minute.

Sandwich ELISA

High-binding 96-well microplates (Greiner Bio-One) were coated overnight with either the primary antibodies of HERM-1811-5 antibody or the ERVK-7 antibody (500ng in 100 μ l PBS per well). The plates were washed 3 times with 300 μ l of wash buffer (0.05% Tween20 in PBS), followed by an hour of blocking with 300 μ l of blocking buffer (2% BSA in wash buffer). Washing was then repeated. MCF-7 cells were lysed as explained above. Acetone precipitated and frozen dried (catalogue#: IRHUPLCP1GM) human placenta were probe sonicated at 45kHz for 2 minutes. Samples (100ul per well) were incubated for 2 hours on the plate shaker at room temperature. HERM-1811-5 or the ERVK-7 were used as secondary antibodies and captured with biotin-conjugated goat-anti-rabbit IgG (Catalog # A16128) and goat-anti-mouse IgG (Catalog # A16094) antibodies. Washing was repeated. 1:1000 dilution of horseradish peroxidase (HRP)

was added for 20 minutes. 100 μ l of tetramethylbenzidine (TMB) was added per well and incubated for 10 minutes at room temperature. The reaction was stopped with 50 μ l of 2M hydrochloric acid (HCL). Negative control consisted of the addition of 2% BSA in wash buffer. Positive control consisted of wells coated with RmAbR001 (#40143-R001), an anti-nucleoprotein antibody to bind to NCAP_SARS2 and captured using a rabbit polyclonal antibody (RpAb T62). Absorbance (OD 450 nm) was measured using FilterMax F5 multi-mode microplate reader (Molecular Devices) with 450NMBW80 absorbance filter.

Immunoprecipitation Protocol

High-binding 96-well microplates (Greiner Bio-One) were coated with 500 ng/well in 100 μ l of HERM 1811-5 (Ango Inc.) antibody and ERVK-7 (ThermoFisher Scientific- PA5-49515) antibody diluted in phosphate-buffered saline (PBS, pH 7.4) and kept overnight at room temperature. Following this, wells were washed 3 times with 300 μ l of wash buffer (0.05% Tween20 in PBS) per well using automated washing plate. For blocking, 6% BSA diluted in wash buffer was utilized. Following this, 3 times washing step took place and 100 μ l of cell lysates were added to each well. The samples were incubated for 2 hours on a plate shaker. Following this, the 3 times washing step was repeated.

Proteomic Sample Preparation

The immunoprecipitated wells were reduced using 1 mM of dithiothreitol at 70°C for 15 min. Following this, 20mM of iodoacetamide was added at room temperature and kept in the dark for one hour. Samples were then digested using 0.25 μ g of SOLu-trypsin per well and incubated at 37°C overnight. The next day, the digestion was stopped using 1% v/v trifluoroacetic acid (TFA).

Nano-Liquid Chromatography and High-Performance Liquid Chromatography and Shotgun Mass Spectrometry Analysis

Following immunoprecipitation and digestion, the samples were analyzed with nano-LC-SRM or UPLC-SRM. A 30-minute gradient was used on the nano-LC where samples were eluted at 300 nl/min. The nano-LC gradient started with 5% of buffer A (95% ACN, 0.1%FA) and 95% of buffer B (95% MS gradient water, 0.1% FA) to 60% of buffer A and 40% of buffer B to 100% of buffer A. On the other hand, a 12-minute gradient was used on the Waters Acquity ultra-performance liquid chromatography at 50µl/min. The gradient started with 95% buffer A (95% MS gradient water, 0.1% FA, 5% DMSO) and 5% of buffer B (95% ACN, 0.1%FA, 5% DMSO) for 1.4 minutes, to 25% of buffer B and 75% of buffer A for 0.7 minutes, to 37% of buffer B and 63% buffer A for 4.1 minutes, to 44% of buffer B and 56% of buffer A for 0.6 minutes, to 95% of buffer B and 5% of buffer A for 0.5 minutes, and to a final concentration of 95% buffer A and 5% buffer B for 1.4 minutes.

Selection of proteotypic tryptic peptides and their optimization for detection using SRM assay

In order to develop the targeted SRM assay, proteotypic tryptic peptides belonging to HERV-K *env* proteins that are shared amongst various classes of HERV-K genes were identified using online databases such as Peptide Atlas and previous literature (10) (**Figure 3.2**). A total of 13 tryptic peptides were optimized by adjusting various parameters such as collision energies, charges, and choosing the best product ion transitions. The specifications of these optimizations are shown in **Table 3.1**.

Table 3.1. Proteotypic tryptic peptides of HERV-K *env* proteins. Optimized parameters enable accurate detection of peptides using SRM assays.

HERV-K tryptic peptides	Precursor Q1 (m/z)	Precursor Charge	Product Q3 (m/z)	Fragment Charge	Fragment Ion type	Collision Energy (V)	Retention Time (min)
YPPICLGR	488.2577	++	715.392	+	y6	23.9	8.3
YPPICLGR	488.2577	++	406.726	++	y7	23.9	8.3
YPPICLGR	488.2577	++	358.1996	++	y6	23.9	8.3
YPPICLGR (Heavy)	493.2618	++	725.4002	+	y6	23.9	8.3
YPPICLGR (Heavy)	493.2618	++	411.7301	++	y7	23.9	8.3
YPPICLGR (Heavy)	493.2618	++	363.2038	++	y6	23.9	8.3
LASQINDLR	515.288	++	916.4847	+	y8	25.2	8.2
LASQINDLR	515.288	++	845.4476	+	y7	25.2	8.2
LASQINDLR	515.288	++	423.2274	++	y7	25.2	8.2
LASQINDLR (Heavy)	520.2921	++	926.4929	+	y8	25.2	8.2
LASQINDLR (Heavy)	520.2921	++	855.4558	+	y7	25.2	8.2
LASQINDLR (Heavy)	520.2921	++	428.2316	++	y7	25.2	8.2
LANQINDLR	528.7935	++	943.4956	+	y8	26.9	8.2
LANQINDLR	528.7935	++	872.4585	+	y7	26.9	8.2
LANQINDLR	528.7935	++	436.7329	++	y7	26.9	8.2
LANQINDLR (Heavy)	533.7976	++	953.503	+	y8	26.9	8.2
LANQINDLR (Heavy)	533.7976	++	882.4667	+	y7	26.9	8.2
LANQINDLR (Heavy)	533.7976	++	441.737	++	y7	26.9	8.2

HERV-K tryptic peptides	Precursor Q1 (m/z)	Precursor Charge	Product Q3 (m/z)	Fragment Charge	Fragment Ion type	Collision Energy (V)	Retention Time (min)
QSVTWLGDR	531.2724	++	747.3784	+	y6	26	8.3
QSVTWLGDR	531.2724	++	646.3307	+	y5	26	8.3
QSVTWLGDR	531.2724	++	460.2514	+	y4	26	8.3
QSVTWLGDR (Heavy)	536.2765	++	757.3867	+	y6	26	8.3
QSVTWLGDR (Heavy)	536.2765	++	656.339	+	y5	26	8.3
QSVTWLGDR (Heavy)	536.2765	++	470.2597	+	y4	26	8.3
QTVIWMGDR	553.2766	++	777.3712	+	y6	26.1	8.4
QTVIWMGDR	553.2766	++	664.2872	+	y5	26.1	8.4
QTVIWMGDR	553.2766	++	478.2078	+	y4	26.1	8.4
QTVIWMGDR (Heavy)	558.2807	++	787.3795	+	y6	26.1	8.4
QTVIWMGDR (Heavy)	558.2807	++	674.2954	+	y5	26.1	8.4
QTVIWMGDR (Heavy)	558.2807	++	488.2161	+	y4	26.1	8.4
MVTSEEQMK	541.7465	++	852.3768	+	y7	27.5	8.1
MVTSEEQMK	541.7465	++	751.3291	+	y6	27.5	8.1
MVTSEEQMK	541.7465	++	231.1162	+	b2	27.5	8.1
MVTSEEQMK (Heavy)	545.7536	++	860.391	+	y7	27.5	8.1
MVTSEEQMK (Heavy)	545.7536	++	759.3433	+	y6	27.5	8.1
MVTSEEQMK (Heavy)	545.7536	++	231.1162	+	b2	27.5	8.1
LWNSQSSIDQK	653.3253	++	1006.48	+	y9	31	8.2
LWNSQSSIDQK	653.3253	++	892.4371	+	y8	31	8.2

HERV-K tryptic peptides	Precursor Q1 (m/z)	Precursor Charge	Product Q3 (m/z)	Fragment Charge	Fragment Ion type	Collision Energy (V)	Retention Time (min)
LWNSQSSIDQK	653.3253	++	677.3464	+	y6	31	8.2
LWNSQSSIDQK (Heavy)	657.3324	++	1014.494	+	y9	31	8.2
LWNSQSSIDQK (Heavy)	657.3324	++	900.4513	+	y8	31	8.2
LWNSQSSIDQK (Heavy)	657.3324	++	685.3606	+	y6	31	8.2
LWNSQAQIDQK	665.8411	++	1031.512	+	y9	31.6	8.2
LWNSQAQIDQK	665.8411	++	917.4687	+	y8	31.6	8.2
LWNSQAQIDQK	665.8411	++	702.3781	+	y6	31.6	8.2
LWNSQAQIDQK (Heavy)	669.8482	++	1039.526	+	y9	31.6	8.2
LWNSQAQIDQK (Heavy)	669.8482	++	925.4829	+	y8	31.6	8.2
LWNSQAQIDQK (Heavy)	669.8482	++	710.3923	+	y6	31.6	8.2
VNCLQDFSYQR	715.3301	++	1216.542	+	y9	35.1	8.2
VNCLQDFSYQR	715.3301	++	608.7744	++	y9	35.1	8.2
VNCLQDFSYQR	715.3301	++	374.1493	+	b3	35.1	8.2
VNCLQDFSYQR (Heavy)	720.3342	++	1226.55	+	y9	35.1	8.2
VNCLQDFSYQR (Heavy)	720.3342	++	613.778	++	y9	35.1	8.2
VNCLQDFSYQR (Heavy)	720.3342	++	374.1493	+	b3	35.1	8.2
VNYLQDFSYQR	716.8464	++	943.4268	+	y7	34.1	8.5
VNYLQDFSYQR	716.8464	++	815.368	+	y6	34.1	8.5
VNYLQDFSYQR	716.8464	++	553.2729	+	y4	34.1	8.5
VNYLQDFSYQR (Heavy)	721.8505	++	953.4351	+	y7	34.1	8.5

HERV-K tryptic peptides	Precursor Q1 (m/z)	Precursor Charge	Product Q3 (m/z)	Fragment Charge	Fragment Ion type	Collision Energy (V)	Retention Time (min)
VNYLQDFSYQR (Heavy)	721.8505	++	825.3765	+	y6	34.1	8.5
VNYLQDFSYQR (Heavy)	721.8505	++	563.281	+	y4	34.1	8.5
VNYLQDFPYQR	721.8568	++	953.4476	+	y7	34.4	8.7
VNYLQDFPYQR	721.8568	++	825.389	+	y6	34.4	8.7
VNYLQDFPYQR	721.8568	++	563.2936	+	y4	34.4	8.7
VNYLQDFPYQR (Heavy)	726.8609	++	963.4558	+	y7	34.4	8.7
VNYLQDFPYQR (Heavy)	726.8609	++	835.3972	+	y6	34.4	8.7
VNYLQDFPYQR (Heavy)	726.8609	++	573.3019	+	y4	34.4	8.7
LQSFYPWEWGE K	785.3723	++	1094.494	+	y8	37.5	9.8
LQSFYPWEWGE K	785.3723	++	931.4308	+	y7	37.5	9.8
LQSFYPWEWGE K	785.3723	++	519.2562	+	y4	37.5	9.8
LQSFYPWEWGE K (Heavy)	789.3794	++	1102.508	+	y8	37.5	9.8
LQSFYPWEWGE K (Heavy)	789.3794	++	939.445	+	y7	37.5	9.8
LQSFYPWEWGE K (Heavy)	789.3794	++	527.2704	+	y4	37.5	9.8
IVSPVSGPEHPE LWR	568.3019	+++	745.8730	++	y13	25.3	8.3
IVSPVSGPEHPE LWR	568.3019	+++	497.5844	+++	y13	25.3	8.3

HERV-K tryptic peptides	Precursor Q1 (m/z)	Precursor Charge	Product Q3 (m/z)	Fragment Charge	Fragment Ion type	Collision Energy (V)	Retention Time (min)
IVSPVSGPEHPE LWR	568.3019	+++	468.5737	+++	y12	25.3	8.3
IVSPVSGPEHPE LWR (Heavy)	571.6380	+++	750.8771	++	y13	25.3	8.3
IVSPVSGPEHPE LWR (Heavy)	571.6380	+++	500.9205	+++	y13	25.3	8.3
IVSPVSGPEHPE LWR (Heavy)	571.6380	+++	471.9098	+++	y12	25.3	8.3

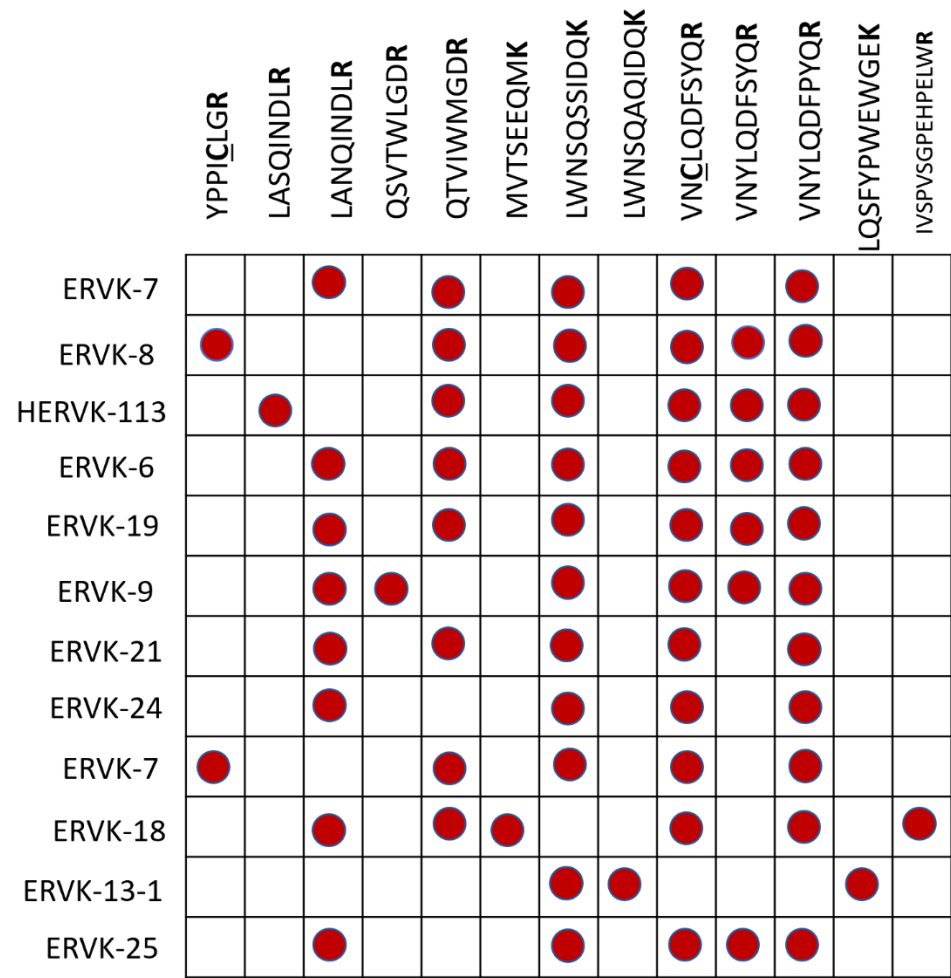


Figure 3.2. Optimized HERV-K *env* proteotypic tryptic peptides shared amongst various HERV-K genes (8).

3.2 Results

3.2.1 Assessment of the HERV-K *env* Protein Expression in MCF-7, MDA-MB-231, and LNCaP Cell Lines

HERV-K *env* protein expression was assessed in two breast cancer (MCF-7, MDA-MB-231) and one prostate cancer (LNCaP) cell line using IA-SRM assays (**Figure 3.3, Figure 3.4**). It was found that there was no expression of these proteins in these cell lines as no peaks of the “light” endogenous peptides were detected in these cell lines. Additionally, the negative control wells which were not coated with any antibody, showed similar abundance of the representative HERV-K *env* tryptic peptides as the wells coated with the HERM-1811-5 and ERVK-7 antibodies.

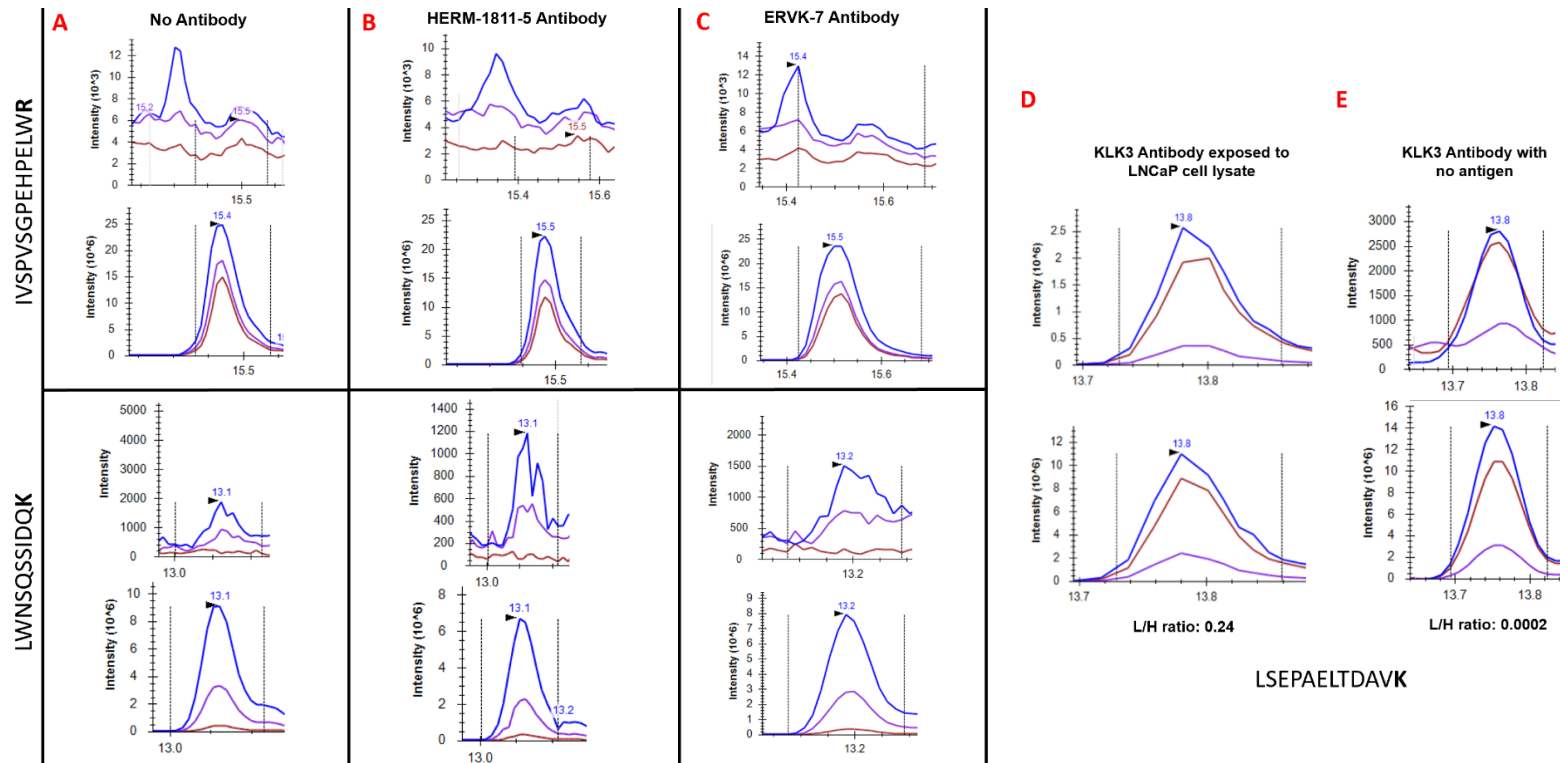


Figure 3.3. L/H ratios from the SRM results of two representative tryptic peptides (IVSPVSGPEHPPELWR, LWNSQSSIDQK) shared by HERV-K *env* proteins tested in MCF-7 cell lysates. IVSPVSGPEHPPELWR L/H ratios of (A) no antibody (0.0001), (B) HERM 1811-5 antibody (0), (C) ERVK7 antibody (0.0002). LWNSQSSIDQK L/H ratios of (A) no antibody (0.0002), (B) HERM 1811-5 (0.001), (C) ERVK7 (0.0002). Positive control: IA-SRM analysis of KLK3 protein (prostate specific antigen) in LNCaP cell line lysates. KLK3 tryptic peptide LSEPAELTDAVK was measured with three SRM transitions, L/H ratios of positive control wells coated with (D) KLK3 antibody and immunocapturing of antigen (0.24), L/H ratios of negative control wells coated with (E) KLK3 antibody with no antigen (0.0002). Bottom rows present the “heavy” isotope-labeled peptide internal standards and top rows present the “light” endogenous tryptic peptides.

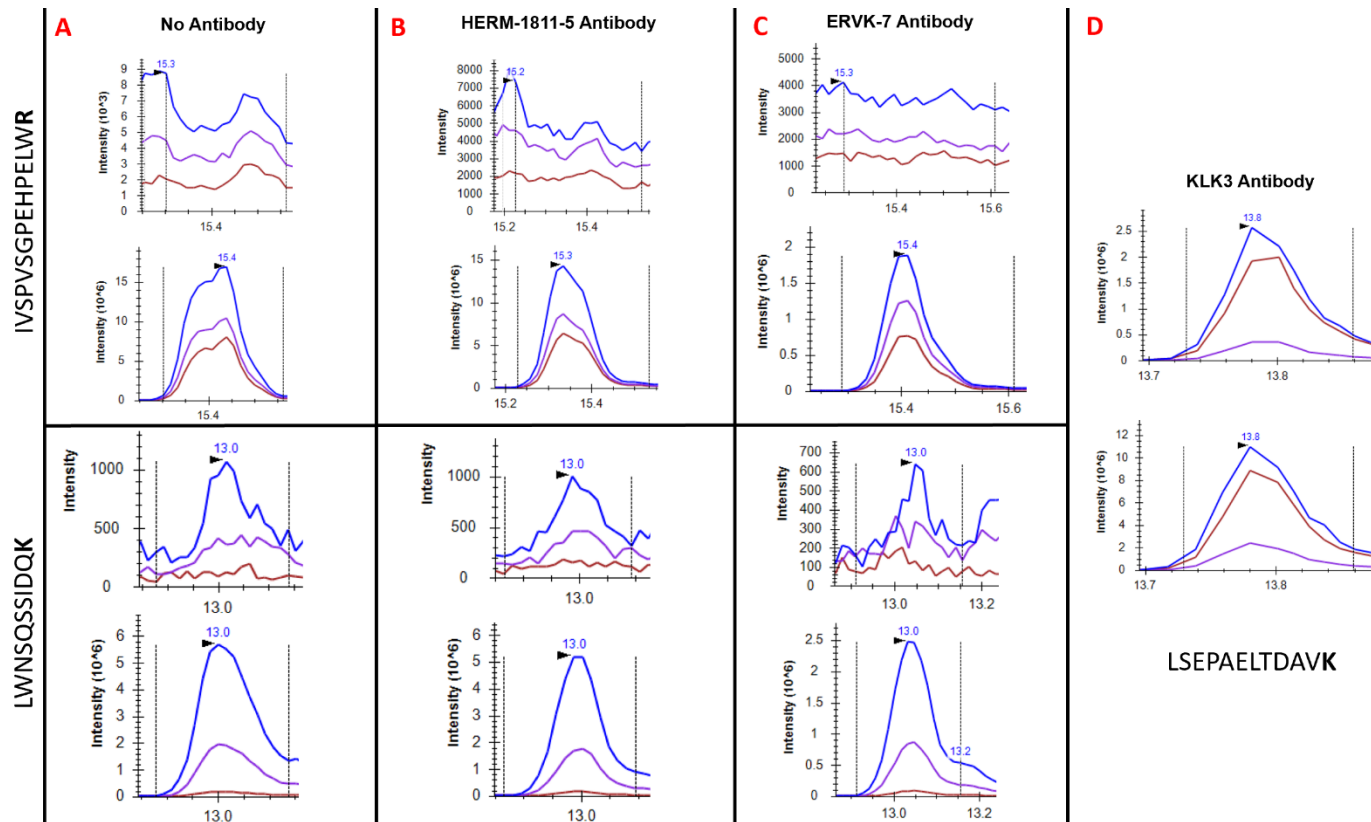


Figure 3.4. SRM results from two representative tryptic peptides (IVSPVSGPEHPELWR, LWNSQSSIDQK) shared by HERV-K *env* proteins tested in LNCaP cell line lysates. IVSPVSGPEHPELWR L/H ratios of (A) no antibody (0.0002), (B) HERM 1811-5 (0.0002), (C) ERVK7 (0.0002). LWNSQSSIDQK L/H ratios of (A) no antibody (0.0001), (B) HERM 1811-5 (0.0002), (C) ERVK7 (0.0002). Positive control: IA-SRM analysis of KLK3 protein (prostate specific antigen) in LNCaP cell line lysates. KLK3 tryptic peptide LSEPAELTDAVK was measured with three SRM transitions, L/H ratios of (D) KLK3 antibody (0.49). Bottom rows present the "heavy" isotope-labeled peptide internal standards and top rows present the "light" endogenous tryptic peptides.

It should be noted that HERV-K *env* proteins (similar to SPIKE_SARS2 spike glycoprotein) are predicted to have the N-term signal peptides and the C-term transmembrane and cytoplasmic regions (12, 13). As a result, the endogenous HERV-K *env* proteins could be localized at the cell surface. Thus, we decided to modify our experimental protocol to ensure that the potential HERV-K *env* proteins expressed at the cell surface were not cleaved during cell passaging using enzymatic (trypsin) cell dissociation media. MCF-7 cells were passaged and detached with the cell dissociation solution non enzymatic (Sigma-Aldrich, catalogue #: C5789). Similar results were found in which HERV-K *env* proteins were not detected (**Figure 3.5**). This was evident as cells exposed to enzyme-free cell dissociation media and exposed to wells coated with PBS (no-antibody controls) had a L/H ratio of 0.0022 versus those coated with HERM-1811-5 had a L/H ratio of 0.0022 and ERVK-7 antibodies had a L/H ratio of 0.0019. Similarly, cells passaged and detached with trypsin and exposed to wells coated with PBS had a L/H ratio of 0.0014 versus those coated with HERM-1811-5 had a L/H ratio of 0.0011 and ERVK-7 antibodies had a L/H ratio of 0.0013.

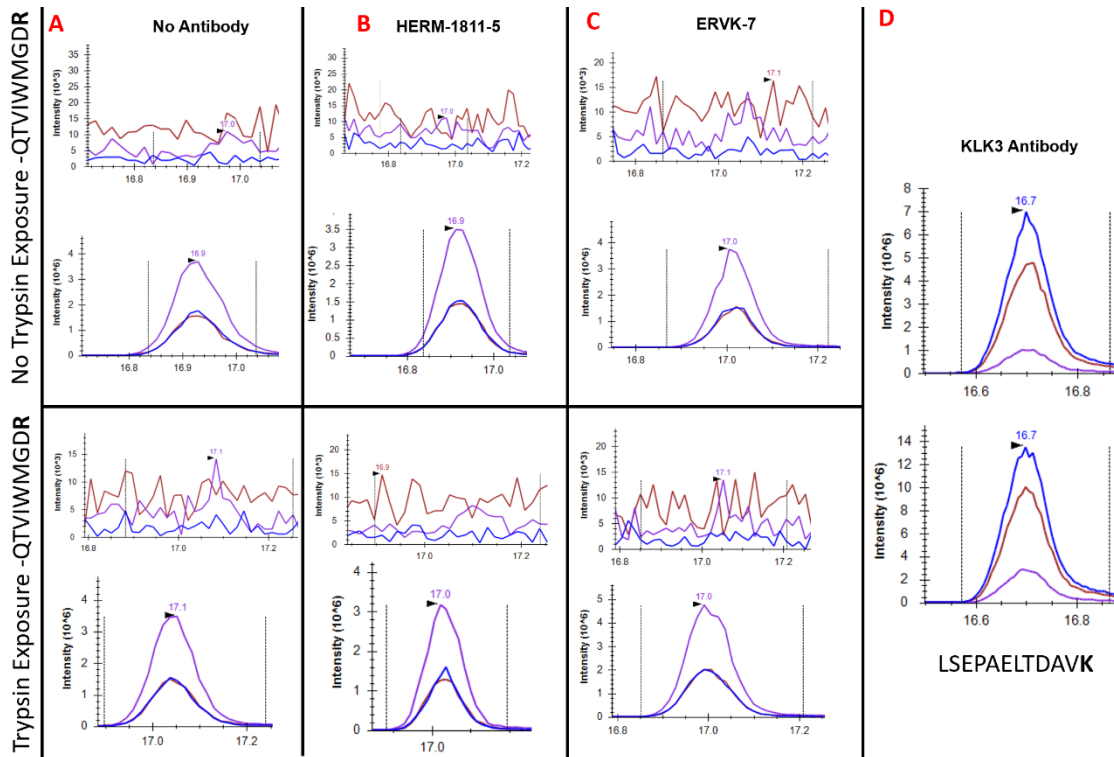


Figure 3.5. SRM results of a representative tryptic peptide (QTVIWMGDR) shared by HERV-K *env* proteins tested in MCF-7 cell lysates cultured and passaged in trypsin exposed versus no-enzyme exposed cells. QTVIWMGDR L/H ratios of no trypsin exposure in (A) no antibody (0.0022), (B)HERM 1811-5 (0.0027), (C) ERVK7 (0.0017) coated wells. QTVIWMGDR L/H ratios of trypsin exposure in (A) no antibody (0.0014), (B) HERM 1811-5 (0.0013), (C) ERVK7 (0.0013) coated wells. Positive control: IA-SRM analysis of KLK3 protein (prostate specific antigen) in LNCaP cell line lysates. KLK3 tryptic peptide LSEPAELTDAVK was measured with three SRM transitions, L/H ratios of (D) KLK3 antibody (0.48). Bottom rows present the” heavy” isotope-labeled peptide internal standards and top rows present the “light” endogenous tryptic peptides

3.2.2 HERV-K Envelope Protein Expression in Placental Tissue

Previous literature has examined the expression of endogenous retroviral envelope HERV group W proteins (HERV-W) in placental tissues, including SYCY1_HUMAN (syncytin-1; ERVW-1 gene) and SYCY2_HUMAN (syncytin-2; ERVFRD-1 gene) in the human placenta (9, 11). These proteins have been shown to result in cell-cell fusion, enabling the placental trophoblastic development (11). We hypothesized that placental tissues could also express HERV-K *env* proteins. As such, we assessed the potential protein expression of HERV-K *env* proteins in the commercially available placental tissues of normal healthy human placental tissues (acetone precipitated and frozen dried; catalogue #: IRHUPLCP1GM) were used to undergo the *in-house* sandwich ELISA (**Table 3.2**). The HERM 1811-5 antibody has a C-terminal epitope of IFEASK and the ERVK-7 antibody has a N-terminal epitope region of VNYLQDFSYQRSLKFRPKGKPCPKKEIPKESKNTE. The results showed that both placental tissue (HERM-ERVK-1/5 dilution: 0.0509, 1/20 dilution: 0.0698; ERVK-HERM-1/5 dilution: 0.0605, 1/20 dilution: 0.0638) and MCF-7 (HERM-ERVK-1/5 dilution: 0.0552, 1/20 dilution: 0.0571; ERVK-HERM-1/5 dilution: 0.0517, 1/20 dilution: 0.062) cell lysates used in this experiment showed similar values as to the negative control of 2% BSA (HERM-ERVK: 0.0632, ERVK-HERM: 0.0555). This reveals that either there is no presence of HERV-K *env* proteins in these human placental tissues and/or that the commercial antibodies do not bind to the *env* proteins.

Table 3.2. ELISA detection of HERV-K *env* proteins in human placenta tissue and MCF-7 cell line.

Primary antibody		Secondary antibody labelled with biotin	Optical Density at 450 nm				
			Freeze Dried Placenta Tissue		MCF-7 Cell Lysate		Negative control
Coated to wells	Free		(1/5)	(1/20)	(1/5)	(1/20)	(2% BSA)
HERM-1811-15 (mouse-anti-human)	ERVK-7 (rabbit-anti-human)	goat-anti-rabbit	0.0509	0.0698	0.0552	0.0571	0.0632
ERVK-7 (rabbit-anti-human)	HERM-1811-5 (mouse-anti-human)	goat-anti-mouse	0.0605	0.0638	0.0517	0.062	0.0555

Note. Plate wells were coated with either HERM-1811-5 or ERVK-7 and were incubated with 1/5 and 1/20 dilutions of placenta tissue or MCF-7 cell lysates; then incubated with ERVK-7 or HERM-1811-5, respectively.

In the absence of positive HERV-K *env* protein control, the validity of the ELISA test was confirmed by coating 2 wells with RmAbR001, an anti-nucleoprotein antibody to NCAP_SARS2 and secondary capture rabbit polyclonal antibody (RpAb T62). OD₄₅₀ (0.1691, 0.1575).

3.2.3 Assessment of Binding of HERV-K *env* Antibodies to their Specific Epitope

In order to examine whether the two commercially ordered antibodies (HERM-1811-5 and ERVK-7) do indeed bind to HERV-K *env* proteins, specific trypsin digestible peptides that are part of the epitope region of these antibodies were synthesized. Following this, the binding level of these antibodies to their corresponding epitopes were assessed (**Figure 3.6**). For the c-terminus, the binding of three (EQIFEASK, EQIFEASKAHLN, GSKLKEQIFEASKAHLNGGPGGLK) different peptides were assessed. For the ERVK-7 antibody, the epitope region peptide (VNYLQDFSYQRSLKFRPKGKPCPKKEIPKESKNTE) was used to assess protein-antibody

affinity. The results revealed that there was no binding between antibodies and their specific epitope regions. This is evident as the peaks detected in antibody coated wells shows similar intensities as those wells coated with no antibody.

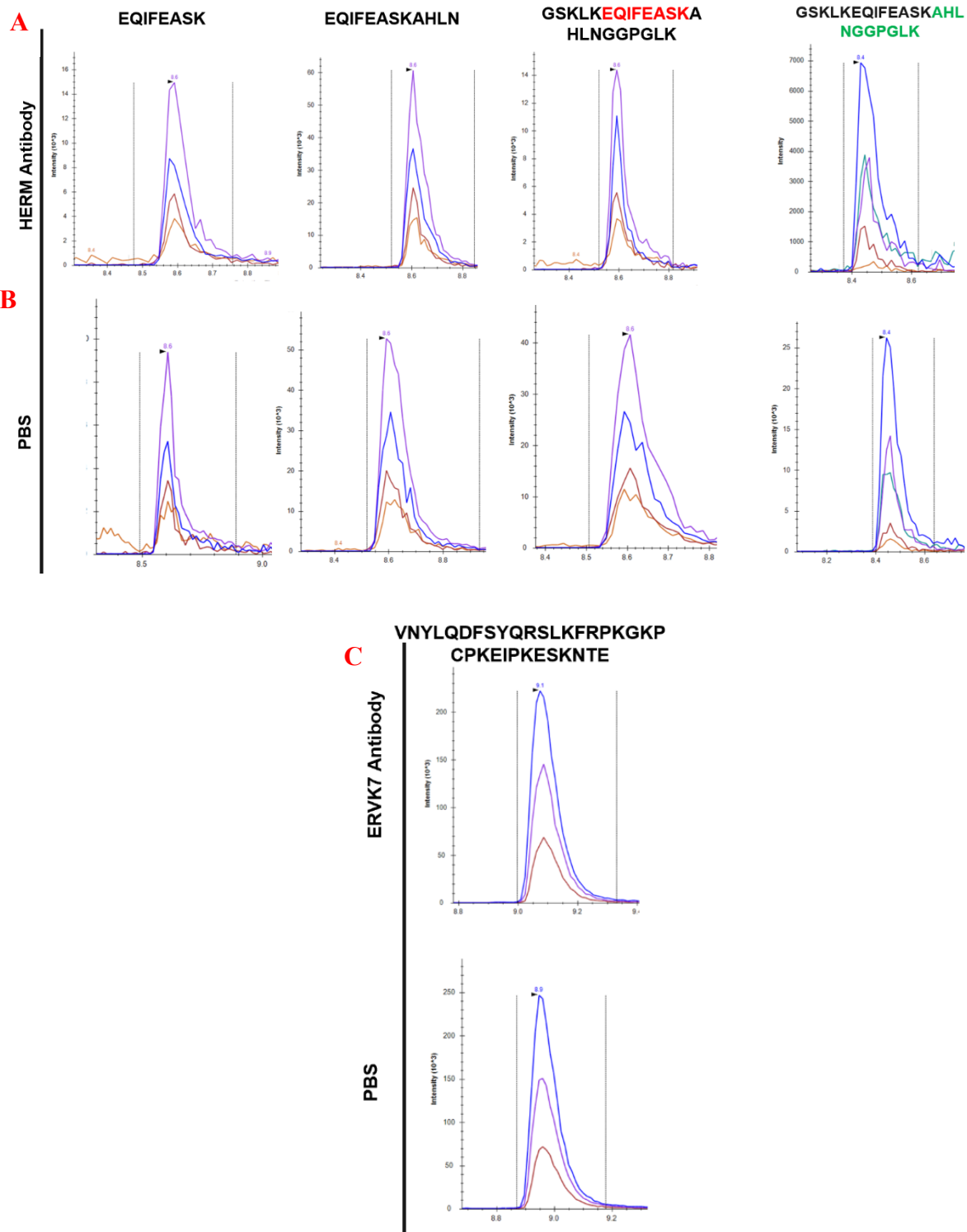


Figure 3.6. Binding of anti-HERV-K *env* antibodies to their specific epitopes. SRM results of assay where wells were exposed to (A) HERM-1811-5, (B) PBS (no antibody) and (C) ERVK-7 antibodies and the capturing of synthetic peptides (EQIFEASK, EQIFEASKAHLN, VNYLQDFS YQ RSLKFRPKGKPCPKEIPKESK NTE) belonging to the epitope region of each antibody.

3.3 Discussion

Based on the performed experiments, HERV-K *env* proteins were not identified in the breast cancer cell lines (MCF-7, MDA-MB-231), prostate cancer cell line (LNCaP), and human placenta tissues. As such it is still unknown whether HERV-K *env* proteins are expressed at the protein level. Additionally, the two commercial antibodies HERM-1811-5 and ERVK-7 may not be suitable for capturing HERV-K *env* proteins and thus not appropriate to be used in our IA-MS assays. These findings are contradictory to previous literature, but it is important to note that those research studies did not assess HERV-K *env* protein expression using highly selective mass spectrometry approaches and were prone to cross-reactivity and false-positive identifications. Wang-Johanning et al. (2007) found that HERV-K *env* mRNA transcripts were found to be expressed at a significantly higher level in ovarian epithelial tumors ($p=0.012$) in comparison to healthy ovarian tissue (4). Similarly at the cell line level, they found HERV-K *env* transcripts to be higher amongst six ovarian cancer cell lines (PA1, SKOV3, OVCA 433, OVCAR3, DOV 13 and OVCA 420) in comparison to non-cancerous ovarian cell lines (NOE113, 114, 116, 119, T29, T72 and T80) (4). HERV-K *env* transcripts were also found to be expressed at higher level in numerous pancreatic cell lines (AsPC-1, BxPC-3, Colo-357, MIA PaCa-2, SU8686, Panc-1 and Panc-2) in comparison to non-malignant pancreatic cell lines (3). Using an *in-house* HERV-K *env* protein antibody (mAB 6H5) and immunofluorescence microscopy Li et al. (2017) demonstrated the expression of HERV-K *env* proteins in pancreatic cancer cell lines, but its absence in non-malignant pancreatic cell line (3). Thus, although HERV-K *env* proteins were not detected using our IA-SRM assay, their expression at the protein level and their potential association with the development of certain diseases needs to be further investigated.

3.4 References

1. Xue B, Sechi LA, Kelvin DJ. Human Endogenous Retrovirus K (HML-2) in Health and Disease. *Front Microbiol.* 2020;11:1690.
2. Wang-Johanning F, Frost AR, Johanning GL, Khazaeli MB, LoBuglio AF, Shaw DR, et al. Expression of human endogenous retrovirus k envelope transcripts in human breast cancer. *Clin Cancer Res.* 2001;7(6):1553-60.
3. Li M, Radvanyi L, Yin B, Rycaj K, Li J, Chivukula R, et al. Downregulation of Human Endogenous Retrovirus Type K (HERV-K) Viral env RNA in Pancreatic Cancer Cells Decreases Cell Proliferation and Tumor Growth. *Clin Cancer Res.* 2017;23(19):5892-911.
4. Wang-Johanning F, Liu J, Rycaj K, Huang M, Tsai K, Rosen DG, et al. Expression of multiple human endogenous retrovirus surface envelope proteins in ovarian cancer. *Int J Cancer.* 2007;120(1):81-90.
5. Groger V, Cynis H. Human Endogenous Retroviruses and Their Putative Role in the Development of Autoimmune Disorders Such as Multiple Sclerosis. *Front Microbiol.* 2018;9:265.
6. Tugnet N, Rylance P, Roden D, Trela M, Nelson P. Human Endogenous Retroviruses (HERVs) and Autoimmune Rheumatic Disease: Is There a Link? *Open Rheumatol J.* 2013;7:13-21.
7. UniProt C. UniProt: the universal protein knowledgebase in 2021. *Nucleic Acids Res.* 2021;49(D1):D480-D9.
8. Medicine USNLo. Constraint-based Multiple Alignment Tool [Available from: https://www.ncbi.nlm.nih.gov/tools/cobalt/re_cobalt.cgi].
9. Chen CP, Chen LF, Yang SR, Chen CY, Ko CC, Chang GD, et al. Functional characterization of the human placental fusogenic membrane protein syncytin 2. *Biol Reprod.* 2008;79(5):815-23.
10. Weldemariam MM, Han CL, Shekari F, Kitata RB, Chuang CY, Hsu WT, et al. Subcellular Proteome Landscape of Human Embryonic Stem Cells Revealed Missing Membrane Proteins. *J Proteome Res.* 2018;17(12):4138-51.
11. Mi S, Lee X, Li X, Veldman GM, Finnerty H, Racie L, et al. Syncytin is a captive retroviral envelope protein involved in human placental morphogenesis. *Nature.* 2000;403(6771):785-9.
12. Michaud HA, de Mulder M, SenGupta D, Deeks SG, Martin JN, Pilcher CD, et al. Trans-activation, post-transcriptional maturation, and induction of antibodies to HERV-K (HML-2) envelope transmembrane protein in HIV-1 infection. *Retrovirology.* 2014;11:10.
13. Morozov VA, Dao Thi VL, Denner J. The transmembrane protein of the human endogenous retrovirus--K (HERV-K) modulates cytokine release and gene expression. *PLoS One.* 2013;8(8):e70399.

4 Conclusions

Immunoassays, such as ELISA, are currently the gold standard methods for detecting proteins in clinical samples (1). In this thesis, immunoaffinity enrichment coupled to mass spectrometry (IA-MS) was assessed as an alternative assay to detect proteins with the high levels of sensitivity and specificity. The applicability of IA-MS assays was showcased through their application in two projects: the detection and quantification of anti-SARS-CoV-2 antibodies (Chapter 2) and the human HERV-K *env* proteins (Chapter 3).

The main conclusion from the Chapter 2 study was that IA-SRM assays could be developed for the serological testing of immunity against SARS-CoV-2 virus. Notably, IgG1 was the most representative antibody isotype for the serological testing of SARS-CoV-2 and for the identification of past infections. Because of the novelty of this SARS-CoV-2 research project, future independent studies are needed to validate antibody cut-offs for the later use of IA-SRM in clinical research and diagnostics. The benefits of having a multiplexing assay were presented in the larger sample set in which combination of IgG1 with IgM antibody subclasses enhances the diagnostic sensitivity and specificity of the assay. This is something particularly important when it comes to antibody-based testing, in which depending on the amount of time post infection, the immunoglobulin subclasses and isotypes vary in abundance due to the class switching phenomenon. Furthermore, by simply coating wells with antigens belonging to different coronaviruses, the immunological responses against other variants and emerging mutants can be measured. Markedly, immunity against four common cold coronaviruses (HKU1, OC43, 229E, and NL63) was assessed and it was found that some circulating levels of long-lasting immunoglobulins such as IgG1 remain in patients post infection while the abundance of other

immunoglobulins such as IgM rapidly decreases due to their short half-life post infection (2). IgG1 was found to have potential prognostic information in which patients who had more severe disease (being taken to the ICU ward) revealed higher levels in comparison to hospitalized patients. Due to the smaller number of non-hospitalized or passed away patients, future studies using larger patient cohorts need to be conducted to investigate whether IgG1 can be predictive of clinical endpoint in patients infected with SARS-CoV-2. Additionally, another avenue to explore is whether saliva samples can be used as an alternative to serological samples using the developed IA-SRM assay for the diagnosis of past SARS-CoV-2 infections. This can be done by obtaining saliva samples collected potentially prior to vaccinations and the COVID-19 pandemic. Furthermore, the diagnostic sensitivity and specificity of the developed assay can be assessed by comparing pre-pandemic or unvaccinated saliva samples with those infected with SARS-CoV-2 or vaccinated. Lastly, incomplete digestion of peptides should be optimized in the future, enabling more robust assay performance.

The main conclusion for the HERV-K *env* protein study (Chapter 3) was that it is still unknown whether HERV-K *env* genes are expressed at the protein level. This ambiguity stems from the unknown performance of the two commercially available antibodies (HERM-1811-5 and ERVK-7). It is also possible that these HERV-K *env* proteins are expressed at extremely low amounts and thus not be suitable for their detection by SRM assays. In future studies, an overexpression of HERV-K *env* proteins can facilitate reassessment of the developed IA-MS assays. Furthermore, the development of an *in-house* antibody that shows a high level of affinity for capturing HERV-K *env* proteins can enhance the immunoaffinity component of IA-SRM assay.

Overall, the use of IA-MS and the development of highly selective targeted methods for the detection of viral antigens and anti-viral antibodies can be applied to a wide array of pathologies and future epidemics, endemics, and pandemics.

4.1 References

1. Thiha A, Ibrahim F. A Colorimetric Enzyme-Linked Immunosorbent Assay (ELISA) Detection Platform for a Point-of-Care Dengue Detection System on a Lab-on-Compact-Disc. *Sensors (Basel)*. 2015;15(5):11431-41.
2. Isho B, Abe KT, Zuo M, Jamal AJ, Rathod B, Wang JH, et al. Persistence of serum and saliva antibody responses to SARS-CoV-2 spike antigens in COVID-19 patients. *Sci Immunol*. 2020;5(52).

References

- Ackermann BL. Understanding the role of immunoaffinity-based mass spectrometry methods for clinical applications. *Clin Chem*. 2012;58(12):1620-2.
- Alhadj M FA. Enzyme Linked Immunosorbent Assay. StatPearls Publishing 2022.
- Arkipova-Jenkins I, Helfand M, Armstrong C, Gean E, Anderson J, Paynter RA, et al. Antibody Response After SARS-CoV-2 Infection and Implications for Immunity : A Rapid Living Review. *Ann Intern Med*. 2021;174(6):811-21.
- Breda A VN, Norberto de Souza O, Garratt RC. *Bioinformatics in Tropical Disease Research: A Practical and Case-Study Approach*. 2006.
- Cardozo KHM, Lebkuchen A, Okai GG, Schuch RA, Viana LG, Olive AN, et al. Establishing a mass spectrometry-based system for rapid detection of SARS-CoV-2 in large clinical sample cohorts. *Nat Commun*. 2020;11(1):6201.
- Cazares LH, Chaerkady R, Samuel Weng SH, Boo CC, Cimbri R, Hsu HE, et al. Development of a Parallel Reaction Monitoring Mass Spectrometry Assay for the Detection of SARS-CoV-2 Spike Glycoprotein and Nucleoprotein. *Anal Chem*. 2020;92(20):13813-21.
- Chen CP, Chen LF, Yang SR, Chen CY, Ko CC, Chang GD, et al. Functional characterization of the human placental fusogenic membrane protein syncytin 2. *Biol Reprod*. 2008;79(5):815-23.
- Chen J, Foroozesh M, Qin Z. Transactivation of human endogenous retroviruses by tumor viruses and their functions in virus-associated malignancies. *Oncogenesis*. 2019;8(1):6.
- Chen Z, Zhang Z, Zhai X, Li Y, Lin L, Zhao H, et al. Rapid and Sensitive Detection of anti-SARS-CoV-2 IgG, Using Lanthanide-Doped Nanoparticles-Based Lateral Flow Immunoassay. *Anal Chem*. 2020;92(10):7226-31.
- Cheng J, Wang L, Rive CM, Holt RA, Morin GB, Chen DDY. Complementary Methods for de Novo Monoclonal Antibody Sequencing to Achieve Complete Sequence Coverage. *J Proteome Res*. 2020;19(7):2700-7.
- Coiras MT, Perez-Brena P, Garcia ML, Casas I. Simultaneous detection of influenza A, B, and C viruses, respiratory syncytial virus, and adenoviruses in clinical samples by multiplex reverse transcription nested-PCR assay. *J Med Virol*. 2003;69(1):132-44.
- Crowther JR. *Systems in ELISA. The Elisa Guidebook*: Humana Press; 2001.
- Dass C. *Fundamentals of Contemporary Mass Spectrometry* 2007. Wiley-Blackwell, Chichester, England.

Dervan E, Bhattacharyya DD, McAuliffe JD, Khan FH, Glynn SA. Ancient Adversary - HERV-K (HML-2) in Cancer. *Front Oncol.* 2021;11:658489.

Desiere F, Deutsch EW, King NL, Nesvizhskii AI, Mallick P, Eng J, et al. The PeptideAtlas project. *Nucleic Acids Res.* 2006;34(Database issue):D655-8.

Dimech W, Panagiotopoulos L, Marler J, Laven N, Leeson S, Dax EM. Evaluation of three immunoassays used for detection of anti-rubella virus immunoglobulin M antibodies. *Clin Diagn Lab Immunol.* 2005;12(9):1104-8.

Faustini SE, Jossi SE, Perez-Toledo M, Shields AM, Allen JD, Watanabe Y, et al. Development of a high-sensitivity ELISA detecting IgG, IgA and IgM antibodies to the SARS-CoV-2 spike glycoprotein in serum and saliva. *Immunology.* 2021;164(1):135-47.

Feng W, Newbigging AM, Le C, Pang B, Peng H, Cao Y, et al. Molecular Diagnosis of COVID-19: Challenges and Research Needs. *Anal Chem.* 2020;92(15):10196-209.

Fournier ML, Gilmore JM, Martin-Brown SA, Washburn MP. Multidimensional separations-based shotgun proteomics. *Chem Rev.* 2007;107(8):3654-86.

Fredolini C, Pathak KV, Paris L, Chapple KM, Tsantilas KA, Rosenow M, et al. Shotgun proteomics coupled to nanoparticle-based biomarker enrichment reveals a novel panel of extracellular matrix proteins as candidate serum protein biomarkers for early-stage breast cancer detection. *Breast Cancer Res.* 2020;22(1):135.

Gauthier DK, Turner JG. Anti-HIV antibody testing: procedures and precautions. *Am J Infect Control.* 1989;17(4):213-25.

Ghaffari A, Meurant R, Ardakani A. COVID-19 Serological Tests: How Well Do They Actually Perform? *Diagnostics (Basel).* 2020;10(7).

Galipeau Y, Greig M, Liu G, Driedger M, Langlois MA. Humoral Responses and Serological Assays in SARS-CoV-2 Infections. *Front Immunol.* 2020;11:610688.

Glish GL, Vachet RW. The basics of mass spectrometry in the twenty-first century. *Nat Rev Drug Discov.* 2003;2(2):140-50.

Gonzalez-Cao M, Iduma P, Karachaliou N, Santarpia M, Blanco J, Rosell R. Human endogenous retroviruses and cancer. *Cancer Biol Med.* 2016;13(4):483-8.

Groger V, Cynis H. Human Endogenous Retroviruses and Their Putative Role in the Development of Autoimmune Disorders Such as Multiple Sclerosis. *Front Microbiol.* 2018;9:265.

Guyen E, Duus K, Lydolph MC, Jorgensen CS, Laursen I, Houen G. Non-specific binding in solid phase immunoassays for autoantibodies correlates with inflammation markers. *J Immunol Methods.* 2014;403(1-2):26-36.

Haag AM. Modern Proteomics – Sample Preparation, Analysis and Practical Applications; Mass Analyzers and Mass Spectrometers: Springer, Cham; 2016.

Ho CS, Lam CW, Chan MH, Cheung RC, Law LK, Lit LC, et al. Electrospray ionisation mass spectrometry: principles and clinical applications. *Clin Biochem Rev.* 2003;24(1):3-12.

Hoofnagle AN, Wener MH. The fundamental flaws of immunoassays and potential solutions using tandem mass spectrometry. *J Immunol Methods.* 2009;347(1-2):3-11.

Ihling C, Tanzler D, Hagemann S, Kehlen A, Huttelmaier S, Arlt C, et al. Mass Spectrometric Identification of SARS-CoV-2 Proteins from Gargle Solution Samples of COVID-19 Patients. *J Proteome Res.* 2020;19(11):4389-92.

Isho B, Abe KT, Zuo M, Jamal AJ, Rathod B, Wang JH, et al. Persistence of serum and saliva antibody responses to SARS-CoV-2 spike antigens in COVID-19 patients. *Sci Immunol.* 2020;5(52).

Janeway CA J, Travers P, Walport M, and Shlomchik MJ. *Immunobiology: The Immune System in Health and Disease.*: New York: Garland Science; 2001.

Kanji JN, Zelyas N, MacDonald C, Pabbaraju K, Khan MN, Prasad A, et al. False negative rate of COVID-19 PCR testing: a discordant testing analysis. *Virology.* 2021;18(1):13.

Kimura T, Rokuhara A, Matsumoto A, Yagi S, Tanaka E, Kiyosawa K, et al. New enzyme immunoassay for detection of hepatitis B virus core antigen (HBcAg) and relation between levels of HBcAg and HBV DNA. *J Clin Microbiol.* 2003;41(5):1901-6.

La'ulu SL, Roberts WL. Performance characteristics of five automated CA 19-9 assays. *Am J Clin Pathol.* 2007;127(3):436-40.

Lan J, Ge J, Yu J, Shan S, Zhou H, Fan S, et al. Structure of the SARS-CoV-2 spike receptor-binding domain bound to the ACE2 receptor. *Nature.* 2020;581(7807):215-20.

Leenaars M, Hendriksen CF. Critical steps in the production of polyclonal and monoclonal antibodies: evaluation and recommendations. *ILAR J.* 2005;46(3):269-79.

Li M, Radvanyi L, Yin B, Rycak K, Li J, Chivukula R, et al. Downregulation of Human Endogenous Retrovirus Type K (HERV-K) Viral env RNA in Pancreatic Cancer Cells Decreases Cell Proliferation and Tumor Growth. *Clin Cancer Res.* 2017;23(19):5892-911.

Liebler DC, Zimmerman LJ. Targeted quantitation of proteins by mass spectrometry. *Biochemistry.* 2013;52(22):3797-806.

Liu G, Rusling JF. COVID-19 Antibody Tests and Their Limitations. *ACS Sens.* 2021;6(3):593-612.

Lu CY, Chang LY, Chen PJ, Xia NS, Shao PL, Huang LM. A highly specific ELISA for diagnosis of 2009 influenza A (H1N1) virus infections. *J Formos Med Assoc.* 2012;111(12):693-7.

Lu RM, Hwang YC, Liu IJ, Lee CC, Tsai HZ, Li HJ, et al. Development of therapeutic antibodies for the treatment of diseases. *J Biomed Sci.* 2020;27(1):1.

MacMullan MA, Ibrayeva A, Trettner K, Deming L, Das S, Tran F, et al. ELISA detection of SARS-CoV-2 antibodies in saliva. *Sci Rep.* 2020;10(1):20818.

Mahase E. Covid-19: FDA authorises neutralising antibody bamlanivimab for non-admitted patients. *BMJ.* 2020;371:m4362.

Marshall MJE, Stopforth RJ, Cragg MS. Therapeutic Antibodies: What Have We Learnt from Targeting CD20 and Where Are We Going? *Front Immunol.* 2017;8:1245.

Medicine USNLo. Constraint-based Multiple Alignment Tool [Available from: https://www.ncbi.nlm.nih.gov/tools/cobalt/re_cobalt.cgi].

Melani RD, Soye BJD, Kafader JO, Forte E, Hollas M, Blagojevic V, et al. Next-generation Serology by Mass Spectrometry: Readout of the SARS-CoV-2 Antibody Repertoire. *medRxiv.* 2021.

Meyer NJ, Gattinoni L, Calfee CS. Acute respiratory distress syndrome. *Lancet.* 2021;398(10300):622-37.

Mi S, Lee X, Li X, Veldman GM, Finnerty H, Racie L, et al. Syncytin is a captive retroviral envelope protein involved in human placental morphogenesis. *Nature.* 2000;403(6771):785-9.

Neubert H, Shuford CM, Olah TV, Garofolo F, Schultz GA, Jones BR, et al. Protein Biomarker Quantification by Immunoaffinity Liquid Chromatography-Tandem Mass Spectrometry: Current State and Future Vision. *Clin Chem.* 2020;66(2):282-301.

Nextprot. Release statistics 2022 [Available from: <https://www.nextprot.org/about/statistics>].

Organization WH. WHO Coronavirus (COVID-19) Dashboard 2022 [Available from: <https://covid19.who.int/>].

Osinalde N, Aloria K, Omaetxebarria MJ, Kratchmarova I. Targeted mass spectrometry: An emerging powerful approach to unblock the bottleneck in phosphoproteomics. *J Chromatogr B Analyt Technol Biomed Life Sci.* 2017;1055-1056:29-38.

Passaes C, Delagreverie HM, Avettand-Fenoel V, David A, Monceaux V, Essat A, et al. Ultrasensitive Detection of p24 in Plasma Samples from People with Primary and Chronic HIV-1 Infection. *J Virol.* 2021;95(14):e0001621.

Peng W, Pronker MF, Snijder J. Mass Spectrometry-Based De Novo Sequencing of Monoclonal Antibodies Using Multiple Proteases and a Dual Fragmentation Scheme. *J Proteome Res.* 2021;20(7):3559-66.

Petersen E, Koopmans M, Go U, Hamer DH, Petrosillo N, Castelli F, et al. Comparing SARS-CoV-2 with SARS-CoV and influenza pandemics. *Lancet Infect Dis.* 2020;20(9):e238-e44.

Petrova OE, Sauer K. High-Performance Liquid Chromatography (HPLC)-Based Detection and Quantitation of Cellular c-di-GMP. *Methods Mol Biol.* 2017;1657:33-43.

Pitt JJ. Principles and applications of liquid chromatography-mass spectrometry in clinical biochemistry. *Clin Biochem Rev.* 2009;30(1):19-34.

Sakamoto S, Putalun W, Vimolmangkang S, Phoolcharoen W, Shoyama Y, Tanaka H, et al. Enzyme-linked immunosorbent assay for the quantitative/qualitative analysis of plant secondary metabolites. *J Nat Med.* 2018;72(1):32-42.

Salavatiha Z, Soleimani-Jelodar R, Jalilvand S. The role of endogenous retroviruses-K in human cancer. *Rev Med Virol.* 2020;30(6):1-13.

Sen KI, Tang WH, Nayak S, Kil YJ, Bern M, Ozoglu B, et al. Automated Antibody De Novo Sequencing and Its Utility in Biopharmaceutical Discovery. *J Am Soc Mass Spectrom.* 2017;28(5):803-10.

SCIEX™ A. Powerful Scan Modes of QTRAP® System Technology 2019 [Available from: <https://sciex.com/content/dam/SCIEX/pdf/tech-notes/all/QTRAP-Scan-Modes.pdf>].

Shabir GA. Development and Validation of a Reversed-phase HPLC Method for the Determination of Hydroxybenzene in a Cream Formulation. *Indian J Pharm Sci.* 2010;72(3):307-11.

Steffen U, Koeleman CA, Sokolova MV, Bang H, Kleyer A, Rech J, et al. IgA subclasses have different effector functions associated with distinct glycosylation profiles. *Nat Commun.* 2020;11(1):120.

Sweeney N, Merrick B, Pedro Galao R, Pickering S, Botgros A, Wilson HD, et al. Clinical utility of targeted SARS-CoV-2 serology testing to aid the diagnosis and management of suspected missed, late or post-COVID-19 infection syndromes: Results from a pilot service implemented during the first pandemic wave. *PLoS One.* 2021;16(4):e0249791.

Sutthent R, Gaudart N, Chokpaibulkit K, Tanliang N, Kanoksinsombath C, Chaisilwatana P. p24 Antigen detection assay modified with a booster step for diagnosis and monitoring of human immunodeficiency virus type 1 infection. *J Clin Microbiol.* 2003;41(3):1016-22.

Thiha A, Ibrahim F. A Colorimetric Enzyme-Linked Immunosorbent Assay (ELISA) Detection Platform for a Point-of-Care Dengue Detection System on a Lab-on-Compact-Disc. *Sensors (Basel).* 2015;15(5):11431-41

Tugnet N, Rylance P, Roden D, Trela M, Nelson P. Human Endogenous Retroviruses (HERVs) and Autoimmune Rheumatic Disease: Is There a Link? *Open Rheumatol J.* 2013;7:13-21.

UniProt C. UniProt: the universal protein knowledgebase in 2021. *Nucleic Acids Res.* 2021;49(D1):D480-D9.

Vernet R, Charrier E, Grogg J, Mach N. A Quantitative ELISA Protocol for Detection of Specific Human IgG against the SARS-CoV-2 Spike Protein. *Vaccines (Basel).* 2021;9(7).

Vivier E, Malissen B. Innate and adaptive immunity: specificities and signaling hierarchies revisited. *Nat Immunol.* 2005;6(1):17-21.

Walls AC, Park YJ, Tortorici MA, Wall A, McGuire AT, Velesler D. Structure, Function, and Antigenicity of the SARS-CoV-2 Spike Glycoprotein. *Cell.* 2020;181(2):281-92 e6.

Wang-Johanning F, Frost AR, Johanning GL, Khazaeli MB, LoBuglio AF, Shaw DR, et al. Expression of human endogenous retrovirus k envelope transcripts in human breast cancer. *Clin Cancer Res.* 2001;7(6):1553-60.

Wang-Johanning F, Liu J, Rycaj K, Huang M, Tsai K, Rosen DG, et al. Expression of multiple human endogenous retrovirus surface envelope proteins in ovarian cancer. *Int J Cancer.* 2007;120(1):81-90.

Waritani T, Chang J, McKinney B, Terato K. An ELISA protocol to improve the accuracy and reliability of serological antibody assays. *MethodsX.* 2017;4:153-65.

Weldemariam MM, Han CL, Shekari F, Kitata RB, Chuang CY, Hsu WT, et al. Subcellular Proteome Landscape of Human Embryonic Stem Cells Revealed Missing Membrane Proteins. *J Proteome Res.* 2018;17(12):4138-51.

Wilson SR, Olsen C, Lundanes E. Nano liquid chromatography columns. *Analyst.* 2019;144(24):7090-104.

Wu AH. A selected history and future of immunoassay development and applications in clinical chemistry. *Clin Chim Acta.* 2006;369(2):119-24.

Xue B, Sechi LA, Kelvin DJ. Human Endogenous Retrovirus K (HML-2) in Health and Disease. *Front Microbiol.* 2020;11:1690.

Yan F, Mo X, Liu J, Ye S, Zeng X, Chen D. Thymic function in the regulation of T cells, and molecular mechanisms underlying the modulation of cytokines and stress signaling (Review). *Mol Med Rep.* 2017;16(5):7175-84.

Yi C, Sun X, Ye J, Ding L, Liu M, Yang Z, et al. Key residues of the receptor binding motif in the spike protein of SARS-CoV-2 that interact with ACE2 and neutralizing antibodies. *Cell Mol Immunol.* 2020;17(6):621-30.

Zahn-Zabal M, Michel PA, Gateau A, Nikitin F, Schaeffer M, Audot E, et al. The neXtProt knowledgebase in 2020: data, tools and usability improvements. *Nucleic Acids Res.* 2020;48(D1):D328-D34.

Zhang Y, Fonslow BR, Shan B, Baek MC, Yates JR, 3rd. Protein analysis by shotgun/bottom-up proteomics. *Chem Rev.* 2013;113(4):2343-94.

Zhou C, Bu G, Sun Y, Ren C, Qu M, Gao Y, et al. Evaluation of serum IgM and IgG antibodies in COVID-19 patients by enzyme linked immunosorbent assay. *J Med Virol.* 2021;93(5):2857-66.